Photonic and Magnetic Nano- and Micro-Particles for Biomedical Applications: Detection and Destruction of Bacterial and Cancer Cells

By

Ron Gordon Smith

A dissertation submitted in partial fulfillment
of the requirements for the degree of
Doctor of Philosophy
(Chemistry)
in the University of Michigan
2013

Doctoral Committee:

Professor Raoul Kopelman, Chair
Professor Theodore G Goodson III
Professor Michael D Morris
Professor Martin A Philbert

Dedication

To my family, especially my wife Janae

Acknowledgements

I would like to thank everybody that has taught me and everybody that has helped me with my research: Brandon McNaughton, Rodney Agayan, Christopher Manion, Suna Im, Matthew Waugh, Tamir Epstein, Yong-Eun Koo, Theodore G Goodson III, Michael D Morris, and Martin A Philbert.

Table of Contents

List of Tables

List of Figures

Chapter 1 Nanometer and Micron-Scale Particles and Their Applications

1.1 Introduction – Nanometer and Micron-Scale Particles

There has been much advancement in engineered particle technology over the last decade. Engineered particles are versatile and are useful tools for various applications from sensing and monitoring, medical therapies, imaging, and as catalysts, to name a few. With this versatility, particles systems can be molded to increase efficacy of the particles in specific biomedical applications. I will discuss functional properties of such particles in three different systems that were studied: photothermal therapy (PTT), photodynamic therapy (PDT), and bacterial detection.

1.1.1 Particle Components

The primary reason for using engineered particles is to take advantage of their chemical, physical, and biophysical properties to facilitate in experiments, analytical measurements, or medical treatments. After reviewing engineered particle systems, there are six major components of particles that can be altered to affect their properties. These components include particle size, shape, material composition, structure of the material, surface modifications to the particle, and chemical agents added to the particles. Engineered particles can be fine-tuned to an application by tweaking each of these components until the desired properties are achieved. In this section, each of the various components of particle will be discussed in more detail, as well as how these modifications affect the particle's properties.

1.1.1.1 Size

Particles are primarily categorized by their size, shape, and material composition. When discussing particle size, particles are often divided into two main groups: nanoparticles and microparticles. Particle size affects the chemical, physical, and biophysical properties of the particle and, therefore, each group has its advantages, depending on the application. Nanoparticles range in size from 1 - 100 nm and have been used for hundreds of years. They are often discussed in biomedical applications and in electronics. In biomedical applications, where the particles need to be internalized, smaller particles are often better because the size of the particle will have minimal physical effects to the cellular structure.

Microparticles range from 0.1 - 100 μm, and because of their size they are often used for different applications. They have been used in applications from magnetic separation, bacterial detection [1], monitoring bacterial cell growth [2], and, as with nanoparticles, drug release studies. The translational movement of magnetic microparticles in magnetic fields has shown to be useful in magnetic separation. [3] [4] [5] The advantage microparticles have over nanoparticles is their large volume to surface area. The increased volume of magnetic material in microparticles allows for separation of cells without leaving particles behind, as does occur when there is inadequate quantity of nanoparticles attached to a cell. Another application for microparticles has been for drug release models. [6] Microparticles are ideal for these two applications and other applications that require higher loads per particle. Larger particles also have some major limitations, with the main limitation being their inability to

be internalized by cells when internalization is required. For applications that require internalization, nanoparticle systems are required.

1.1.1.2 Shape

Particles come various shapes, such as spheres [7], rods [8] [9] [10] [11], nanocages [12], prisms [13], hollow spheres [14] [15], spheroids, discs [16], and cubes [12]. The shape of metal nanoparticles can be controlled by changing either the concentration or type of surfactant, reducing agent, metal precursor, temperature, or reaction time. [17] Depending on the material type of the particle, this can have varying effects on the properties of the particles. The main physical and biophysical properties affected include drag coefficients, plasmon absorption, light scattering, fluorescence, cytotoxicity, and cellular uptake.

In biological conditions the shape of particles can affect the way the particles interact with cells. Examples of this include toxicity, cellular uptake, uptake rate, and binding efficiency. Particle shape also affects the drag coefficient of the particle, which is very important when using magnetic particles in rotating magnetic fields.

1.1.1.3 Materials

Particles can be manufactured from a wide range of materials. These materials can be separated into different categories: metals, inorganic, semiconductors, organic, or a combination of two or more materials. The material composition of the particle affects biodegradability, toxicity, structure, ability to adsorb or absorb molecules, ability to attach to other molecules, and solubility. Each material has its own unique properties, and these properties can be tuned and tweaked to improve the effectiveness of the particles. Often people forget that not only does the material composition change

the functionality of the particle, but also the material structure, i.e. porosity, changes the functionality of the particle. This section will further explain the different materials that can be used, give some examples of each, and mention a few of their properties.

The first category of materials discussed in this thesis is metals. Some of the most common metals used are gold [12] [14] [18] [19] [20], silver [12] [18], platinum [17], and palladium. [17] Gold and silver nanoparticles are commonly used for imaging [19], thermal therapies [19], and microbial detection using SERS [21]. Silver nanoparticles are also good reducing agents, which is the reason for their antimicrobial properties. [22] The ability of nanoparticles to function as metal catalysts, i.e. platinum and palladium nanoparticles, is often overlooked by those in biological fields. The catalytic properties not only work well in synthesis, but when they occur in the body they can lead to side effects too.

The second major category of particles is inorganic particles. A few of the most common include silica [23], iron oxide [24], zinc oxide [25], and titanium (IV) oxide [25]. These particles heave been used for applications such as MRI imaging [24], magnetic separation [3] [4] [5], bacterial growth dynamics [1], and sunscreen [25].

The next category is semiconductor particles. Of special interest are semiconductor particles called quantum dots. [26] Quantum dots are often made with two parts, a stabilizing shell such as ZnS, and an internal semiconductor core such as CdSe. These types of particles are easily designed to fluoresce at specific wavelengths with a narrow emission band [27] [28]. They have a few advantages over fluorescent dyes. Quantum dots do not photobleach as easily as fluorescent dyes, have a stronger luminescence, are easier to tune to fluorescent wavelengths by varying the size of the

nanocrystal, and their fluorescent band width is thinner than fluorescent dyes. The reason quantum dots have not replaced dyes is because they can be difficult to synthesize and can be toxic to cells if not coated. They are becoming more common as they have become more commercially available.

The last major category is organic nanoparticles, which include (but are not limited to) both biological and polymer particles. Organic particles can be made from liposomes [29], micelles, carbon nanotubes [30], fullerene [31] viral derived capsid, proteins, other natural polymers [32], and synthetic polymers. [32] [33] [34] The number of polymers that can be used in particle formation is limitless, but some of the more popular polymers for biological applications are polyacrylamide (PAA) [7], poly(lactic-co-glycolic acid) (PLGA) [35] [36], polyethylene glycol (PEG) [32], and polyethylenimine (PEI) [37]. Other synthetic polymers that are often used include sol-gel [38], polyglutamic acid (PGA), polylactic acid (PLA), polycarprolactone (PCL), and N-(2-hydroxypropyl\)-methylacrylamide copolymer (HPMA). [32] Some common natural polymers are heparin, dextran, albumin, gelatin, alginate, collagen, and chitosan. [32] There are many great reviews available on the different polymers that are used to form particles. [32]

Not only are there different polymers, there are different polymer architectures as well: linear, cross-linked, star, and dendrimers, to name a few. Most polymer architectures used for particles are random and not extremely uniform, such is the case of all the polymers listed above. Dendrimers, on the other hand, are extremely uniform in size but can be very difficult to synthesize and can also be expensive. [39] In most cases, there is no need for the amount of uniformity of dendrimers. Often it is important

to sacrifice some perfection to lower the costs of the therapy. This increases the availability of the product and can lead to higher profits.

Often the properties of a material are not optimal, and it is necessary to employ a combination of the different materials. For example, many metallic, inorganic, and semiconductor nanoparticles will often have polymer coatings to decrease surface interactions in biological environments. [35] [36] [40] [41] In some cases organic/inorganic particles are coated with metals, as in gold nanoshells. Gold nanoshells have an adsorption band in the infrared, and gold spheres of the same size absorb in the green of the visible spectrum. [42] The capability to combine different materials from the various categories increases the ability to tailor the nanoparticle to the desired functionality.

Materials have a range of different architectural structures, such as crystalline, amorphous, porous, or gelatinous structures. As particles can have varying size and shapes, particles can have various degrees of a structure type which will also affect the properties of the particles. The structure will have an effect on solubility of particles, biodegradability, loading efficiencies, leaching of load, binding affinity, surface modifications, and cytotoxicity. Organic materials are one of the primary materials used when a porous particle is required, but other compounds such silicates can also be used. For example, groups have used 130 nm mesoporous silica particles for drug delivery of paclitaxel. [23] [43] This type of particle has about 750 pores on the surface. [43] Some material structures can be easily altered by slight changes to the starting materials or quantities used in the composition of particles. For example, changing the quantity of cross-linkers or the length of monomers in a polymer is a common method of

changing particle structure with minimal change to surface functionality. This is the technique used to change the porosity of the particle in order to increase the amount of compounds loaded into the particle. Loading will be discussed in greater detail in a later section.

1.1.1.4 Surface Modifications

During the design phase it is often determined that the current material for the particle is not ideal. Changing the material can be a huge undertaking and it is often easier to change the properties of the particle by modifying the surface of the particle. Surface modifications can affect solubility, stability, surface charge, the electrical double layer around the particles, biodegradability, cytotoxicity, drag, surface activity [17], and cellular flow. Some of these surface modifications have been well studied, making it easy to find protocols and other aids to perform the modification. Surface modifications are made by attaching proteins [44], peptides [33] [44] [45], small molecules, polymers [35] [36] [40] [41] [46], metals [47], surfactants [48]**,** or inorganic materials to the surface of the particle [26]. They are attached by using a variety of covalent bonds, physical connections, or intermolecular forces such as ionic, London dispersion, or dipole-dipole. The type of connection affects the stability of the modifications, and it also affects other properties such as toxicity. The most common surface modification is the addition of polyethylene glycol (PEG).

Polyethylene glycol can increase biocompatibility [40] [49], limit nonspecific binding [49], increase the lifespan of particles in blood [40] [47] [49], and slow the uptake by the reticuloendothelial system (RES). [35] [36] [40] [41] The amount of improvement for each of these changes will depend on the particle material, shape, and

size. For example, PEGylated gold particles can have about a 10-fold higher concentration in blood after a half hour than unmodified gold particles. [40] In the case of biocompatibility, unmodified liposomes are readily attacked by the body, and it is difficult to get enough particles to their destination. PEGylated liposomes are more biocompatible and more will arrive to the destination before being targeted by the body. [41] The improvements in biocompatibility do not eliminated all toxicity. In the case of 13 nm gold nanoparticles in mice, the particles were still toxic after PEGylation. [49]

Polyethylene glycol is not the only surface polymer modification for particles. There is a more detailed list of polymer modifications provided by Grupta et al. [47] Surface modifications are not only for biological purposes but can also be used to lower surface activity, which has been shown by the difference in catalytic activity between platinum nanoparticles and platinum nanoparticles coated with either polyvinylpyrrolidone (PVP) or with tetradecyl trimethyl ammonium bromide (TTAB). [17]

1.1.1.4.1 Uptake

Surface modifications also affect the rate and quantity of particle uptake by cells. The charge of the particle, which can easily be changed by surface modifications, is the biggest determinations of cellular uptake. Positively charged particles gain entry into cells more readily than their negatively charged or charge neutral counterparts. [50] Manipulating the charge can be accomplished through the adsorption or covalent linking of small molecules, polymers, proteins, peptides, and surfactants. For a positive charge, proteins, peptides, etc., are loaded with amine functional groups and then for negatively charged particles usually they are loaded with carboxyl functional groups. Arginine and lysine based peptides are used in nature to increase the positive charge in

order to increase the amount of cellular uptake and the rate of cellular uptake. A commonly used peptide in the laboratory is TAT peptide [33], an arginine rich peptide found on the surface of HIV that increases the internalization of the virus. When modifying PAA with TAT peptide, particles have shown to need 4 times shorter incubation times. [33] Other arginine rich peptides, beside TAT peptide, also function well at increasing uptake and rate of uptake. [45] In fact, quantum dots with a 9 residue biotinylated L-arginine peptide showed an increase in uptake by about 2 orders of magnitude.

Other surface modifications that have been used to improve cellular uptake include (but are not limited to) polyethylenimine (PEI) [23], polylysine, antennapedia [51], transportan sequences [52], and citric acid. [53] These surface modifications do not necessarily need to be covalently linked to the surface in order to function. For example, short chain PEI can form complexes with mesoporous silica nanoparticles to increase uptake. It is important to remember that surface modifications used to increase uptake will affect the toxicity of the particle, as is the case of particles functionalized with PEI. [37] [54] [55]

1.1.1.4.2 Targeting

Cellular targeting is an important function of particles that is possible because of surface modifications. Targeting has been used for a variety of biomedical applications including cell separation, real-time tracking of biomolecules [56], cancer targeting [57], imaging, sensing, tumor delineation [58] [59], and drug delivery [39]. Targeting can increase the population of particles binding to targeted cells, increase the uptake of particles, decrease the minimal effective concentration of particles, and lower the

effective cytotoxicity of particles. There are two different types of targeting: passive targeting and dynamic targeting.

Passive targeting takes advantage of leaky vasculatures often encountered in tumors. The primary method that will be discussed will be the enhanced permeability and retention (EPR) effect. [41] [60] The EPR effect is caused by tumor having extensive angiogenesis, leaky vasculature, and sometimes poor lymphatic drainage. [34] [59] [60] [61] [62] [63] Because of these attributes of tumors, small particles and molecules such as drugs, dyes, and imaging agents, accumulate in tumors faster than in most other organs. [60] Researchers have been taking advantage of the leaky vasculature of tumor cells for decades. [62]

The next method of targeting is active targeting, using targeting moieties to increase the concentration of particles attached to specific cells. [58] [64] [65] Targeting moieties can be surface-conjugated proteins, aptamers, small molecules, large molecules, or single strand DNA. In order to target cancer cells selectively, targeting moieties need to take advantage of the over-expression of proteins, or any other unique attribute of the cell.

Antibodies are a common tool of targeting, but are expensive to produce. The antibody anti-EGFR (anti-epidermal growth factor) is an example of an antibody that can be used to target epithelial cervical cancers. The cervical cancer over-expresses the epidermal growth factor, therefore increasing the binding affinity of particles with anti-EGFR targeting. Anti-EGFR gold nanoparticles have been used to increase the amount of particles binding to SiHa, HOC, and HSC cancerous cells. [14] [15] [66] Many tumors

also over-express vascular endothelial growth factor (VEGF) or its equivalent vascular permeability factor (VPF), which also can be used for targeting. [60]

Another targeting moiety can be a peptide. The F3 peptide is a prime example of a peptide used to increase the concentration of particles in tumors. The F3 peptide has been used to target angiogenic vasculature in solid tumors as well as certain tumor cells. [33] [34] It interacts with a cell surface receptor called nucleolin. A common cell line MDA-MB-435, a human melanoma, is a good cell line for the F3 peptide because it expresses high quantities of nucleolin. [33] [34] Not only can particles be targeted to specific cells they can be targeted to regions in specific cells. Research has shown that 30 nm PEGylated gold particles with RGD and NLS peptide (KKKRK) target the nuclei of HSC cells, a human oral squamous cell carcinoma, and does not target normal cells. [67]

The last group to be mentioned is aptamers. Aptamers have a great potential as being a faster and easier method of targeting tumors, but they have had limited usage because of patents. There are many methods of targeting particles to various types of antigens, and often it is necessary to experiment with various targeting moieties to find the ideal targeting moiety.

It is important to remember when targeting cells that the particle size affects both the binding and the uptake into the cell. [68] Larger targeted particles have smaller k_d values, or higher binding affinity, than small particles. Not only does it affect the binding affinity, but the increase in binding affinity affects the particle uptake. Initially, as targeted particles increase in size, uptake also increases along with binding. At even larger particle sizes, internalization is hindered. These two competing effects result in

there being a specific size that is optimal for internalization. Herceptin-GNP is a good example of how size of particles affects uptake.

1.1.1.4.3 Cytotoxicity

Surface modifications can be used to change the cytotoxicity particles. In many cases, the particles can be adjusted to acceptable toxicity ranges so that collateral damage to healthy tissues is minimalized. This would be the case for drug delivery particles that are delivering a very toxic drug. The most common modification to lower the cytotoxicity of particles, as previously mentioned, is attaching PEG. Another surface modification used is polyvinyl alcohol, which has been used with platinum nanoparticles. [69] Even though a modification has functioned well in one case, it does not mean it will function for all cases. This has been observed with iron oxide particles coated in polyvinyl alcohol, which can cause apoptosis. [46] Some surface modifications can be altered to become less cytotoxic. For example, PEI toxicity, believed to arise from the "proton sponge" effect, increases as the polymer increases in length. So with PEI it is ideal to use shorter polymer chains, under 10 kD. [23] [37]

Surface modifications affect an array of characteristics such as toxicity, targeting, uptake, rate of particle uptake, rate of consumption, surface activity and blood lifetime. Adjusting the amount and the type of surface modifications can easily shift particle characteristics within their ideal range.

1.1.1.5 Chemical Agents

There are many different chemical agents, such as thermal dyes, contrast agents, sensing agents, photosensitizers, DNA, or drugs that do not function well by themselves in a given environment. The chemical agents' environment can result in low

solubility, aggregation, chemical debilitation, chemical reactions, short lifetimes, and chemical build up at locations other than the target. Loading chemical agents into the particle, or in some cases attaching them onto the surface of the particle, can prevent many of the issues that arise from the interaction of the chemical agents with the environment. Generally this is done by loading the chemical agents into chemically and biologically inert particles. Loading efficiency, or binding efficiency, depends on various different characteristics of the particle matrix and agent. The major characteristics are the hydrophobicity, size, charge, and functionality. [70] Another characteristic unique to the particle that affects loading is the pore size. Currently there is a wide range of recipes for many of the matrix materials. The different recipes can alter some the characteristics of the particle allowing for some adjustments to increase loading or surface attachment. Surface attachment usually happens after the particles are formed, but loading chemical agents into the particles can be either through congruent-loading (during synthesis of particles) and post-loading (after synthesis of particles). The three main methods of keeping the chemical agent with the particle are physical encapsulation, intermolecular forces, and covalent linkage.

Physical encapsulation is when the structure of the particle prevents the chemical agent from leaving the particle, as with air in a balloon. It is one of the primary methodologies of adding chemical agents to particles. With physical encapsulation, the chemical agent is either encapsulated during the particle formation (congruent-loading) or loaded into the particle after the particle has been formed (post-loading). Post-loading is a simple technique of adding the agent to a particle solution, allowing the agents to penetrate into the particle. The addition of chemical agents is highly

dependent on the structure of the particle, i.e. porosity and rigidity. The particles are than washed to remove any chemical agents that may come out later. Loading efficiency depends heavily on the system and sometimes post-loading will have better results than congruent-loading.

Intermolecular forces, such as charge-charge, London dispersion, hydrogen bonding, and dipole-dipole interactions, are another method for binding chemical agents to particles. This is very similar to a sponge that holds water, since one of the reasons that the water stays inside the sponge is because of the interactions the water has with the sponge. There is often a combination of intermolecular forces and physical encapsulation used. The intermolecular forces may just slow the leaching of the chemical agent into the environment a little, and so it may be necessary to increase the physical encapsulation to slow the leaching even more. As with physical encapsulation, chemical agents can be added congruently or after synthesis of the particles.

Often the intermolecular forces are simplified even further, and researchers just look at the hydrophobicity of the dye and particle. When choosing a particle matrix, one wants the particle to have similar hydrophobicity. If the chemical agent is hydrophobic, then the particle should also be hydrophobic on the inside so that the chemical agent stays in the particle. [70] If the hydrophobicity is the opposite the chemical agents will often prefer not to be in the particle and will leach out of the particle. When sensing analytes, the hydrophobicity of the matrix material should match that of the analyte. For example, PAA particles work well for ion sensors [71] [72] [73] [74] [75] due to their neutral and hydrophilic nature, which allow ions into their matrix; while hydrophobic matrices, like organically modified silicate, are better suited for oxygen sensors. [76] [77]

Bioaffinity interactions, which also fall under intermolecular forces, can be used to attach various agents to the particle surface or to the inside of the matrix. One of the most common bioaffinity interactions is the streptavidin biotin interaction. This has been used for decades to attach various molecules, often antibodies, to the surface of particles. As with all of the intermolecular forces, the loading efficiency depends heavily on the characteristics of the matrix material and how they match up with the chemical agent.

Covalent linking is the last, and best, method of increasing loading efficiency. Unlike the other two, which generally leach the chemical agents, covalently bound chemical agents can be designed to never leach. This method is ideal for systems where the chemical agent can be permanently or semi-permanently attached to the matrix without affecting the function of the particle. The chemical agent can either be covalently linked to the surface of the particle after particle synthesis, or connected internally before or after particle synthesis. Sometimes it is advantageous to redesign the chemical agent to be a monomer unit, so it can be copolymerized with a polymer matrix. This can lead to high loading percentages. Generally the covalent bond between chemical agent and particle are done using reactions that combine any combination of amine, carboxyl, or thiol functional groups. There are various coupling reagents on the market, such as NHS and sulfo-NHS, to assist in covalently binding chemical agents with the particle. Protocols are well understood and often can be found on the websites of the companies that manufacture the coupling reagents.

1.1.2 Particle Attributes

The deeper scientists delve into particles, the more excited they become about their many attributes. Many of these attributes have been discussed previously, but will be discussed in further depth in this section. These attributes are the reason why nanoparticles are being used for therapies such as drug delivery, photothermal therapy, and also for sensors. Of the many attributes of particles, there are five major attributes that will be discussed: protection, biodegradability, bioelimination, solubility, and effects on cells.

1.1.2.1 Protection

Protection is a two part functionality of particles. The particle matrix can shield the load from interacting with the environment [78] [79], or shield the cells from interacting with the load of the particle [7] [23] [33]. This is most often seen with polymers that have chemicals incorporated in to their matrix. The polymer prevents or hinders most cellular materials from entering the matrix, or the payload from exiting the polymer. Since the payload interaction with the cells is limited, the toxicity of the payload can be minimized and can also prevent chemical reactions between the payload and the body. This brings in the possibility of introducing toxic chemicals into the body and limiting their side effects. A couple of ideal candidates for decreasing toxicity are drugs, such as chemotherapies, and toxic imaging agents. [80] One example of this is Camptothecin, which has a drop in toxicity when it is encapsulated in a PEGylated β-cyclodextrin nanoparticle. [80] Going the other direction, particles have shown the ability to shield the payload from enzymes, serum, and leukocytes. For example methylene blue, a photosynthesizer for photodynamic therapy and contrast

agent, is not stable in the body because proteins, NADH, and diaphorase, react with it to turn it into leukomethylene blue, a white inactive form that cannot produce Reactive Oxygen Species (ROS). [7] [38] [71] [73] [79] This shielding or protection is not limited to chemical interactions, but also shields chemical agents from degradation caused by electromagnetic radiation. The G2 dye photobleaches within 3 min when exposed to a 1.5mW 630 nm laser, but when it is covalently encapsulated in a particle it takes 39 min to photobleach the dye. [33] The protection can be used to prevent other interactions with dye that would give false positives when sensing. [71] [73] The G2 dye, used for measuring oxygen through fluorescence, has a critical decrease in accuracy in the presence of BSA and NO. [33] In fact, BSA interferes so much that it can cause a 550% increase in fluorescence of free G2 dye. [33] Nitric oxide, though not as extreme, can cause a 32% change in fluorescence to free G2 dye. [33] When the G2 dye is covalently linked to a particle, the interference, in similar environments, only causes a fluorescent change of less than 0.3% and 2% respectively. [33]

1.1.2.2 Biodegradability and Bioelimination

Biodegradability is often described as materials that will degrade in nature, but with particles, it usually refers to a particle's ability to degrade *in vivo*. There have been numerous studies on the bioelimination of particles that biodegrade and particles that do not biodegrade, formed with stable bonds. [32] [40] [81] [60] [82] [83] Particles do not necessarily need to biodegrade to be bioeliminated, but particles that are biodegradable into fragments smaller than 10 nm can be filtered by the renal system. [61] [84] The particles not eliminated by the renal system are eliminated by the Reticuloendothelial System (RES), also known as the Mononuclear Phagocyte System. [32] [60] The RES

removes foreign material by opsonization followed by phagocytosis by macrophages. [60] Kupffer cells of the RES are liver macrophages that are in direct contact with blood, which are the primary cells that remove larger particles to be excreted out with feces. [81] [82] They remove endogenous material such as old or damaged erythrocytes, immune complexes, viruses, bacteria, toxins, cancer cells, apoptotic cells, and other cellular debris. [81] [82] The Kupffer cells either degrade the particles in the lysosomes, or the particles have to be exocytosed. [82] Non-biodegradable particles that are exocytosed will generally remain within the cells for a considerable time, in some cases 6 months, before being exocytosed. [82] [83] The particles are exocytosed to the surrounding hepatocytes and then later release with the bile so that they can be eliminated out of the body through the feces. [81] [83]

The fact that the particles can be bioeliminated is not the important part of bioelimination. The rate of bioelimination, or when bioelimination begins, is also important in particle design. If particles have too short of a blood life, bioelimination begins too quickly, the particles may not be therapeutically affective, as has been seen with some drug-carrying particles. [41] There are a few characteristics that affect the rate of bioelimination. RES uptake depends on particle size, surface charge and surface hydrophobicity. [60] The chance of being captured by RES dramatically increases as particles become bigger than 100 nm. [32] [60] [84] Surface modifications also affect the biodegradability of the particle. For smaller particles, renal elimination can be prevented by altering the surface charge of the particle to be more neutral or anionic. [60] When trying to avoid RES, the smaller the charge also lowers phagocytosis by macrophages.

Biodegradation is mainly controlled by the matrix material. One can choose from a variety of matrix materials. Some of the most common include albumin, chitosan, heparin, polylactic acid (PLA), polyglycolic acid (PGA) and polylactic-co-glycolic acid (PLGA), with PLGA being the most popular because its by-products are nontoxic and can be further metabolized. [41] [60] PLGA has been used for years in drug delivery research. Some particle matrices can be chemically altered from being extremely stable to being biodegradable. For example polyacrylamide, which has non-biodegradable bonds between monomer units, can be made with biodegradable or non-biodegradable cross-linkers. The biodegradable cross-linkers will not provide a pathway for the particles to break down to monomer units, but will allow the matrix to break down to a size that can be filtered by the kidneys or ease elimination by the RES. Biodegradable linkages can also be used in linking drug molecules to particles. The linkages allow the particle to release the drug at the ideal time after it arrives into the tumor. [32] PH-sensitive linkers, such as hydrozone and cis-aconityl, are prime examples of using biodegradable linkages to control the release of drugs. [85] [86]

1.1.2.3 Solubility

Solubility issues plague the pharmaceutical world with ideal designer drugs, dyes, or imaging agents being insoluble or inadequately soluble to be therapeutically effective. Many of these are hydrophobic agents that not only are not very soluble, but incorporate themselves into the lipid bilayer or fat. As mentioned, particle systems can be designed to carry both hydrophilic and hydrophobic loads to a source by changing the particle matrix. [23] To increase the load delivered to cells, hydrophobic particles need to be modified to have hydrophilic surfaces. Particles are ideal for many drugs,

dyes, proteins, and other molecules that have solubilities lower than the desired or required concentrations. Camptothecin, a potential drug for cancer, could not be used effectively because of its hydrophobicity. [80] Using particles, the solubility of Camptothecin can be increased 1000 fold.

1.1.2.4 Particles and Cells

Much of this dissertation discusses the interaction of particles with various types of cells. The two main subjects that will be discussed are; how particle size, shape, and surface chemistry affect cellular-particle interactions, and also methods of getting particles into cells.

1.1.2.4.1 Various Particle Attributes and Cellular Response

Many of the factors that affect the uptake of particles have been mentioned previously. There are various things that affect cellular uptake and cellular response: size of the particle [16] [53] [68] [87], shape of particle [16] [53] [87], surface chemistry [8] [16] [23] [88], temperature of the surrounding medium [53], and the cell type [26] [46]. This section will mostly review the attributes of particles and how particles affect cells, with only minor facts about how temperature and cell type affect uptake and cellular response.

Size has been shown to affect rate of internalization, pathway of cellular uptake [16] [53] [68] [87] [89], localization of particles, and toxicity. [53] Particle size and how it affects rate is intuitive: generally, the larger the particles the slower they are taken into the cell. [53] Particles are not only affected by size, but also by surface functionalization, leading to a dynamic relationship between the two attributes. Uptake often increases with size, due to improved binding with the surface of the cells. [68]

Albumin-coated drug delivery nanoparticles that went through clathrin-mediated endocytosis, which will be discussed later, have 5-10 times greater uptake when they range in size from 20 to 40 nm in size than their 10 nm counterpart. [90] Particle uptake peaks once the effect from the particle size overcomes the improved uptake from increased binding. The most efficient size for endocytosis ranges from 25-50 nm for gold nanoparticles. [53]

As mentioned, there are size limitations to particle uptake because large particles cannot be endocytosed by the cells. HeLa cells are known to invaginate PRINT particles with a dimension up to 3 μm. [16] PRINT particles are derived from trimethyloylpropane ethoxylate triacrylate, polyethylene glycol monomethylether monomethacrylate, 2-aminoethylmethacrylate hydrochloride, and 2,2-diethoxyacetophe none. Particle size also affects localization of particles within the cells and the body. . Some extremely small particles can pass through the blood-brain barrier. As mentioned previously, size can also affect uptake by the RES or filtration by the renal system. This is seen with dendrimers that are less than 7 nm, which not only allows them to escape the vasculature to target tumors, but also allows them be filtered by the renal system for removal from the body. [39]

Toxicity also depends on the size of the particles. This has been observed with silver nanoparticles and microbes. The microbial response to silver nanoparticles is stronger with smaller particles. [22] Another example is with naked gold spheres, or spheres without chemicals attached to the surface. Naked gold spheres are often considered nontoxic, but particles 8 to 37 nm do show toxicity. [91]

It is important to remember that an increase in particle size can have both positive and negative effects to uptake, bioelimination, toxicity, and terminus. Tuning particles to the ideal size can be difficult with all of these variables dependent on size.

The shape of the particle is also known to affect cellular uptake and cellular response. [53] As mentioned before, some of the more recognized shapes used in particle applications include spheres, rods, tubes, cubes, and ellipsoids, sometimes referred to as rice. Rates and quantity of cellular uptake do depend on the shape of the particle, but there is no underlining rule known for all types of particles and cell types. In the case of PRINT particles, particles of equal volume were taken up faster when they had higher aspect ratios. [16] The opposite is true for gold nanorods where a higher aspect ratio means slower and lower uptake. [53] In fact, the particle uptake increases as the particle becomes more spherical.

There are many different materials in particles with a core of gold, silver, carbon [92], polymers, or iron oxides but it is the surface chemistry and structure of the particle that has the most affect on cytotoxicity, amount of uptake, rate of uptake, and where the particles accumulate. [8] [16] [23] [53] [88] With this in mind, the cellular response can be altered by coating, or modifying the surface of the particles with different polymers, metals, proteins, peptides, DNA, aptamers, and small molecules.

As previously mentioned, the surface charge is one the simplest methods of affecting cellular uptake. The rule of thumb is that as you increase the negative charge, the slower the uptake, while an increase of positive charge increases the uptake into the cells. [8] [16] [23] PRINT particles with various charges are a great example of how charge affects cellular uptake. [16] Another good example is capped gold nanorods.

Positively capped polyallylamine nanorods showed an uptake of about 2320 particles per cell, while negatively charged PAA capped nanorods showed an uptake of about 270 nanoparticles per cell. [9] Surfaces of particle are not always stable, which can result in abnormal cellular uptake with what would appear to be positively charged particles. In the case of positively charged CTAB (Cetyl trimethylammonium bromide)-capped gold nanorods, they are introduced to cells with CTAB, but the CTAB is quickly replaced by extracellular proteins such as BSA. [9] Even if the particles remain positive, it does not mean that the particles will have better plasma compatibility. [88] Sometimes there are trade-offs when manipulating the surface of the particle.

The cytotoxic cellular response to particles can often be minimalized by altering surface chemistry. Many quantum dots are known to be cytotoxic, and therefore, they are coated with molecules such as thioglycerol, cystenamine, and MUA to try to limit cytotoxicity. [27]

Chemicals adsorbed or absorbed by the particles can also be cytotoxic. These chemicals often include drugs, dyes, proteins, peptides, impurities, and remnant starting materials, such as surfactants or monomers. Remnant starting materials is the main reason most particle synthesis require multiple washings. Impurities, such as endotoxins and starting materials, often result in an induced inflammatory response if not removed. [88] So it is vital in many cases to work in clean environments and be diligent in washing the particles.

Many have misconceptions about the final particle having similar cytotoxic effects as the starting materials. Polyacrylamide is a good example of a particle system in which the monomer unit is toxic, but the polymer is not toxic. This will be discussed in

much greater detail later in the chapter. It is important to be mindful of the different materials used in the particle system. Each chemical can drastically change the cellular response to the particle.

1.1.2.4.2 Particle Delivery into Mammalian Cells

After choosing the particle matrix, it is necessary to determine how the particle will be delivered to the cell. There are multiple different methods of intracellular delivery of nanoparticles. The different methods can be divided into two different groups: physical force and unaided-internalization.

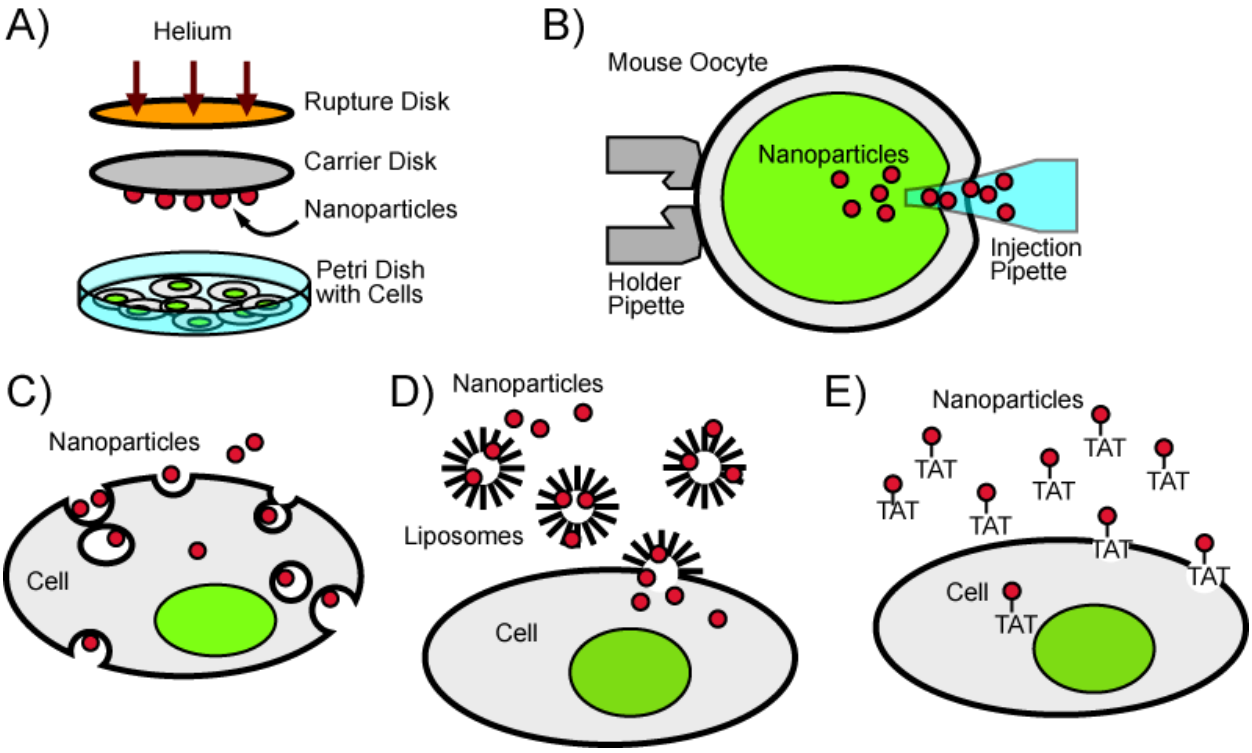

Figure 1.1: These are some various methods of delivering nanoparticles into mammalian cells or cells for bioanalysis or therapy. They are separated into two major categories of physical insertion (Figure A and B), and unaided-internalization, or chemically assisted delivery (Figures C-E). Figure (A) is Gene gun, (B) Picoinjection, (C) Endocytosis (nonspecific or receptor mediated), (D) Liposomal delivery, and (E) Surface modified particles, with the membrane-penetration peptide TAT being the example. [93]

1.1.2.4.3 Forced intracellular delivery

Forced intracellular delivery is when mechanical means are used to force the particles into the cell. The two most common methods that are used are gene gun and picoinjection. [38] [71] [76] [94] Gene gun uses pressurized helium to propel the particles that are attached to a carrier disk into the cells, as can be seen by Figure 1.1. Even though many would assume that gene gun is extremely invasive, cell viability is still about 99%. [95] Picoinjection is another method of physically inserting particles into cells, and is accomplished with a very small needle. It is ideal to have all the particles inserted into the cell, but this method does have its limitations and problems. First, this technique is very invasive to the cell, damaging cell membrane and damaging internal cellular structure. The other issue with this technique is the limitation on the number of cells that can be injected, since cells are injected one at a time. Neither of these two methods functions well for *in vivo*.

1.1.2.4.4 Unaided-internalization or Chemically Assisted Internalization

The next method of internalizing particles is unaided-internalization, or chemically assisted internalization. This method has the potential to function well *in vivo* and *in vitro*, but depends heavily on the type of particle system. Internalization, or in other words, endocytosis, of the particles can be extremely quick and take only minutes, while other are extremely slow and can take days to be endocytosed. If the particle uptake is not ideal, surface-conjugated translocation proteins or peptides [58] [96] [97], such as the membrane penetrating TAT peptide [56] [98], are prime method of changing uptake. Incorporating the particle into liposomes is another method to assist in delivering the particles into the cells. [95] The three methods of unaided-internalization and chemically

assisted internalization, can be seen in Figure 1.1. Each of these methods of internalization results in negligible physical perturbation. Even though the particles don't cause physical damage to the cell, the particle can still be extremely toxic.

For unaided-internalization, particles are internalized through the various endocytotic pathways. The two main endocytotic pathways are phagocytosis and pinocytosis. The pinocytotic pathways include macropinocytosis, caveolae-mediated endocytosis, clathrin-mediated endocytosis, and caveolae/clathrin independent endocytosis. [88] There are multiple variables that affect the pathway of internalization. The pathway can be affected by the energy, cellular environment, cell type, particle shape, particle size, and surface functionality of the particle. Particles don't necessarily have to go through just one type of pathway. Particles a 150-200 nm that were formed by Particle Replication In Non-wetting Templates (PRINT) went through multiple pathways when entering cells. [16] Carboxyl modified polystyrene nanoparticles of 24 nm diameter were endocytosed by clathrin, caveolin, and cholesterol independent pathways. [53] There are multiple methods to determine the mannerism of uptake, and reviews explaining how to determine and monitor cellular uptake. [99] .

1.1.2.4.5 Cellular Response

There are many different ways that cells can respond to particles that may or may not lead to cell death. Particles can cause an adjuvant response, inflammatory response, antigenicity, and production of nitric oxide, just to name a few. Adjuvant response is an augmented immune response towards antigens. One example is lipid-coated polysaccharide nanoparticles, which induce 4 x production of immunoglobulin G when immunized with alum adjuvant. [88] Cells can also have an inflammatory

response and produce cytokines. This has been observed with PLGA based nanoparticles, oligonucleotides in T cells, and with unpurified carbon nanotubes. [88] The third type mentioned is antigenicity, or an antibody response. Most particles studied do not invoke this response, but one of the few that does is fullerene. [88] Also cells can produce NO, as in aortic endothelial cells during uptake of polysiloxane particles. [100] *In vivo* not only has same response as *in* vitro but also larger issues can arise from interactions of the body with particles. There is the possibility that microparticles could cause strokes. [60] Not all cellular responses have a negative impact on the body. Particles can be changed to invoke a positive cellular response. When gold colloidal particles were coated with P1 or P2 peptide, they caused angiogenesis, or formation of blood vessels, which is important in healing wounds. [101]

1.1.3 Particle Applications

Now that particle design, particle attributes, and how they interact with cells has been discussed, it is important to discuss how these particle features can be applied in research and medicine. There are four main applications of particle systems that will be described. The applications are analytical measurements, imaging, therapies, and for catalytic activity.

1.1.3.1 Imaging

Imaging is an important part of understanding how the body works and implementing various therapies. Researchers and medical professionals often use nanoparticles in imaging to label cells, parts of cells, and processes occurring within cells. This has been done mostly with dye molecules, but of late many researchers have discovered the advantages of using nanoparticles in imaging. A couple of the

most common problems with imaging cells with dye molecules are that the dye molecules photobleach with time and are negatively impacted by cell medium. Metallic particles, which do not photobleach, are one type of particle that can be used in cell imaging because of their high scattering ability that can be seen using darkfield microscopy. [14] [15] [19] [66] Dyes incorporated in polymer matrices can also be used in enhancing functionality of fluorescent dyes. As mentioned earlier, the polymer matrix protects the dye from interactions with cells, but it can stabilize the dye, slowing photobleaching rates. [33] Quantum dots, a type of inorganic particle, do not photobleach and also have thin spectra bands. By using quantum dots of different spectral wavelengths and targeted to different cellular components, multiple cellular components can be imaged simultaneously. Medicinally, particle systems function well as contrast agents to distinguish between healthy cells and tumor cells. Currently images of tumors using MRI are being enhanced by magnetic particles, such as iron oxide [102] or gadolinium, to aid in diagnosing patients with cancer. Dye molecules or dyes incorporated in a polymer matrix can help surgeons locate and remove tumors. This is referred as tumor delineation and will be discussed further in chapter 2.

1.1.3.2 Analytical Measurements

Nanoparticles have been used for over a decade in analytical measurements as probes [7] [19] [33] [45] [66] or PEBBLES (photonic explorer for biomedical use with biologically localized embedding). [103] [104] Analytical measurements include quantification and location of cells, proteins, ions, metabolites, and small molecules such as oxygen. [33] Nanoparticles can also be used to measure distances, translocation speeds, translocation rates, cell related forces, and different reaction

dynamics. They can also be used to measure distances below the diffraction limit by using two different colored nanoparticles. [90] There is often overlap between cellular imaging and analytical measurements. Many of the particles used for analytical measurements can be applied in imaging to locate the items being measured. There are a few main requirements that need to be met to do intracellular measurements. The probe needs to be in a cell-permeable form, inert as much as possible, and sensitive enough to do the measurement. Even after fulfilling these requirements, one must remember that the physical presence of the probe might perturb cellular processes, decreasing accuracy of the measurement. Also the intracellular measurements can be skewed by sequestration to specific organelles inside a cell, like the lysosomes. As with imaging, one can use fluorescent particles, quantum dots [45], dye filled particles [33], and gold particles [19] [66]. Magnetic microparticles also can be useful in detecting proteins, DNA, detecting bacteria, and measuring bacterial growth, either by magnetic separation techniques or magnetic rotation.

1.1.3.3 Therapy

Particles, mostly simple particles like gold, have been used for several decades as therapeutic agents. By 1972, liposomes were used to help inject proteins in to rats and radioactive particles to follow liposome concentrations throughout the body. [78] There are multiple therapies in use today: drug delivery, gene therapy, photothermal therapy (PTT), and photodynamic therapy (PDT). In this section drug delivery and gene therapy will be discussed. Both PTT and PDT will be discussed in greater detail in later sections.

Many drugs have very adverse side effects and some of most promising drugs are extremely toxic. In order to limit side effects, scientists have been contemplating how to deliver drugs to specific sites in the body and limit the concentration of drugs that are in the other parts of the body. Another issue in delivering drugs is keeping drug concentrations in the therapeutic range. It is difficult to keep drugs in the therapeutic range because the concentration of drugs in the body shoots up and then drops after each dose. The rate of increase and decrease is not the same for each person either. Another issue of keeping particles in the therapeutic range is when the therapeutic range overlaps with toxic range of the drug. This is often the case with current cancer drugs and many promising cancer drugs that have not been used as of yet because of their high toxicity. Last of all drugs are not always hydrophilic and have very low solubilities in water, which can make it impossible to get drug concentrations to even reach the therapeutic range. Particles have shown to resolve or lower the severity of these issues.

The concept of particles transporting drugs to cells is not a new idea. Particles have been used since at least 1975 try to increase uptake of drugs. [6] Liposomes, 1-10 μm in size, were loaded with radioactive ion $^{22}Na+$ and $^{85}Rb^{+}$ for cancer therapies. [6] Other large particles, micron and larger, have been used for controlled release of drugs. Controlling the release of the drugs helps keep the drug concentrations within the therapeutic range, as well as keeping the drug concentrations from spiking into, or too much into the toxic range. By varying the synthesis and chemistry of PLGA, researchers have determined how to change the rate of release of different drugs. [60] Microparticles do have a few advantages for drug release. First, they have a larger

loading capacity than that of smaller particles. [60] They will also remain in the tissue of the injection site, increasing the concentration of drugs at the target location. [60] This is another method of passive targeting, besides using passive or dynamic targeting, to increase the drug's effectiveness. As mentioned earlier, nanoparticles on the other hand have higher penetration depth, higher uptake into cells, can enter the tumor through EPR effect, can exit the vasculature to enter cells, and are more readily bioeliminated. [39] With the decrease in size, however, other issues arise. Certain tumor cells are known to able to pump out small drug molecules or probes.

The hydrophilicity of the particle matrix is vital for drug loading, and the hydrophilicity of the particle surface is important in determining the solubility of the particle in the body. Hydrophobic drugs, previously unsuitable for drug therapy, can now be incorporated in hydrophobic particles with hydrophilic surfaces to make them suitable for drug therapy, such as the aforementioned Camptothecin, which had a 1000 fold increase in solubility. [43] [80]

Small molecule drugs are not the only therapeutic agent that can be delivered. Nanoparticles can also be used in gene therapy to deliver DNA to cells. [20] The release of DNA from gold nanorods was controlled by using light to melt the nanorods. This is another method besides biodegradation and pH-sensitive to control the release of drugs or genes. [32] [85] [86]

Particles have shown great potential in future drug applications. With targeting, improving cellular uptake, controlling drug release, and improving solubility, particles can be used to decrease toxicity of drugs and improve their effectiveness.

1.1.3.4 Catalytic Activity

Often forgotten by the biological community is the catalytic activity of different types of particles, usually metallic particles. For example, palladium is effective as a catalyst for hydrogenation of nitrobenzene. [17] Though this work will not discuss this further, it is important to remember the different functionalities of particles, in case they do affect future results.

1.1.3.5 Combination

Each of the aforementioned applications can also be used in conjunction with another application. Imaging and analytical measurements in combination are very common. Also nanoparticles loaded with contrast imaging agents and therapeutic agents, instead of sensing elements, can be used. [59] [104] [105] For example, research groups have used dye loaded polymer particles, iron oxide particles, and multifunctional quantum dot *in vivo* for cancer imaging and therapy. [58] [59] [106] Later chapters will discuss combination applications in more detail.

1.2 Photothermal Therapy

1.2.1 Introduction

Mammalian cells have ideal operating temperatures, and once the cell undergoes hyperthermia and is heated out of this range, cells begin to die. This is the concept behind thermal therapy, the precursor to photothermal therapy. Though simple, as are many ideas in science, taking advantage of this attribute could lead to the cure or to effective treatments for many ailments. Thermal therapy has had its downfalls, and with the advent of new methods, such as photothermal therapy, there is renewed interest in using thermal therapy as an effective tool in combating cancer. In this

section we will discuss the history of hyperthermia, what is hyperthermia, the cellular response to hyperthermia, photothermal therapy as a method of inducing hyperthermia, and how the body responses to photothermal therapy.

1.2.2 Hyperthermia

1.2.2.1 History of Hyperthermia

Some of the first work using heat as a therapy was in 1910, and it used temperatures ranging from 50-55°C to kill the tumor cells. [107] Although the initial studies ranged from 50-55°C, most of the following studies in the early years ranged from 42-43°C. [108] Initially full body heating tests were done with little or no advantage and so most opted for local or regional heating. [109] Many of these tests were done with water baths or semi localized heat sources (heated objects) with some success. Other options for localized heating included external microwave applicators, ultrasound beams, small magnetic induction coils, and radiofrequency plate applicators. [109] [110] [111] With the minimal success of thermal therapy by itself, researchers began exploring it as an adjuvant with other therapies, such as radiation therapy [107] [112], alcohol [112], or just simple resection of the tumor. For example, the radioresistant melanoma, S91, can survive x-ray radiation doses of 1000 r. When the melanoma was pretreated with thermal therapy at 44°C for 30 min, there was complete regression in 20 of the 25 mice. [112] Likewise, the treatment of S180 sarcoma by just heating the cells 15 min increased the efficacy from 25 % to 75% cell death at 1000 r. [112] It was shown that the combination of the two therapies were more effective. Often it was difficult to heat the tumor because of location, shape, or size leading to one of the

reasons why today in medicine it is not a common practice and is often considered still experimental. [113]

1.2.2.2 What is Hyperthermia

Hyperthermia is defined as the heating of tissue above standard conditions, 37.5°C in the case of most mammalian cells. It has been tested thoroughly in the past, and most tests range from 39-45°C. [108] [114] [115] [116] [117] [118] [119] There is mild hyperthermia, ranges from 39-41°C [108] [117] [118] [119], and standard hyperthermia, ranges from 42-45 °C. [108] [114] [115] [116] [117] [120] Changes in cellular activity do arise from mild hyperthermia, but cell death isn't noticed until 42°C and above. [117] Any temperature above 45 - 46°C generally causes necrosis and is often not discussed when discussing hyperthermia.

1.2.2.3 Mode of Cell Death

Before the effects of hyperthermia are discussed, it is important to discuss the two main courses of cell death: apoptosis and necrosis. Apoptosis is an orderly programmed cell death and is the common course for cell death. The main signaling pathways for apoptosis include death receptors, mitochondria, and ER (endoplasmic reticulum). [121] During apoptosis, cells release multiple proteases that trigger intercellular connections to be eliminated, cells to shrink, cytoplasm to condense, cytoskeleton to collapse, nucleus to collapse, and then the cells to bleb. [120] The expression of caspase-8 or caspase-9 proteases initiates this cascade to cell death. [122] After blebbing, the cells are then eliminated by phagocytosis. The activation of cells to express the proteases necessary to cause cell death can be caused by multiple factors, such as viral infections, normal cell death, and DNA mutations. In the case

when cells are in state of hyperthermia, apoptosis occurs from 41-46°C. [122] [123] [124] This pathway is the ideal pathway when killing cancer cells with any of the many different therapies available. The reason this pathway is ideal is because there is no inflammatory response, which could hinder phagocytotic uptake of the dead cells.

Necrosis, the other method of cell death, is caused by cellular trauma. The trauma can be caused by such conditions as anaerobic environments, excessive heat, extreme cold, or a mechanical damage to the cellular structure. Necrotic cells essentially explode, leaking cellular contents such as cytoplasm, enzymes, and cytokines into the interstitial fluid. Cytokines often induce an inflammatory response, which can cause complications in the host. In thermal therapy, necrosis occurs from 46-70°C and is often called thermoablation. [10] [122] [123] [124] As with many rules, exceptions have been observed and researchers have shown that sustained temperatures of 43°C can also cause necrosis. [125] Necrosis is also seen when cells are killed using micro explosions. [10] Fundamentally base protein denaturing or caused by strong acid and bases as well. [122] Often there are regions in which necrosis is surrounded by a mixture of necrotic cells and apoptotic cells, with the very outer layer being apoptotic. [122]

1.2.2.4 Cellular Responses to Hyperthermia

Cellular response to hyperthermia is dependent on several variables. A few of the variables include cell type, vasculature, blood flow, and thermotolerance. Not only do these influence the potency of hyperthermia, but many of the variables are also affected by hyperthermic conditions. The heat that is used to target tumors is often applied, or spills over, to the healthy surrounding tissues. Healthy tissue reacts

differently than cancerous tissue to hyperthermia. In this section, the hyperthermic effects on blood flow, pH, and oxygen concentrations in tumor cells and healthy cells will be compared, and then thermotolerance of cells will be discussed.

In most studies targeting cancer, healthy cells are inadvertently heated as well. When heating healthy cells to 42-45°C for 1 h the blood flow increases 3 to 4 fold, with the flow peaking about 1 h after heating. [114] [115] This has been observed using multiple types of tissue. [115] The increase in blood flow regulates the temperature of tissue, making hyperthermia less effective at killing outer cells of the tumor. [115] Once the blood flow increases, the healthy cells temperature lowers 1.0-1.5°C for muscle and 0.5°C for skin. [115] Blood flow and oxygen concentrations are correlated, resulting in an increase of oxygen uptake, observed skin, lymph nodes, and lung tissue. [117] The pH of the muscle tissue that surrounds a tumor during hyperthermia also increases. [115] All of the mentioned effects are common for healthy tissue during hyperthermia.

The effects on cancer cells and their vasculature are very dependent on the type of tumor and the stage of the tumor. Before describing the effects of hyperthermia on tumor cells, it is important to understand tumor vasculature. The tumor vasculature is similar to that of healthy tissue when it is small, but it changes drastically as it increases in size. First the capillaries of tumors are irregular with a lot bends, twists, distortions, and dilations. Second, as the tumor grows, the capillaries tend to elongate with an increased amount of networking. These two differences from healthy tissue spread the pressure away from the host arteriole more than it would with healthy tissue and vasculature. [114] For this reason tumors do not act the same as healthy tissue with changes in blood pressure, oxygen concentration, oxygen uptake, and changes in pH.

The blood flow to tumors during and after hyperthermia depends on the size of the tumor, temperature, time heated, and tumor type. [114] [115] [118] As previously mentioned, the vasculature pressure decreases drastically as the tumor increases. Commonly, the blood flow increases a little when heated from 41-42°C but drastically decreases when the temperature is greater than 42°C. [114] [115] [118] With smaller tumors, < 0.7 g, blood flow increases even when even heated above 43°C for 1 h. [115] The smaller the tumor, the greater the increases in blood flow with heating. [115] For larger tumors heated above 42°C, the blood flow decreases more rapidly with an increase in the size of the tumor. [115] This is what should be expected because the vasculature and surrounding environment resembles healthy tissue more and more as the tumor decreases in size. As with healthy cells, changes in blood flow are not immediate and they do not return to normal immediately after hyperthermic conditions. It is not uncommon for it to require a few hours proceeding hyperthermia for blood flow to return to normal. Knowing this, it may be better to keep the tumor in hyperthermic conditions for longer periods of times so that the blood flow is even lower to the tumors, and the tumors are under harsh conditions for longer periods**.** [115] Another fact that is often overlooked is that there are many variations in tumors and they are affected differently by hyperthermia. SCK tumors and Walker tumors under similar conditions showed that SCK tumors had a higher blood flow than Walker tumors. [115]

There are two effects that come from the differences in blood flow between tumors and healthy tissue. Tumor cells will have higher temperature than healthy tissue, and it will take longer for tumors to return to normal operating temperatures. This is because blood flow regulates the temperature of cells, and the lower blood flow

of tumors makes it more difficult to regulate their temperature. This weakness of tumors is one reason that thermal therapies are promising.

The behavior of oxygen concentration is similar to that of the blood flow. Oxygen concentration increases with temperatures 37-39.5°Cb but decreases with temperatures above 42°C - 43°C. [108] [117] [118] [126] [127] [128] In the intermediate range, ~41°C, there are no statistical significant changes in O_2 concentration. [129] Oxygen concentrations are dependent on both blood circulation and oxygen consumption rates**.** [130] The oxygen consumption rate reverses from increasing at temperatures of 41-42°C, to decreasing at temperatures above 42°C. [128] As blood flow decreases, oxygen consumption also decreases. [129] The relaxation time in tumors cells can take several days to return normal. [117] [131] When implementing hyperthermia as an adjunct therapy, a decrease in oxygen concentration can hinder the functionality of the other therapy. To increase oxygen uptake into cells, there are different drugs, such as Nicotinamide, that can be used. [118] [132] In the case of radio therapy, Nicotinamide increases the damage caused by radiation therapy. [118] [132] Unfortunately, the induced increase in oxygen uptake does not appear to change the effectiveness of lone hyperthermia. [132]

Not only do the blood and oxygen levels decrease, so do nutrient levels, rate of DNA synthesis, protein synthesis, and the pH level of tumors. [114] [115] [128] [129] [133] [134] Nutrient consumption follows the same pattern as oxygen consumption; it increases at lower temperatures, is neutral around 41°C, and it decreases above 42°C. [128] [129] These effects may differ when there are other factors involved, such as radiotherapy. [135]

Cells are known to be able to adapt to certain changes in their environments. Over 50 years ago, Crile discovered that tumors previously heated to hyperthermic conditions were more resilient, or thermotolerant, to future increases in temperature. [112] [136] [137] Thermotolerance is not unique to cancerous tissue, and is also seen healthy tissue. [112] [115] [116] [137] [138] It develops after short exposures, around 30 min, of lethal temperatures ranging from 43-45°C, but it can also occur during continuous heating of 3 or more hours at nonlethal temperatures ranging from 39.5-41.5°C. [120] These are the common conditions that cause thermotolerance. Some cell lines will deviate from the norm and require more or less heat to become thermotolerant. [133] The period between dosages, usually 0.5 to 12 h, is important in determining how much resistance cells will have to future hyperthermic conditions. [108] [116] [127] [137] Thermotolerance can also occur during constant heating, but it appears to only slow the rate of death a little. [116]

Tumor cells are more heat-sensitive than normal tissue due to the lack of blood flow, which makes it difficult to compensate for changes in temperature like in healthy tissue. [115] Not being able to conform to changes in heat, the amount of oxygen and nutrients to tumor vasculature lower. [114] In tandem with lower interstitial pH, the vasculature collapses with the center of the tumor being the more sensitive to the changes than the periphery. [114] [135] Hyperthermia affects other biological processes, such as nitric oxide synthase production and overall tumoural nitric oxide production, and there are other sources of information that discusses in greater detail the effects of hyperthermia. [108] [118] Even though there are many similarities between tumors, the efficacy of thermal therapy depends on the type of tumor. [112]

Various healthy cells also react differently to hyperthermic conditions and can affect results *in vivo*. [112]

1.2.3 Photothermal Therapy (PTT)

Photothermal therapy is a type of thermal therapy that uses light to heat tissue. The interest in thermal therapy to treat cancer has recently increased because of the hype around the properties of gold nanoparticles. Gold particles have strong absorption cross-sections, high scattering ability, are easily tunable, and have minor toxicity (with some controversy about toxicity). The strong absorption cross-section, along with the ease of tuning the absorption peak, prompted researchers to test gold nanoparticles as possible heat sources when they absorb electromagnetic radiation. Groups have used many varieties of gold nanoparticles; nanorods, spheres, nanocages, and nanoshells. [11] [12] [14] Nanorods are one of the more exciting of the gold particles because of the ease of tuning their wavelength by adjusting their aspect ratio.

Dye molecules, such as Indocyanine Green, have also been used as photosensitizers, or light absorbers, in PTT. [139] Gold particles are considered better because of their high absorbing cross-section. In the case of 40 nm gold sphere, the cross section is 5 orders of magnitude greater than Indocyanine Green molecule. [140] [141] This comparison is often made, but the conclusion that many have drawn from it is not completely accurate. Of course a large particle will have a much larger absorbing cross-section than a single molecule but there will be more dye molecules than particles. This will be discussed in further detail in chapter 2.

Photothermal therapy does not require particles to function. A very strong light source, usually a laser, can often heat up the target enough to accomplish the task, as

in photothermolysis (e.g. laser hair removal). The main issue with this technique is that targeting is only as good as the aim and the absorption of the target. The laser light scatters through the cellular mediums, which results in collateral damage to surrounding tissue. Particles have a dual utility; they increase absorption at the target and can improve targeting. If the dual utilities are used in conjunction, the light intensity and particle concentration can be tuned so that surrounding tissue will never reach the heat threshold that causes cell death, but the target will surpass the threshold.

In order to minimize collateral damage, a couple of strategies should be observed. First, the light source should be focused on to the target to minimize damage to the surrounding tissue. In the case of particles, the light should not be absorbed by the cells, but by the particles that have been targeted to the tumors. The stray light not absorbed by particles will also diffuse over a larger volume before being absorbed. This way, any stray light will not heat up the surrounding cells much and it can penetrate deeper. Some groups say the optical window of tissue is between 650 nm to 900 nm, but it depends on the type of tissue. [142] [143] [144] Other groups say the optical window is closer 700 nm to 1100 nm [30] or 600 to 1300 nm. [145] [146] [147] The ability of the system to kill tumors increases if the particles are tuned to absorb in this range and a light source emits in this range.

When considering a particle, it is important to remember some of the previously mentioned attributes of particles. Particles should be designed to minimize toxicity, increase bioelimination, and maximize absorption at the target site. The matrix material, surface coatings, size, and shape all need to be adjusted to minimize toxicity and improve bioelimination. Particles may need to be actively targeted to be effective and

prevent damage to other surrounding tissue. [125] In the case of tumors, passive targeting through the EPR effect may be sufficient. Surface chemistry is the major variable in EPR uptake.

The particle density from the amount of particles taken in affects the total absorption. With a higher absorption comes a higher temperature, which makes the particles more efficient at killing cells. Changes in size, shape, and an increase in dye loading can also increase absorption. Size and shape changes not only change the absorption cross-section of particles, but they also affect cellular uptake of the particles. Increasing the dye loading usually will increase the absorbing cross-section of the particle. If there is too much dye, the dye molecules can interact, effectively lower their absorption. This is very dependent on the dye molecule, as well as on the matrix material.

There will be differences between *in vivo* and *in* vitro results caused by blood flow, heterogeneity of tissue, variations in optical window, scattering, and deviations in particle concentrations. These differences need to be taken into consideration when adapting the system to *in vivo*.

1.2.3.1 Coomassie Blue Polyacrylamide Nanoparticles for PTT (Discussed in Chapter 2)

Currently gold is the primary method for particle PTT, and chapter 2 will discuss the results of a competing method using Coomassie Blue conjugated in a polyacrylamide nanoparticle. Competing treatment methods are often used for different scenarios such as hypersensitivity, lower costs, lower toxicity, alternative side effects, improved bioelimination, improved functionality, lower long term effects, ease of use,

and some nonsensical reasons such as pretty color and name. Some of these reasons will be discussed in greater detail in chapter 2. A Coomassie Blue derivative was synthesized to copolymerize with polyacrylamide. Nanoparticles were synthesized using reverse micelle, and cross linked with a biodegradable cross-linker, N-(3-Aminopropyl) methacrylamide hydrochloride (APMA). Particles had an average size of 96 nm, with a large size distribution. The particles were incubated with HeLa cells of varying concentrations for approximately 24 h before being excited with a LED array. CB-PAA particles showed promising results and were able to kill almost all of the cells. Cell death was dependent on particle concentration and exposure time, as would be assumed. Methods of improving the technique and particle system will be discussed in greater detail in chapter 2.

1.3 Photodynamic Therapy

1.3.1 Introduction

Photothermal therapy is one possible method to fight diseases, but another alternative is photodynamic therapy (PDT). Advancements in photodynamic therapy have led to new therapies that are currently going through FDA trials or are currently in use. PDT is a three-component system that produces reactive oxygen species when they are all present: photosensitizer (PS), excitation source, and oxygen. [148] The therapy is based on energy transfer from a photosensitizer, which has been excited by a light source, to oxygen. This creates a reactive oxygen species (ROS), singlet oxygen in this case, that is toxic. The unstable ROS species can be used as therapeutic agent to combat cancer or bacterial infections. This section will discuss the production of dyes, singlet oxygen production, and PDT.

1.3.2 Dyes

There are several different dyes that have been used as photosensitizers. One of the initial and most popular dye was Photofrin®, which is FDA approved. [146] Other PS dyes include toluidine blue O, methylene blue, chlorin e6, 5-aminolevulinic acid (ALA), naphthalocyanines, HPPH, phthalocyanines, Levulan®, Radachlorin®, Visudyne®, and Foscan®. [146] [149] [150] [151] [152] Photosensitizers will have varying quantum efficiencies, excitation frequencies, excitation bandwidths, cellular stability, dark toxicity (cytotoxicity of the dye when there is no excitation), and potential to photobleach. Each of the attributes has to be taken into account when determining which photosensitizer will function best. Another dye that has been used is Indocyanine Green (ICG). Indocyanine Green has absorption peak around 810 nm, with quantum yield of 10-20 %. It functions as a photosensitizer for both PDT and PTT by changing between CW lasers and a high energy pulsed laser. [139] [153] It is important to remember that photodynamic PS dyes will also create heat when excited. Not all energy will result in a ROS because of quantum efficiency, and so a lot of the absorbed light will be converted into heat. Cells may not heat enough to kill cells, but the heat produced during illumination can affect results.

1.3.3 Singlet Oxygen Production

There are two types of ROS species generated. Type I produces free radicals, or superoxide ions, from hydrogen or electron transfer. Type II is an inversion of the spin of one of the electrons in π* orbitals making the electrons paired in the highest occupied orbital. This is the case of singlet oxygen, the main ROS that will be discussed. Singlet oxygen production is dependent on three components:

photosensitizer (PS), oxygen, and excitation source. [148] In the presence of PS and excitation source, the PS can absorb photons to excite it from an electronic ground state to a short-lived electronic excited state (S_1 ~ 10^{-6} s). [148] In the excited state, the PS can decay back to the ground state through fluorescence, or it can be converted into an electronically excited triplet state. In the triplet state, (T_1~10^{-2} s), there can be phosphorescence back to ground state, or an energy transfer to triplet oxygen when oxygen is present. The energy transfer converts triplet oxygen to a higher energy singlet state (Figure 1.2).

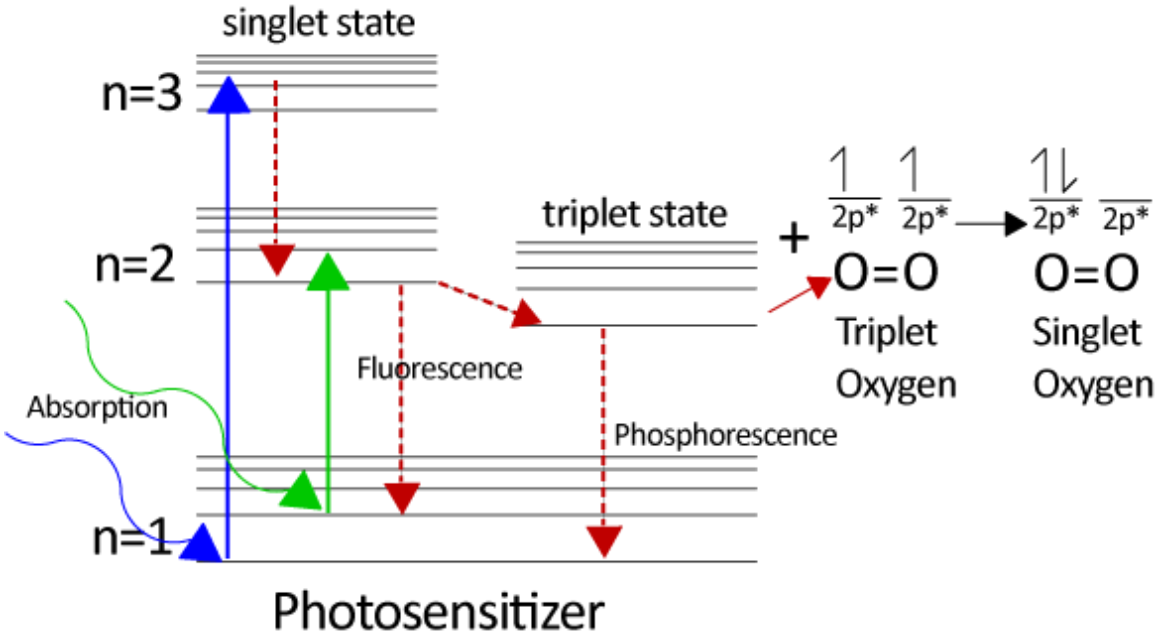

Figure 1.2: This is a Jablonski diagram showing the energy states of the photosensitizer and the energy transfer to oxygen. The photosensitizer is in the singlet state and can absorb a band of frequencies. Fluorescence is the most common pathway, but there can be an intersystem crossing to a triplet state. The energy transition back to the singlet ground state is forbidden and slower than fluorescence, which allows for the energy transfer to triplet oxygen. This converts triplet oxygen to a higher energy and unstable singlet state. In the singlet state, the electrons are paired instead of being unpaired in the π* orbital.

The ability of photosensitizer at converting absorbed light to into singlet oxygen is represented by the quantum yield. For example, methylene blue has a quantum yield of

Φ_Δ ~ 0.5 [34], and Rose Bangel red has a quantum yield of Φ_Δ = 0.75 [154]. The closer the quantum yield is to 1, the more efficient the PS at transferring energy. The higher the quantum yield, the better it is because less PS is required to accomplish the same goal.

Singlet oxygen is highly unstable, very reactive, and at high enough concentrations, it is very toxic. The life span of singlet oxygen is dependent on environmental conditions, and generally ranges from 3.1-4.6 μs in water. [155] In organic solvents, the lifetimes are anywhere from a few microseconds, all the way up to a few milliseconds, but most are in the 10-500 μs range. [155] For cellular systems, the lifetimes are 100 ns in lipids and 250 ns in cytoplasm [146]. Because of the short lifespans, singlet oxygen activity is restricted to 10 nm in organic solvents and it is predicted to be 45 nm in cellular media, but it is not clear how the authors arrived at this number. [146] [156] One of the methods of measuring singlet oxygen production can be done by using anthracene-9,10-dipropionic acid disodium salt, a singlet oxygen sensitive dye.

1.3.4 Photodynamic Therapy

The three components photosensitizer, excitation source, and oxygen, required for singlet oxygen production have already been mentioned, but for photodynamic therapy there are a few more requirements. Requirements include singlet oxygen production in the correct location, system that produces reactive oxygen species (ROS) at correct wavelength, dye that has a high enough quantum yield, a strong enough light source, and ROS concentrations within therapeutic range. Producing the singlet oxygen in the correct location is paramount on functionality. Since singlet oxygen has

such a short lifespan, the dye or particle must be close enough to actually affect the target. In the case of bacteria, researchers use dyes that penetrate into the bacteria because of the difficulty of killing the bacteria from the outside. This is the same with mammalian cells and particles entering the cells. The ideal wavelength for most applications is within the optical window, as described in the PTT section. This allows for higher concentrations of singlet oxygen production at further depths from the surface. The light source also has to be tuned to that wavelength. The dye used within the particle, or as free dye, also needs to have a high quantum yield. When the dye has a low quantum yield it may be difficult to get enough dye, or dye loaded particles, at the correct location to be effective. The light source not only needs to be tuned to the dye, but it also need to emit a high enough intensity to produce enough singlet oxygen at the required depths. Just as with PTT, lasers are the most common method with a few groups working with LED arrays. Taking the previous four requirements into account, the particle or dye system can produce enough singlet oxygen to be therapeutic. Altering them can increase the effectiveness of the system that is being used.

There are currently a lot of different systems in use today. Both dyes and particle systems have been used in photodynamic therapy to fight a various range of cancers and bacterial infections. **Figure 1.3** is a prime example of a particle system that was designed and tested by our group to combat brain tumors. It uses a methylene blue dye incorporated into a polyacrylamide matrix. The PEG is attached to the surface to increase biocompatibility and lifetime in blood. F3 peptide is attached to the surface to target the tumor. ICG is another known system that has been used multiple times to treat cancer. [139] [141] [157]

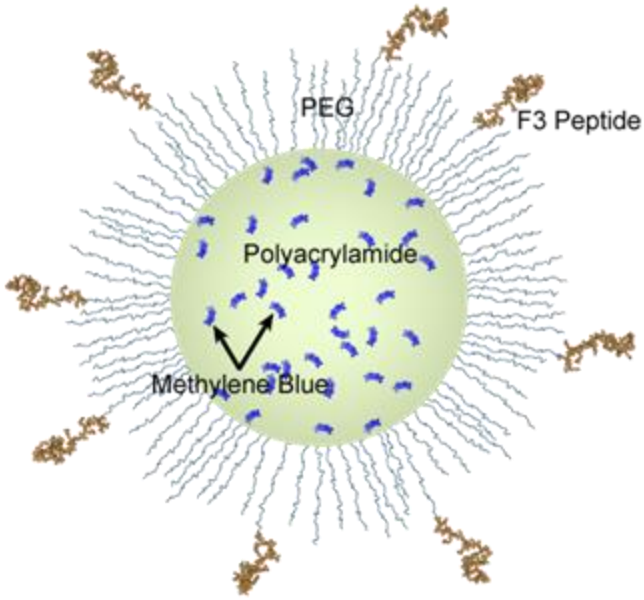

Figure 1.3: Example of a therapeutic nanoparticle used for photodynamic therapy on tumor cells. In this example the methylene blue photosensitizer is loaded into a polyacrylamide matrix. The polymer matrix can be functionalized with many different molecules, such as is represented by the PEG. These surface molecules can change the behavior of the particle, such as PEG is used to increase plasma half-life and reduce nonspecific binding. Other groups can be functionalized to the surface, such as targeting moieties. In the figure above, the F3 peptide is used as a targeting moiety so that the particle targets tumor cells. **[93]**

1.3.5 PDT on Bacteria (Discussed in Chapter 3)

Nonconjugated methylene blue polyacrylamide particles have been used previously in photodynamic therapy. [158] In chapter 3, a conjugated methylene blue polyacrylamide nanoparticle was fabricated to test for improvements in effectiveness in killing bacteria. It was hypothesized that conjugating methylene blue could increase the singlet oxygen around the cells by increasing the concentration of methylene blue. Targeting particles to specific cells could also be used to increase the therapeutic ability of the particles. In both cases results were contrary to the hypothesized results. There were issues with both results that might explain what had happened. They will be discussed more in chapter 3.

1.4 Nonlinear Rotation

Magnetic particles have been used over the past several years for multiple purposes. One of their most common uses is the magnetic separation of analytes, ranging from bacteria cells, peptides, proteins, and DNA, through translational motion. Magnetic particles do not only move side to side but they can also rotate in a magnetic field. The rotation dynamics, when the particle cannot rotate the same speed as the magnetic field due to drag, allows one to measure changes in drag caused by viscosity changes, shape changes, temperature changes, etc. This section will describe the dynamics of particle rotation in a magnetic field, types of particles, and some of the work that has been done in the field.

1.4.1 Rotation of Magnetic Particles

When ferromagnetic, superparamagnetic, or paramagnetic particles are placed in a rotating magnetic field, the particles will rotate. The magnetic dipole, permanent or induced, will always want to align itself with the magnetic field. When the magnetic field is rotating, the particle will also try to rotate. This is best described by the figure below, where $\boldsymbol{\varphi}$ represents the phase lag, $\boldsymbol{\beta}$ represents the magnetic field, and $\mathbf{m}$ represents the dipole moment of the particle (permanent for ferromagnetic, or induced for paramagnetic or superparamagnetic particles).

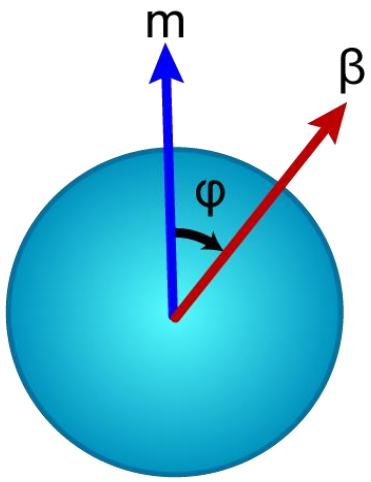

Figure 1.4: This is a simple magnetic particle in a magnetic field. During rotation the magnetic moment (**m**) lags behind the magnetic field (**β**) by the angle (**φ**).

There are two phases for the rotation dynamics of the magnetic particles. The first phase is the linear phase, also called the synchronous regime, where the particle rotates at the same frequency as the rotating magnetic field. It is best represented by the following equation

$$\langle \dot{\theta} \rangle = \Omega, \;\; \Omega < \Omega_c \qquad (1.1)$$

where $\langle \dot{\theta} \rangle$ is the particle's average rotation rate, **Ω** is the driving frequency of the external magnetic field, and $\mathbf{\Omega_c}$ is the critical slipping frequency. In this regime, the phase lag is fixed with only minor fluctuations, depending on the drag caused by the solution's interaction with the particle. If the magnetic field rotation frequency is increased, so does the lag between the magnetic dipole of the particle and the magnetic field. As the particle increases in frequency, the phase lag will increase until the phase lag is over 180° and the particle will prefer to rotate in the opposition direction to align itself with the magnetic field. This point in the change of rotation dynamics, or slip in the

rotation of the particle, is called the critical slipping frequency ($\boldsymbol{\Omega_c}$). Mathematically, for a sphere, it can be represented by the following equation below.

$$\Omega_c = \frac{mB}{\kappa \eta V} \tag{1.2}$$

In the equation **m** is the strength of the magnetic moment of the sphere, **B** is the external magnetic field amplitude, **κ** is the shape factor, **η** is the dynamic viscosity of the surrounding fluid, and **V** is the volume of the particle. This equation only holds true to particles with low Reynolds number (<< 1), or in other terms, the particle moment of inertia is negligible and does not affect particle rotation.

The regime where the particle rotation is slipping is described as the nonlinear phase, or the asynchronous phase. The following equation describes the rotation dynamics of particle.

$$\langle \dot{\theta} \rangle = \Omega - \sqrt{\Omega^2 - \Omega_c^2}, \ \ \Omega > \Omega_c \tag{1.3}$$

The nonlinear rotational dynamics of a magnetic particle, when driven by a rotating magnetic field, depends both on environmental conditions and on properties of the particle. [159] [160] [161] In the nonlinear phase, the magnetic torque on the particle is not great enough to keep the particle in phase with the magnetic field because of the drag. The particle continues to rotate in the state but just at slower frequency than the magnetic field, which can be seen in Figure 1.5. [162] [163] It often appears as a oscillating particle, where the magnetic dipole is slowly making a full rotation. This regime is dependent on the particle volume, drag, and shape factor. Because of this dependence, particles can be used to measure changes in volume, drag, or shape factor.

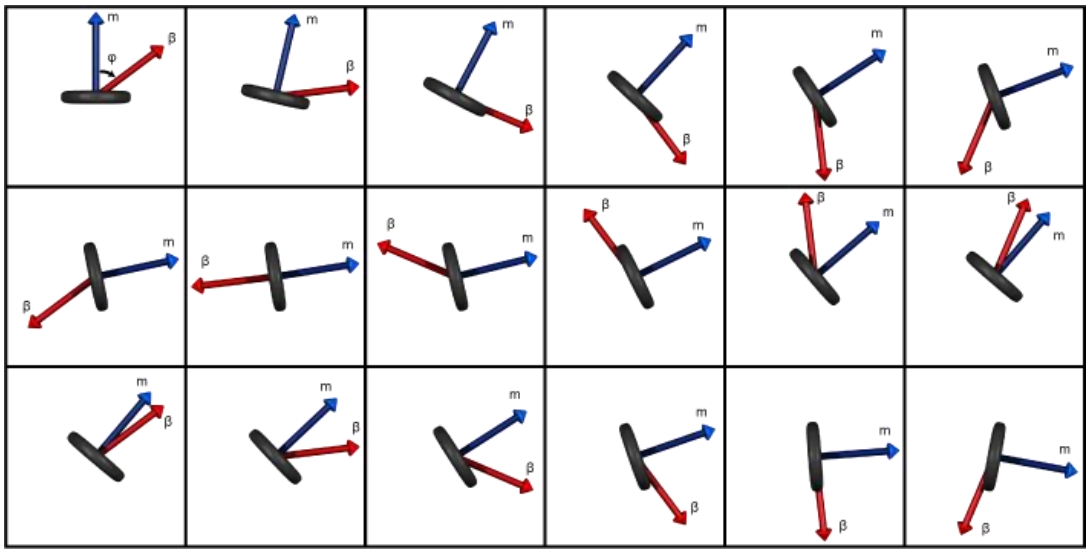

Figure 1.5: The diagram shows the behavior of a magnetic particle rotating asynchronously. The particle's magnetic moment is represented by the red arrow, and the magnetic field is represented by the blue arrow. Initially the rotation starts in phase, but by the 8th image, the particle is rotating in the other direction. In this case, the magnetic field rotates about eight times before the particle completes one full revolution.

There are various types of magnetic particles: particles with a solid magnetic core, particles with multiple smaller magnetic particles within the particle matrix, and particles coated with magnetic material. The most common magnetic material is iron oxide, but nickel and cobalt also work. Each of the particle types has their advantages. For example, nonmagnetic particles can be coated on one side of the particle with vapor deposition creating Janus particles or MagMOONs. MagMOONs can be used to increase the signal-to-noise ratio by locking on to the frequency of rotating particles at a known rotating frequency. [164]

1.4.2 Nonlinear Rotation Results

As previously mentioned, bacteria strains are becoming more antibiotic resistant. A possible solution is to determine the antibiotic that actually works, instead of determining the bacterial phenotype. The best method to do this is by monitoring the

cellular growth and division of the bacteria in an antibiotic solution of varying concentrations. No cellular growth means cell death has occurred or cell division has been inhibited. In the research, we worked on determining the cellular growth of varying bacteria strains using magnetic particle rotation in the asynchronous phase, or nonlinear phase. Included in this chapter are magnetic particles, magnetic particle rotation, and a summary of results.

1.5 Summary of Remaining Chapters

In summary, photothermal therapy tests on cancer cells are described and discussed in Chapter 2, photodynamic therapy tests on bacteria are described and discussed in Chapter 3, detection of bacterial binding using magnetic microparticles is described in Chapter 4, and overall conclusions and suggestions for future work are given in Chapter 5.

Some figures of this thesis have been taken from published works:

Chapter 1- Yong-Eun Koo Lee, Raoul Kopelman, and Ron Smith, “Nanoparticle PEBBLE Sensors in Live Cells and *in Vivo*”, Annual Review of Analytical Chemistry **2009,** 1(2):57-76. Chapter 4 - Brandon H. McNaughton, Rodney R. Agayan, Roy Clarke, Ron G. Smith, and Raoul Kopelman , “Single bacterial cell detection with nonlinear rotational frequency shifts of driven magnetic microspheres”, Applied Physics Letters, **2007**, 91, 224105.

Chapter 2 Photothermal Therapy using CB-PAA Nanoparticles on HeLa Cells

2.1 Abstract

A Coomassie Blue derivative was synthesized with a PAA nanoparticle delivery system to be used for photothermal therapy (PTT) on tumor cells. The Coomassie Blue derivative was synthesized in the lab, and was then copolymerized with acrylamide to form a nanoparticle, with Coomassie Blue accounting for 17% of total mass. Using endocytosis, the Coomassie Blue polyacrylamide (CB-PAA) particles were internalized by HeLa cells, and then exposed to a 590 nm LED light source. Cell death was measured using varying light intensities, exposure times, and concentrations of CB-PAA. When the cells were incubated with 1.2 mg/mL of CB-PAA nanoparticles and exposed to 25.4 ± 1.6 mW/cm^2 for 40 minutes, there was 97% cell death using a Live Dead assay. Cell death took approximately 2.5 h to complete.

2.2 Introduction

There have been many advances in the field of photothermal therapy to treat cancer. Groups have mostly emphasized gold particles, specifically gold nanorods, as the photosensitizer. With very little research done outside of gold nanoparticles, there is a great chance of finding a viable option to gold. It was hypothesized that Coomassie Blue polyacrylamide particle, which has a strong absorption band on the edge of the visible range, could be used to transfer heat to kill the cancer. The particle matrix was

used as a delivery system that can increase targeting ability of the dye to tumor cells, and minimalize the dyes interaction with the body. This chapter will discuss some general information of why new therapies are important to combat cancer, some properties of cancer, other cancer therapies, information about HeLa cells, properties of polyacrylamide (PAA), and toxicity. Then it will discuss the experiment and the results of using Coomassie Blue polyacrylamide (CB-PAA) nanoparticles to kill HeLa cell.

2.2.1 Cancer

In the year 2008 there was an estimated 7.6 million people that die from cancer worldwide. [165] Of these 7.6 million, there were nearly 114,000 brain nervous system tumors in the developing countries alone. Cancer is genetic mutated cells that grow uncontrollably, and can often metastasize to other parts of the body, killing the host. The origins of cancer and its classifications are going to be discussed, not only to be informative, but to better understand how to design therapies to target cancer. Many of the best therapies come from understanding the origins of the disease.

2.2.1.1 Characterization

There are over a hundred different types of cancer, and also multiple different ways of categorizing cancer. [166] Cancer is usually categorized by the location of the tumor. There are different terms to describe the location of the tumor. Examples include leukemia (bone marrow or blood cancer), carcinomas (cancer of tissue that separate the body from the outside, like lung and prostate cancer), adenocarcinoma (cancer in the glands as in breast cancer), lymphoma (cancer of the lymphatic system), sarcoma (cancer of connective tissue), colon cancer, brain cancer, and many more. There are also many subcategories, such as small cell lung cancer (SCLC) and non-

small cell lung cancer (NSCLC), of which SCLC grows faster and metastasizes earlier. [167] Tumors can be found as single cells, strands, files, clusters, or sheets. [168] They are categorized into two main categories: malignant and nonmalignant. Malignant tumors grow uncontrollably (cancer), and nonmalignant, or benign tumors, are confined, as in moles. Most, about 90%, of cancer related deaths are caused after the cancer has metastasized to other parts of the body. [168]

2.2.1.2 Etiology

There are three main causes of tumors: high energy radiation, chemical, and viral. High energy electromagnetic radiation, ionizing radiation, and particle radiation can all cause mutations in cells. Electromagnetic radiation needs to have a frequency of at least 2.4 x 10^{15} Hz (125 nm) in order to be over the 10 eV threshold to ionize molecules. [169] Non-ionizing radiation, such as UV-B (315 nm to 280 nm with energies of 3.94–4.43 eV), is also known to cause cancer, but there is some argument about whether the weaker UV-A can cause cancer. [170] [171] UV-B rays don't ionize the molecules in cells, but are strong enough to cause reactions in the cells, which in turn can cause mutations. The major sources of high energy electromagnetic radiation come from solar radiation, x-rays, and radioactive decay.

Besides electromagnetic radiation, cancer can be caused by high energy particles, α and β particles. Both types of particles are results of radioactive decay. An α-particle is comprised of 2 protons and 2 neutrons. It has a shallow penetration depth that depends on the type of tissue. A thin layer of dead skin on the epidermis is usually enough to block α-particles from damaging healthy tissue. There are two forms of β decay: electron (β-) or a positron (β+). Beta particles have a deeper penetration than α-

particles, and penetrate about 4.6 mm, on average, in soft tissue. [172] Alpha particles do not penetrate as far, but they can be even more dangerous because of their high ionizing potential that comes from their strong positive charge.

The next major cause of cancer is chemicals. There are thousands of known chemicals that cause cancer. The leading cause of cancer by chemicals is still smoking. By 2011, researchers had discovered 8889 chemical constituents in cigarette smoke. [173] [174] Of these chemicals they know of at least 45 compounds that do, or are suspected of, causing cancer. [175] These chemicals, and other chemicals, can be separated into multiple different groups. The groups include high energy molecules, natural toxins, mutagens, inflammatory chemicals, and others.

Unstable molecules, or high energy molecules, can come from high energy radiation, the body, or from chemicals in the environment. High energy molecules include free radicals, reactive oxygen species (ROS), or ions. [176] [177] Generally antioxidants, such as vitamin c, vitamin e, and polyphenols, scavenge many of these high energy molecules. [176]

Another common set of chemicals that cause cancer are benzene and phenols, which lead to Leukemia and Hodgkin lymphoma. There still is some confusion on the method in which benzene causes cancer, but it is believed that benzene causes cells to increase ROS production that damages the DNA. [178] [179] It also affects the transcription of the erythroid related genes in the erythroid progenitor cells causing erythropoietic depression, or lower red blood cell production. [180] Another example is the natural forming silicate, asbestos, which is used for insulation and to reinforce concrete. Asbestos imbeds in mesothelial cells and can cause mesothelioma. [181]

[182] [183] The method it causes cancer is unknown, but there are couple hypothesized paths: a direct path of damaging DNA and an indirect path caused by an inflammatory response. [181] The inflammatory response leads to a release of ROS (by the body), RNS (Reactive Nitrogen Species), cytokines, chemokines, and growth factors. This is followed by DNA damage, disruption of mitosis, and/or apoptosis/necrosis. The final steps in the mechanism caused by the inflammatory response is activation of intracellular signaling pathways, resistance to apoptosis, sustained cell proliferation, impaired DNA repair, chromosomal and epigenetic alterations, inactivation of tumor suppressor genes, and activation of oncogenes. Carbon nanotubes may have similar effects to cells, but many believe oxidative stress is caused by impurities in with the carbon nanotubes, and not by the nanotubes themselves. Some studies have shown that cleaned particles have no acute toxicity to lung cells. [92] Not all chemical carcinogens are man-made. There are also natural toxins, such as aflatoxin B1, which can lead to cancer.

The last cause of cancer that will be discussed is viruses. Virus strains alter the DNA sequence to produce new viruses, and some strains can cause cancer. A few of the strains that are known to cause cancer include, but are not limited to, Hepatitis B, Human Papilloma, and VX-2 Shope virus papilloma for white rabbits. [117] The causes of cancer are very important, and can sometimes lead to better therapies to prevent or combat cancer.

2.2.1.3 Methods of Combating Cancer: Issues and Advantages

There are several strategies that are implemented to treat, with the goal to cure, cancer. Treatments depend on the type of cancer, location, how aggressive the cancer

is, and the type of patient. The main treatments are surgery, chemotherapy, and radiation. Great improvements in these fields have led to increases in survival rates of patients. There are also many more improvements and new therapies that are in development.

The Practice Guideline for many cancers, as in colon cancer and liver cancer, is the resection or the surgical removal of the tumor. [184] On tumors that can be removed, or mostly removed surgically, it is the first choice. The ease of surgery depends on the shape of the tumor, if it is spherical, and if it is intertwined with the other tissue. When performing a resection, it is recommended to remove 1 cm surrounding the tumor, which does not work when there is vital surrounding tissues. [185] Resection does have an advantage of being the only curative method for various types of tumors, as with colon cancer. There have been great strides made in resection as a treatment. With Colorectal Liver Metastases resections, with intent of curing, the patient improved from 69% effective to 87% effective from 1970 to 1992. [185] Some of the new work that is exciting is in tumor delineation, or use of dyes or other items to increase contrast between the tumor and healthy tissue for resection. CB-PAA particles, because of their strong blue color, may be useful for tumor delineation.

There are many different chemotherapy drugs currently used to treat cancer. Many of the drugs are used for multiple tumor types, and some drugs are designed to target specific tumors. Chemotherapy drugs are known for their adverse side effects ranging from nausea, vomiting, depressed immune system, immune disorders, and loss of hair. [146] Some side effects have been extremely reduced by modifications to the structure of the drugs, as is the case with cisplatin and carboplatin. [186]

Chemotherapy is often used as adjuvant treatment with other treatments, like resection. Several examples of drugs that have been studied for adjuvant therapy in stage II and III colon cancer and metastatic colorectal cancer include 5-fluorouracil, capecitabine, oxaliplatin, and irinotecan. [184] [187]

As mentioned in chapter 1, there have been some advances in drug delivery using nanoparticles. Natural origin particles have been used since 1975 to try to increase the uptake of drugs. [6] More recently, there are particle-based drug systems like Abraxane (paclitaxel in an albumin particle), Brakiva (topotecan in liposomes), CRLX101 (camptothecin conjugated to a cyclodextrin-polyethylene glycol copolymer) [80], and MTX (MTX incorporated in a dendrimer) [39]. Nanoparticles function well at increasing the quantity of drugs delivered to the tumor through the EPR effect [41] [80], controlling release of the drug [6] [60], and targeting. [39] The increased drug concentrations localized at the tumor also function well at lowering side effects by lowering the effective dose required to be effective.

There are various types of radiation therapy, such as gamma rays and x-rays. The problem with radiation therapies is the adverse side effects that not only can kill cancer, but can also cause cancer. Besides causing cancer, radiation also causes severe damage to epithelial surfaces, infertility, and swelling of soft tissues. [146] In the past, thermotherapy had been used in conjunction with radiation therapy. [132] Mild hyperthermic conditions improved the effectiveness of radiation therapy. Besides thermotherapy, other adjunctive therapies include using drugs like nicotinamide to increase the oxygen concentration in the cells, which is needed since hypoxic cancer cells are radioresistant. [118] [132]

Several of the new methods to fight cancer include photodynamic therapy [146], photothermal therapy [14], other thermal therapies [110] [147], and gene therapy [55]. Many of these methods try to take advantage of the unique qualities of tumors, such as Enhanced Permeability Retention (EPR), fast growth, lower pH, increased concentration of certain proteins, etc. [188] It is not where cancer and healthy tissue are similar that most of advances in therapy will occur, but where they differ.

2.2.2 Toxicity

One of the most important factors, if not the most important factor in choosing a polymer matrix, is toxicity. Toxicity depends on a lot of different factors. Many of these factors, such as cell type, have been previously mentioned in chapter 1. [46] Below is a chart of responses to toxins, effects to the body, and some initial tests done to determine overall toxicity of particles, drugs, etc. [81]

Responses	Effects	Initial Evaluation Tests
Histopathological changes	Hypersensitivity	Cytotoxicity
Humoral responses	• Type I - anaphylactic	Sensitization
Host resistance	• Type II - cytotoxic	Irritation or intracutaneous reactivity
Clinical systems	• Type II - immune complex	Systemic toxicity
Cellular Responses	• Type IV - cell-mediated (delayed)	Subchronic toxicity
• T cells	Chronic inflammation	Systemic toxicity (acute)
• Natural Killer cells	Immunosuppression	Subchronic toxicity (subacute toxicity)
• Macrophages	Immunostimulation	Genotoxicity
• Granulocytes	Autoimmunity	Implantation
		Hemocompatablitiy
		Supplementary evaluation tests
		• Chronic toxicity

• Carcinogenicity
• Reproductive/developmental
• Biodegradation

Table 2.1: This is a table of the different responses to toxins, effects they have to the body, and some evaluation tests to determine toxicity. [81]

Cytotoxicity tests, such as MTT assay, though important and often one of the only tests done to declare a system nontoxic, are not the only tests to determine toxicity. There are a lot of steps and processes to determine the overall toxicity of a system.

2.2.3 Polyacrylamide

Polyacrylamide (PAA) was chosen as a delivery system because it is known to be safe and is a common polymer used in purifying drinking water, oil recovery, oil well drilling fluids, fracturing aids, wastewater treatment processes as flocculants, in soil conditioning and stabilization, as emollients in some personal care and grooming products, grout, dye acceptor, mineral processing, paint softener, paper manufacturing, and paper board manufacturing. [189] [190] [191] [192] It has also has been used for years in biological applications, such as breast implants. [193] [194] [195] Except for a few examples that are more likely caused by other issues, PAA shows little or no toxicity, even in extreme concentrations. [34] [189] [192] [196] In most cases, there are no issues and the body just coats the PAA with a cellular membrane that has thin fibers of connective tissue that integrate the PAA with the surrounding tissue. [194] [197] [198] Besides it having low toxicity, PAA is used because it has a high hydrophilicity [34], low cost to produce, easy to conjugate, and can be cross-linked with biodegradable linkers.

Polyacrylamide is polymerized through a free radical reaction of the monomer acrylamide. In the presence of water, the polyacrylamide absorbs the moisture, swells,

and forms a hydrogel. For many applications, including breast augmentation, the hydrogel is usually around 2.5% cross-linked polyacrylamide. [193] [194]

2.2.3.1 Toxicity of Polyacrylamide and Starting Materials

The toxicity of PAA has been studied since the early 50's, and because of its low toxicity, it has been used in biological applications in China and Europe since 1997. [189] [198] As of 2000, over 30,000 patients have been injected with bulk polyacrylamide for aesthetic and plastic surgery in the Soviet Union. [194] Some complications have arisen from using it in cosmetic surgery applications. [193] [194] [195] There were 15 cases of complications from the reviewed cases in the years 2004 to 2007. Of the 15 cases of complications, most of them had inflammation, granulomas, and cellular membrane around injections. [193] [194] [197] The injections or the implants of PAA gel were ranging from cheeks, nose, eyelids, breasts, and one penis. Out of the 15, 5 required surgical removal of the PAA, usually squeezed out of a small incision. [193] Seven of the eight of the granuloma patients tested positive for bacteria in the PAA. When compared to other dermal fillers, it appears to have fewer toxicity issues. There have been some cases in which some issues have been observed such as inflammation (due to infection), hematoma, multiple induration and lumps, persistent mastodynia, mastalgia, and lactation. [194] [195] [199] Most issues that arise can be easily attributed to bad medical practice, and not from the toxicity of PAA. [195] Other studies have been done in other mammals to test toxicity and other possible effects. In pigs, there were no significant issues from PAA gel. [197] The most dangerous part of injecting it into pigs came from infections caused by contamination or unclean practices.

[197] Polyacrylamide still has ideal characteristics for a dermal filler, but needs more studies into complications. [193] [198]

The bulk properties often differ than that of particles made of the same material. Unlike bulk PAA, polyacrylamide nanoparticles are still in the earlier stages of use, and have only been used in animals. Polyacrylamide nanoparticles also show very little, if any toxicity. When Fisher344 rats were injected with PEGylated PAA particles, no toxicity was observed, even when the rat was injected with 5 and 50 mg/kg. [81] At 500 mg/kg of PAA, the rats showed no inflammatory response, but they did have modest elevation in alkaline phosphatase, which could mean there were issues with the liver removing the particles from the rat. *In vitro*, PAA nanoparticles do not show any MTT toxicity in C6 glioma, A549, MBA-MB-435, and MCF-7 when incubated in 4 mg/mL for 24 h. [33] This was also confirmed with F3 methylene blue PAA nanoparticles that showed no, or limited dark toxicity *in vitro* 9L, MDA-MB-435, and F98. [34] There is some information that anionic PAA may be toxic at high molecular weights, but this toxicity is often attributed to the unreacted AA monomer units. [192]

There are a few ways polyacrylamide can be toxic: residual acrylamide (AA) [191], residual surfactants, chemical contaminants, and/or biological contaminants. Acrylamide is an acute eye irritant, skin irritant, respiratory tract irritant [189], neurotoxin [191] [192] [196], causes axonopathy in human and animals [196], and in acute conditions, it affects the kidneys, liver, and lowers the reproductive rates in females and males (lower sperm count). [191] [192] Most of the issues that arise are reversible with time, depending on the exposure. [196] Acrylamide injected intraperitoneally (IP) with dosages of 30 mg/kg/day only takes 2-10 days to show neurotoxicity in cats and rats.

[192] That would be equivalent to 1.8 gram/day injected in a 60 kilogram person. For oral toxicity, the LD50 is about 150-180 mg/kg in rats, guinea pigs, and rabbits. [192] The restriction on oral consumption of acrylamide is 0.5 μg/kg/day (regarded as 1000-fold safety level). [192] The average daily oral exposure of AA for a United States citizen is about 0.4 μg/kg/day. [191]

Polyacrylamide particles are formed in a reverse micelle reaction that requires surfactants to stabilize the cells of hydrophilic reactants and reaction solvents. After the reaction has concluded, there is surfactant attached to the surface of the particles that needs to be washed and removed. The remaining surfactant, if not enough is removed, can be toxic and can cause adverse cellular reactions. The two surfactants that are commonly used in the reaction are Brij 30 and AOT. Many of the values for toxicity are for oral consumption, which does not accurately portray how the body will interact with intravenous injection. In the case of Brij 30, the intravenously LD_{50} (lethal dose required to kill 50%) is 27 mg/kg for a rat and 100 mg/kg for a mouse. [81] For AOT the LD_{50} is 60 mg/kg in a mouse. [81] To remove the excess starting materials and remove contaminations, it is necessary to wash the particles thoroughly. These will probably be two biggest causes of any toxicity observed.

2.2.4 Accumulation, Biodegradability, and Bioelimination

Where particles accumulate in the body and in cells has a lot to do with how they are bioeliminated. Nonbiodegrable PEGylated PAA and standard PAA larger than 10nm accumulated mostly in the liver and spleen. [81] The liver and the spleen are part of the RES, and is the pathway to remove large biocontaminates. The particles were not discovered in the vascular lumen of the renal glomerulous, as would be expected,

because the kidneys can only filter into the nephron only those objects smaller than 10 nm. Moreover, the particles used in the study could not biodegrade into smaller fragments or dissolve completely. [32] [60] If the particles are not eliminated, buildup can cause long-term adverse outcomes and limit the amount of treatment that can be administered.

As mentioned in chapter 1, one method to increase bioelimination is by making the particle matrix biodegradable. Polyacrylamide chains do not biodegrade into its monomer unit or any smaller unit. [81] [192] The backbone of PAA is extremely stable and does not breakdown without photodegradation, mechanical breakage, heat (200-300°C), or free radical degradation. [189] [190] [192] It is not clear from the available literature whether or not acrylamide is one of resulting products liberated from metabolic breakdown of the particle. [189]

When forming a cross-linked PAA matrix, the cross-linker can be biodegradable. If the linker is biodegradable, the resulting products can be small enough to be eliminated renally, or easier to pass through the reticular endothelial system (RES). The more biodegradable cross-linkers (glycerols) used, the more likely the particles were to pass through urine vs. feces. [81] When injecting a rat with nonbiodegrable PEGylated PAA, about 4% was excreted within 5 days, with the remaining recovered in the liver. [81] Whereas particles synthesized with 10% biodegradable cross-linkers had about 10% excreted in the first five days. After 42 days, about 17% of the particles were excreted. PAA goes through a 2-phase degradation, with the first phase of elimination peaking around day 1, and the second phase starting after 14 days, and elimination jetting up at day 35. The increase in elimination is a good sign for minimizing potential

issues arising from long term exposure to PAA and making PAA a good candidate for a particle matrix.

2.2.5 Dye

When choosing the dye for photothermal therapy, there were a couple of characteristics that were desired. First, the dye needed to be in the optical window of cells, absorbing near, or in, the infrared. The original dye also needed to be nontoxic to increase the possibility that the derivative would be nontoxic. Thirdly, the derivative of the dye needed to be easy to synthesize and have high incorporation in to the particle to increase its total absorption. Lastly, the dye should also be blue so that it can serve a dual purpose as a photosensitizer and a contrast agent for tumor delineation. It was determined that Coomassie Blue fulfilled these properties. Coomassie Blue is a very common dye used in protein staining, and it has a strong absorption band around 595 nm. The dye, Coomassie Blue, is nontoxic up to extremely high concentrations, but this does not mean that the derivative is nontoxic or it being connected to PAA is nontoxic. [200]

A derivative of Coomassie Blue G250 was synthesized by Michael Nie, a member of the Kopelman Group, to increase dye incorporation. The derivative could act either as monomer unit, or as a biodegradable cross-linker to copolymerize with PAA. Altering the dye was done on the sulfur groups to minimize affect to dye and changes to toxicity. N-(3-Aminopropyl) methacrylamide hydrochloride (APMA) was attached by the terminal amine to make the new derivative, which can be seen in Figure 2.2.

2.2.6 HeLa Cells

When choosing a cell line, it was decided that a very common strain, HeLa cells, would be best for initial tests. HeLa cells, one of the most recognized cell strains, were discovered in 1951 by George Gey at John Hopkins Hospital in Baltimore. [201] The cells came from aggressive glandular cervical cancer found in a young black lady named Henrietta Lacks. Usually most cervical cancers are slow growing, but HeLa cells come from aggressive cervical cancer. Not only are the generation times on the order of 24 h, but this rare adenocarcinoma is also resistant to radiation. [201] [202] The cells were excised from a purple lesion to become the first stable human continuous cell line. [202]

2.2.7 Photothermal Therapy

The ideal temperature range for photothermal therapy is 42°C - 45°C, where cell death has a higher probability to occur by apoptosis than necrosis, which is usually at temperatures above 45°C. [120] In this temperature range, and with higher concentrations of particles in the targeted cells, there will be minimal damage to the surrounding tissue. This is the reason that this type of photothermal therapy was chosen. There are other thermal therapies that include photothermal ablation (pressure), magnetic hyperthermia, microwaves, ultrasound, or photothermolysis, but many of them cause collateral damage, are not precise, cannot target, or have side effects.

2.3 Experimental

2.3.1 Initial PTT Experiments with Methylene Blue Derivative Particles

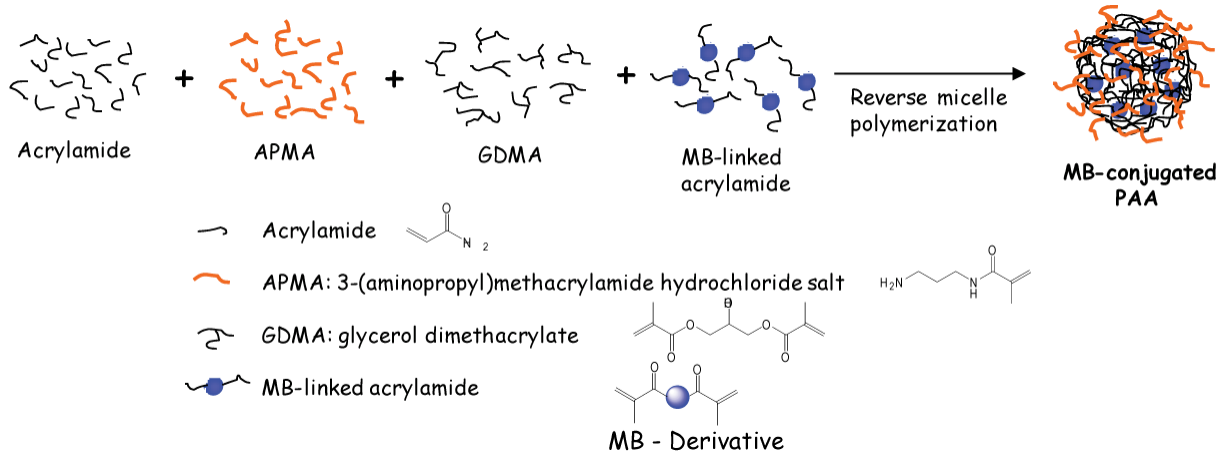

Figure 2.1: This is a diagram of the synthesis of the methylene blue polyacrylamide nanoparticles. The starting materials were mixed and added to hexane surfactant solution to produce reverse micelles (hydrophobic solvent with insides of micelles being hydrophilic).

Particles were synthesized by the above reaction (Figure 2.1). Michael Nie synthesized the methylene blue derivative and Matt Waugh synthesized the particles. After the synthesis, the volatile hexanes were then removed using Büch RII Rotavapor. The particles were then washed in an Amicon cell 7 times with ethanol, and then 10 times with Millipore water. After the particles were washed, they were lyophilized in a Thermo Electron Corp ModulyoD freeze dryer and stored at room temperature for future experiments. Michael Nie confirmed that these particles did not produce singlet oxygen by using ADP method.

2.3.2 Coomassie Blue Derivative Particle Synthesis

In one container, 165 mg of Coomassie Blue derivative was mixed with 0.8 mL of anhydrous dimethyl formamide (DMF) from Sigma Aldrich, and 1.0 mL of Brij 30 from Sigma Aldrich. In a separate container, 610 mg of acrylamide from Sigma Aldrich was

mixed with 40 mg of N-(3-Aminopropyl)methacrylamide hydrochloride (APMA) from Polysciences Inc., and 1.2 mL of water (Milli-Q water coming from a Millipore A10 water purification system). In a 250 mL round bottom flask containing a magnetic stir rod, 4.8 g of Dioctyl sodium sulfosuccinate (AOT) from Sigma Aldrich was mixed with 8.5 mL of Brij 30, and 60 mL of deoxygenated hexanes from Sigma Aldrich. The contents of the first two containers were added to the round bottom flask. The resulting solution was then mixed and bubbled under an inert environment for 20 min. Added to this solution was 400 µL of a freshly made solution of 66% w/v APS from Sigma Aldrich in Millipore water, and 200 µL of N,N,N′,N′-Tetramethylethylenediamine (TEMED) from Sigma Aldrich. The final solution was continually mixed for 1 h under an inert environment. The diagram of the synthesis can be seen in the figure below.

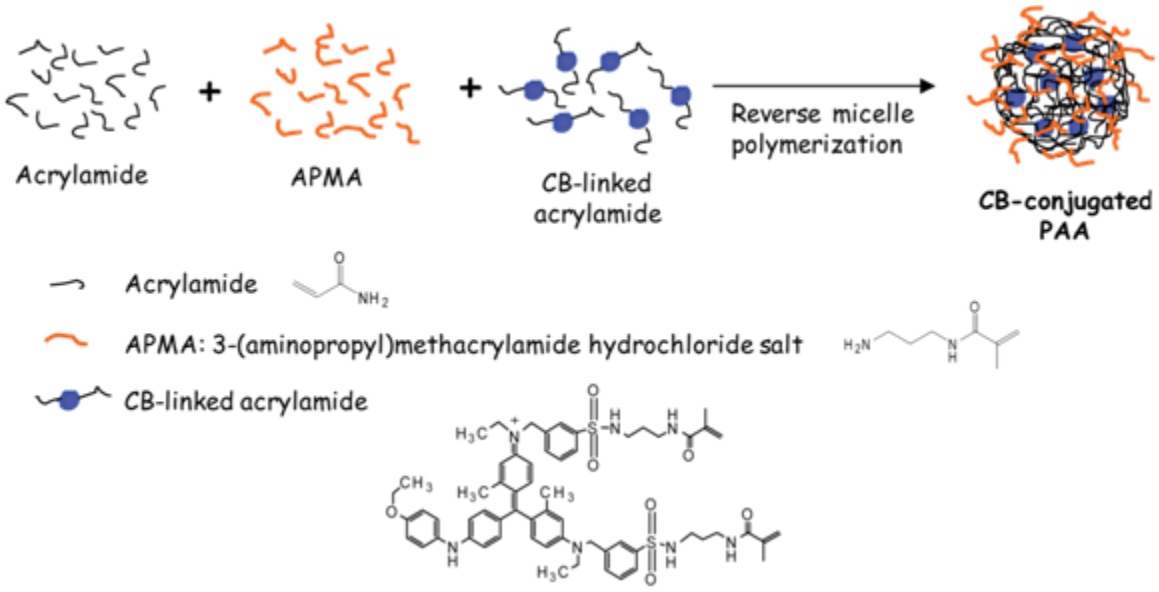

Figure 2.2: Diagrams shows the synthesis of the CB-PAA nanoparticles. Starting materials were prepared and added to hexane surfactant solution to produce reverse micelles (hydrophobic solvent with insides of micelles being hydrophilic). The reaction was initiated with APS and TEMED while being constantly stirred under argon.

The volatile hexanes were then removed using Büch RII Rotavapor. The remaining product was washed in an Amicon Cell using a 300,000 NMWL Millipore Ultrafiltration Membrane. The solution was washed 10 times with 200-proof ethanol from Decon Labs Inc., followed by 10 washes with Millipore water. The washing was performed in a 200 mL Amicon Cell. For each rinse, the solution containing the particles dropped down to about 10-20 mL before more ethanol or water was added. Large aggregates were then removed by centrifuging at 5000 RCF for 7 minutes. The soluble product was passed through a 0.2 μm filter from Whatman to remove large particles. The filtered product was then lyophilized using a Thermo Electron Corp ModulyoD freeze dryer and stored at room temperature for future experiments.

For the experiments that had the particles incubated with HeLa cells, particles were resuspended in 11995 DMEM growth media from Gibco. The solutions were then passed through a 2.2 μm filter from Whatman, followed by a 0.2 μm filter.

A small amount of CB-PAA nanoparticles were resuspended in Millipore water to give a concentration of 0.5 mg/mL. The particles were characterized by taking size and zeta potential measurements in a DelsaNano particle sizer. In order to determine the amount of Coomassie Blue derivative in the particles, a calibration curve (Figure 2.9) was created comparing the absorption of Coomassie Blue derivative to its concentration. This was accomplished by taking absorption spectra of different concentrations of Coomassie Blue derivate that had been dissolved in small quantity of DMF and the rest Millipore water. From this, it was possible to determine the concentration of dye for a given mass of particles in solution.

2.3.3 LED Array Light Source

The excitation source used was an LED array created to maximize the 600 nm absorption peek of the CB-PAA particles. An array of 256 wide angle LEDs from Kingbright Corporation, with an emission peak at 590 nm, were soldered onto a fiberglass PCB board. Wide angle LEDs and mirrors around the perimeter of the array were used to increase uniformity of light hitting the samples. The deviation of the irradiance at the face of the mirrors is 6%. A fan was placed on the top of the LED array to keep the temperature of the array down and to minimalize heating of the cells through convection. The general design of the LED array can be seen in Figure 2.3. An adjustable power supply was used to control power output of the LED array.

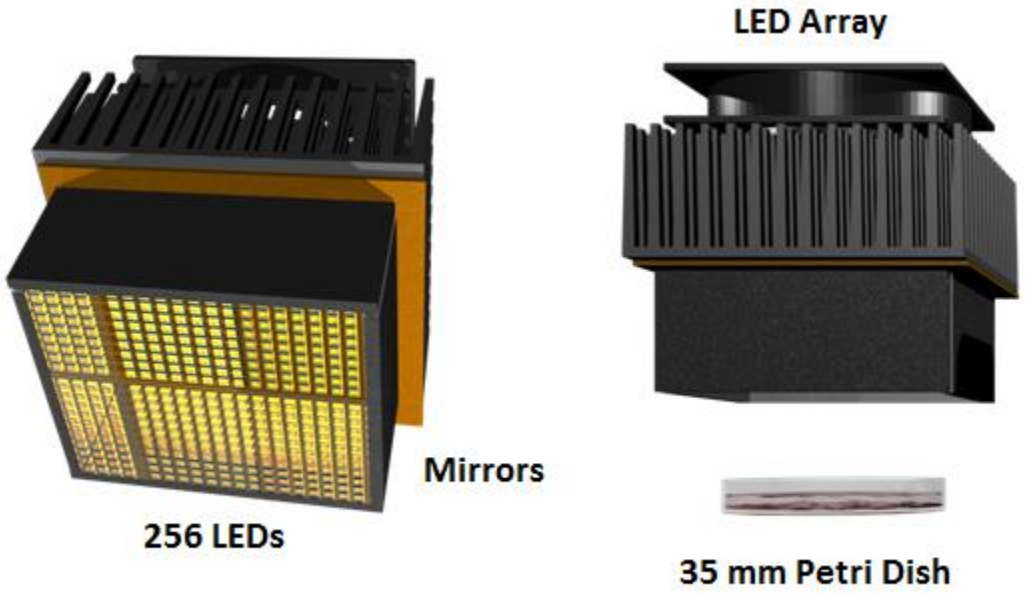

Figure 2.3: Design of the LED array and experimental setup. The 256 LEDS with an absorption peak centered at 590 nm were surrounded by 4 mirrors. A fan was placed on top to keep the LED array from overheating or from heating the samples by convection. The illustration on the right represents how the LED array was placed down on top of the petri dish.

2.3.4 Live Dead Assay

Experiments were done using a Live Dead fluorescence assay. The HeLa cells or 9L cells used in the experiments were incubated with calcein AM dissolved in DMF from Sigma Aldrich to stain the live cells green, and propidium iodide to stain the nucleus of the dead cells red. Cells were then imaged on an IX71 Olympus microscope using a FITC filter set to image the live cells, and rhodamine filter set to image the dead cells. Experimental setup can be seen in Figure 2.4. Ten images using each filter set were taken at different locations across the 35 mm petri dish to increase accuracy of counts. Cells were then counted manually, or by using ImageJ imaging software.

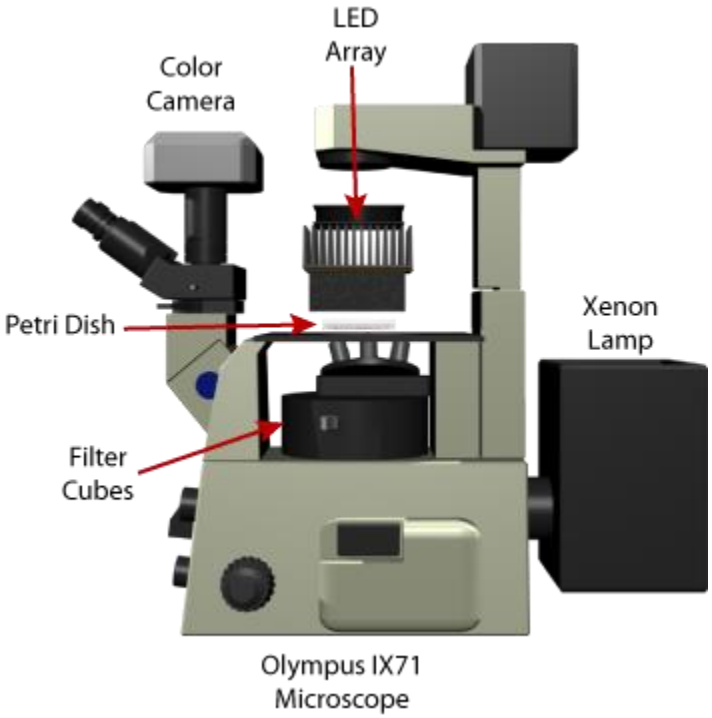

Figure 2.4: Experimental setup to measure the vitality of cells using a LIVE DEAD assay. Cells were in a petri dish on the microscope during illumination by the LED array. LED array was removed during measurements to remove reflections off the LED array. Dyes were excited with Xenon Lamp that was filtered with filter cubes. Images were taken with color camera and then later analyzed.

2.3.5 PTT using Methylene Blue Polyacrylamide Particles

Matt Waugh, with my assistance, did the following experiment. Particles were resuspended in water, then filtered through a 2 μm filter, 1 μm filter, and then a 0.22μm filter. Particles were added to the growth media to make the various concentrations. The 9L cells were than incubated with the particles. Cells were then washed and placed in DPBS. The live dead assay reagents were then added to the solution. Cells were illuminated with 590 nm LED array with an intensity of 20 ± 1 mW /cm^2. Cell counts were done immediately following excitation.

2.3.6 CB-PAA Particle Concentration with Different Time Exposures

HeLa cells were cultured for one day in a 35 mm petri dish, and then rinsed twice with DPBS. Different concentrations of particles dissolved in 11995 DMEM were added to each dish and allowed to incubate for approximately 24 hrs. Cells were then rinsed twice with DPBS, and then 0.75 mL of DPBS was added. The live dead assay was done and cells were imaged. The cells were then placed under the LED with an intensity 25.4 ± 1.6 mW/cm^2 for the allotted time. Cells were imaged and counted again, as in the live dead assay. The imaging and counting was then repeated 2.5 h after exposure. There was a difference of up to 10% decrease in live cells between using DPBS and DMEM 21063 from Gibco.

2.3.7 Effect on Cell Death with Incubation Times

As with previous experiments, cells were prepared with 0.8 mg/mL CB-PAA particles. The cells were then incubated for varying times before washing twice with DPBS, and then adding 0.75 mL of DMEM 21063 from Gibco. Live dead assay

counting and imaging were done as they were previously: before exposure and 2.5 h after exposure. Cells were exposed at 25.4 ± 1.6 mW/cm^2 for 40 min.

2.3.8 The Effect of Light Intensity on Mortality

Again, HeLa cells were cultured for one day in a 35 mm petri dish, and then rinsed twice with DPBS. Each petri dish was incubated for approximately 24 h with 0.8 mg/mL CB-PAA particles. After the incubation, the cells were rinsed twice with DPBS, and then 0.75 mL of DMEM 21063 was added. Live dead assay was performed, and the HeLa cells were exposed to varying intensities of 590 nm light from the LED array for 40 min. The percentage of living cells were then determined from images taken 2.5 h after exposure.

2.3.9 MTT Assay

HeLa cells were cultured until confluent. The cells were then trypsinized and diluted in 11995 DMEM media. A hemocytometer was used to find the concentration of the cells, and then 5000 cells were placed in each well of a 96-well plate. The cells were then incubated for 24 h in an incubator. The cells were washed once with DPBS. Then 12 wells of each different concentration of CB-PAA particles were added to the 96-well plate. The particles were then incubated with the cells for approximately 1 h, and then washed twice with DPBS. After the 2 rinses, the MTT reagent dissolved in DMEM 21063 was added, with a final concentration of 0.5 mg/mL. The cells were allowed to incubate for 4 h and then the solution was removed. After the MTT reagent solutions were removed, 0.2 mL of anhydrous DMF was added to each well. The plate was placed on a rocker and allowed to rock for 5 h. The dish was then placed in a Biochrom Anthos 2010 plate reader and the intensity measurements were taken 570

nm. The concentration of the particles was not high enough to affect the absorption by the plate reader.

2.3.10 Heat Due to Particles

About 0.5 mL CB-PAA particles, with a concentration 1.2 mg/mL, were placed in the bottom of a 10 mL snap cap culture tube (See Figure 2.5). A small thermocouple was placed in the solution to measure the temperature of the solution as it was excited by the LED array. The LED array was turned on and the temperature was measured intermittently. Particles were excited for ~20 min at 25.4 ± mW/cm^2. The temperature change was 5.6 +/- 0.1°C, compared to a blank solution using a thermocouple.

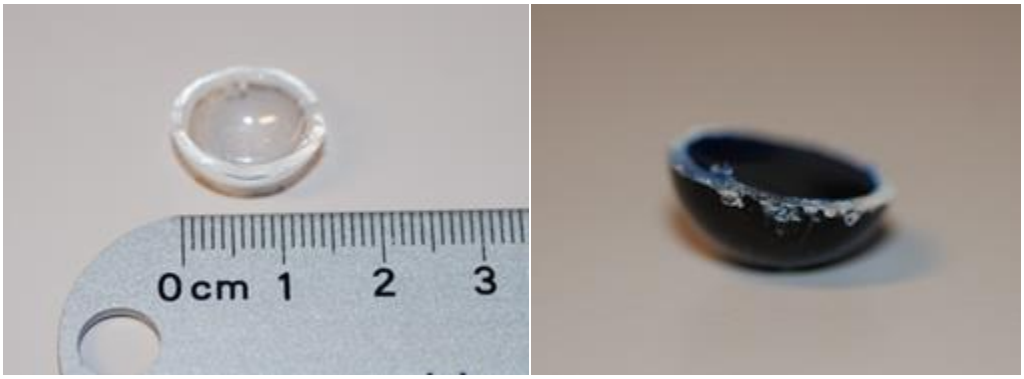

Figure 2.5: The bottom of a 10 mL snap cap culture tube was cut off. It was filled with 0.5 mL of a 1.2 mg/mL solution of CB-PAA. The temperature was measured as it was exposed to the 25.4 ± mW/cm^2 LED array.

2.4 Results

2.4.1 Methylene Blue Polyacrylamide Nanoparticles

Methylene blue particles were characterized by Michael Nie and Matt Waugh. There was high dye loading and the particles were determined not to produce singlet oxygen. Given that information, it was determined that the methylene blue particles would kill the cell by photothermal therapy, and not by photodynamic therapy. When we tested the 9L cells, they showed a lot of promise. Cell death was about the same for

0.1 to 0.4 mg/mL, and was obviously faster with the 0.8 mg/mL. The reference cells were not affected by the LED array, which is expected. After 20 min exposure, there was about 95% to 99% cell death for all cases. This information convinced us to try the CB-PAA particles because of their deeper color and availability of the Coomassie Blue derivative. The synthesis of the methylene blue particles was more difficult than Coomassie Blue derivative. Once the methylene blue derivative ran out, and the 9L cells became contaminated, it was decided to no longer pursue these particles.

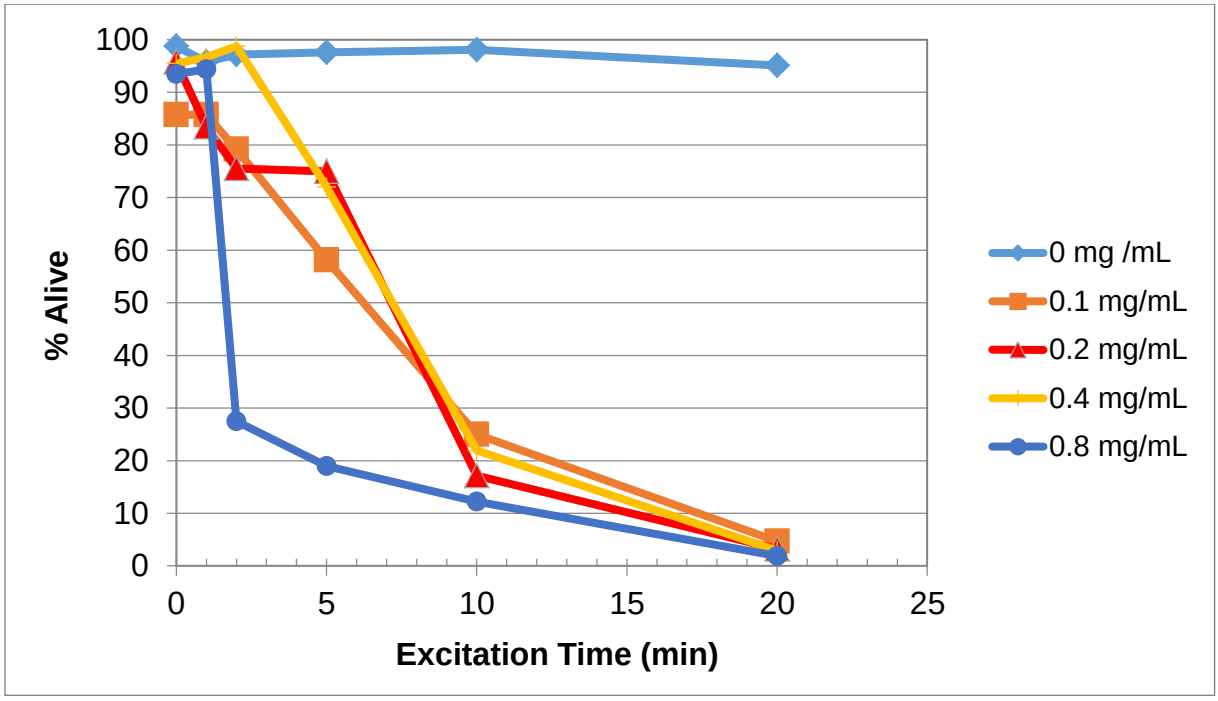

Figure 2.6: PTT using methylene blue polyacrylamide nanoparticles on 9L cells. Methylene blue polyacrylamide particles at various exposure times, up to 20 minutes. Concentrations ranged between the reference and 0.8 mg/mL.

2.4.2 Characterization of the CB-PAA Nanoparticles

After the synthesis of the CB-PAA nanoparticles, average particle size was determined using dynamic light scattering to be 96 nm with a large distribution, as can be seen in Figure 2.7, and the zeta potential to be +6.9 mV. The particle did not show a shift in its absorbance peak, as can be seen by Figure 2.8. Using a calibration curve

created from the Coomassie Blue derivative free dye, the Coomassie Blue derivative incorporation was determined to be 17% by mass. This was determined by using the calibration curve that can be found in Figure 2.9. Assuming the density due to PAA in water was about 0.1 g/cm^3, it was estimated that there were 2400 dye molecules per nanoparticle. The extinction coefficient was determined to about 1.4 x 10^8 M^{-1}cm^{-1}.

There were some issues with the particles. The solubility of the CB-PAA particles was not very high, and it also decreased with time. Second, solutions of the resuspended lyophilized $_{particles}$ contained visible aggregates that had to be removed through filtration.

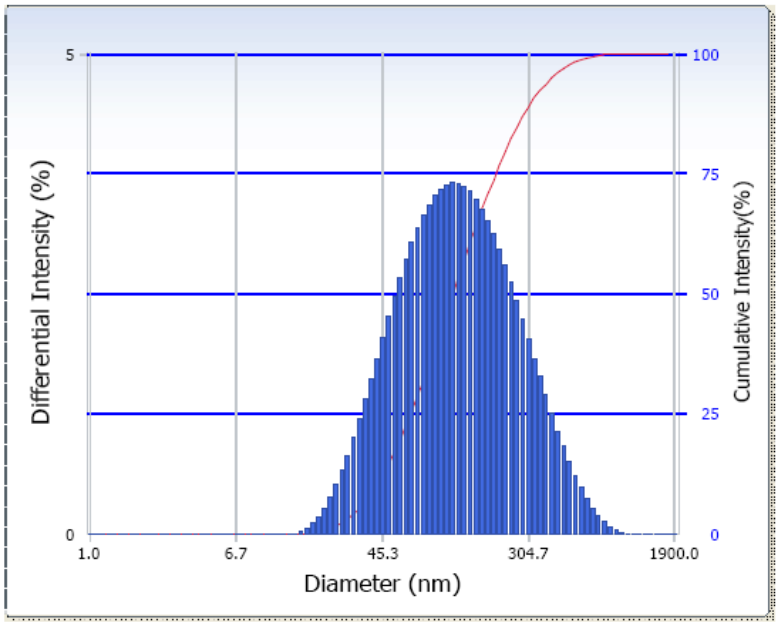

Figure 2.7: Particle size distribution using dynamic light scattering on a DelsaNano particle sizer. The particles are at a concentration of 0.5 mg/mL in Millipore Ultrapure water. This is after filtering the particles through 0.22 µm filter.

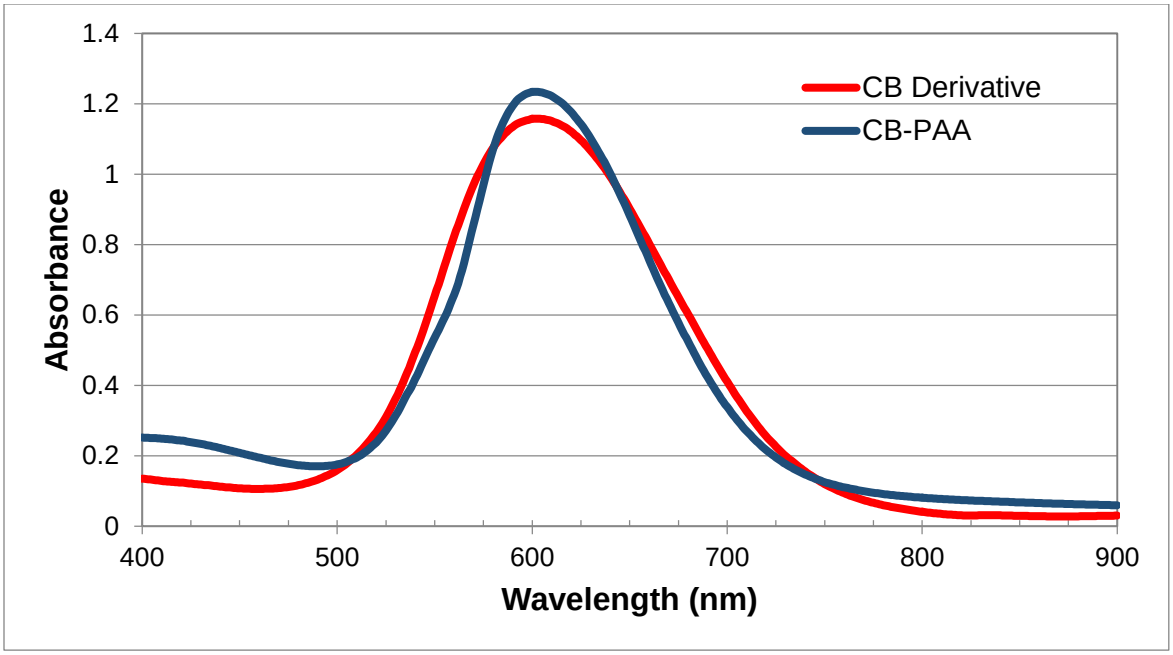

Figure 2.8: UV-Vis spectra of the 31 μM Coomassie Blue derivative and the Coomassie Blue polyacrylamide particle at a concentration of 0.25 mg/mL. The Coomassie Blue derivative was initially dissolved in the minimal amount of DMF, and then diluted to the concentration using water.

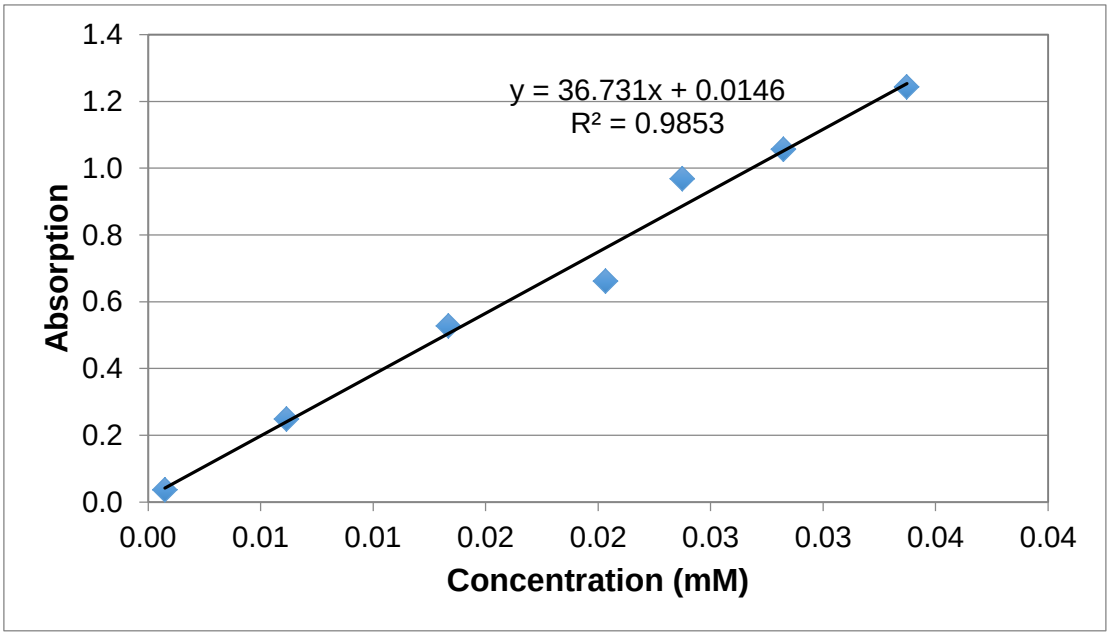

Figure 2.9: Calibration curve of the Coomassie Blue derivative showing the effect concentration has on absorbance. Dye was dissolved in a minimum amount of DMF, and then diluted with water for all points. The plot information was to determine the amount of dye that was present in the particles.

When preparing the particles for experiments, the particles were filtered through multiple filters. Absorption spectra of known concentrations, ranging from 0.01 mg/mL to 0.35 mg/mL of CB-PAA particles, were taken to make a calibration curve. The spectra are visible in Figure 2.10. From the spectra, there is no visible shift as the concentrations get larger, which denotes no interference between particles at those concentrations, but this is impossible to determine with concentrations up to 1.2 mg/mL. The calibration curve of the particles is in Figure 2.11. To determine the concentration of particles for experiments, filtered particles were diluted with growth media by known values and then fitted with the calibration curve. The concentration of the filter product was calculated, and the initial solution was diluted accordingly for the experiments.

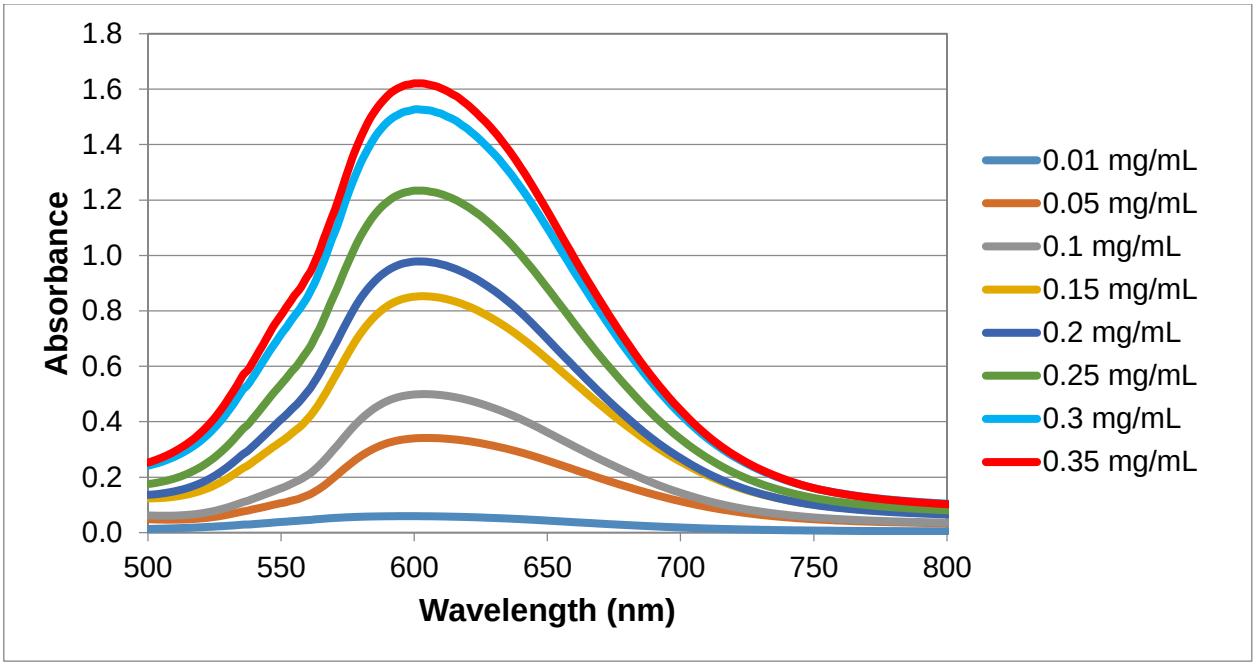

Figure 2.10: Absorption spectra of CB-PAA particles at varying concentrations ranging from 0.01 mg/mL to 0.35 mg/mL. Particles were diluted in 11995 DMEM growth media from Gibco. The reference cell for all the spectra contained growth medium to eliminate any shifts caused by the growth media.

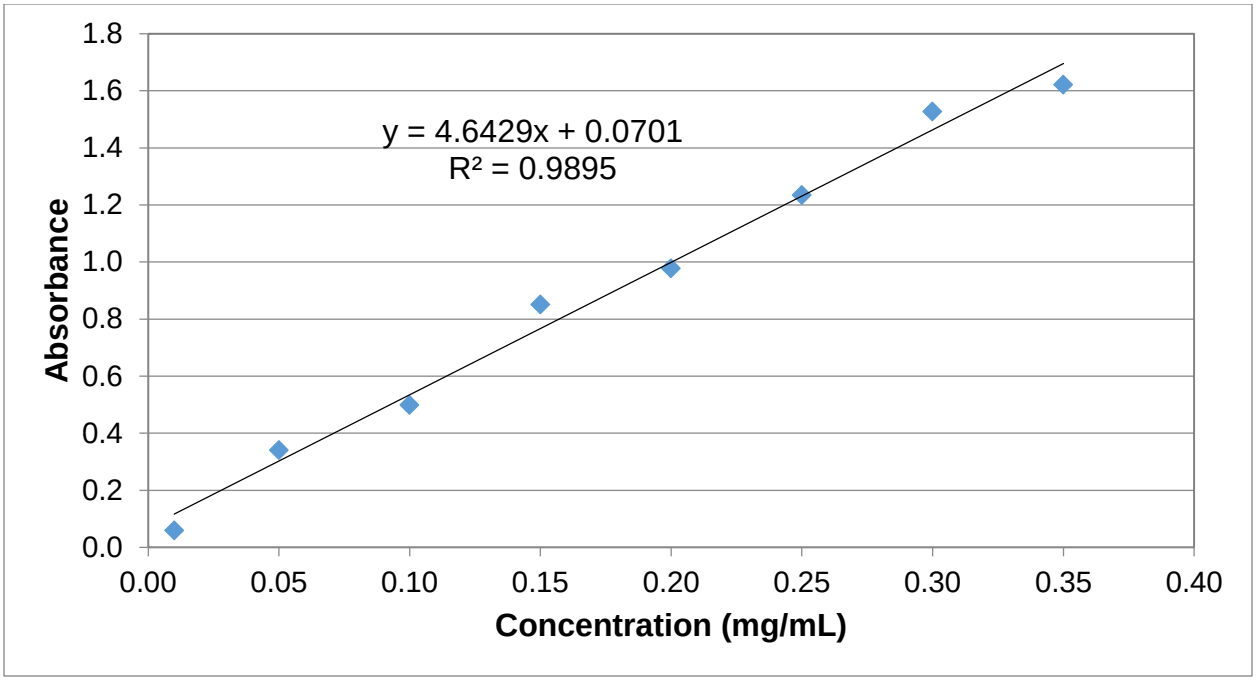

Figure 2.11: The calibration curve of particles was taken at varying concentrations up to 0.35 mg/mL. Concentrations above 0.35 mg/mL were obviously out of the linear phase and not represented in the plot.

2.4.3 Relation of Cell Death to Exposure Time and Concentration of Particles

HeLa cells were incubated with varying concentrations of CB-PAA, and then exposed to light for varying amounts of time to examine the relationship between cell death, exposure time, and concentration of CB-PAA particles. First, CB-PAA particles were solubilized in growth media due to their low solubility, and also to provide the HeLa cells with enough nutrients to grow during incubation. After the particles had been filtered to remove aggregates, they were added to previously washed HeLa cells. Growth media was added to each petri dish to change the concentration of particles to the desired amount. Cells were incubated for a minimum of 24 h before they were washed twice with DPBS to remove free floating particles. The extra particles were removed so that the intensity of light at the cells was uniform between different concentrations. Also, the particles were removed to ensure that cell death was not a

result of the heating of the solution, but the heating of the cells themselves. One milliliter of DPBS, and not growth media, was added to each petri dish because the growth media available at the time contained phenol red, which can scatter and absorb some of the light. There was a slight hint of blue on the surface of the petri dish from the particles being absorbed by, or attached to, the HeLa cells. In order to measure cell viability, calcein AM and propidium iodide were used to perform a live dead assay. The two dyes were added to each dish and allowed to incubate with the HeLa cells for 10-15 min in the incubator. Fluorescent images were taken at 10 different positions on the petri dish as a reference. The petri dish was then placed under the 590 nm LED array with intensity 25.4 ± 1.6 mW/cm^2.

To confirm that it was not the heating of the solution that caused cell death during exposure to the light source, the solution temperature was measured, using a thermocouple, to be 23 °C before, and 29°C during exposure. This was the same for all concentrations, including the petri dishes with no particles. The temperature was approximately 34°C when the solution in the petri dish had a concentration CB-PAA of 1.2 mg/mL, which is below the incubation temperature of the cells. This was tested using the bottom of the culture tube as seen in Figure 2.5.

Cell death did not occur immediately, as can be seen by Figure 2.17. Where the incubation concentration of CB-PAA was 1.2 mg/mL, 97% of the cells were dead after 2.5 h. Since the cells were in DPBS, they could not be left indefinitely or they would have died from lack of nutrients. Based on this information, fluorescent images were taken at 2.5 h after exposure to the LED array for all samples. The fluorescent images were taken in similar locations on the petri dishes, and were then counted manually or

by using a script in ImageJ. An example set of images can be seen in Figure 2.12. Cell counts were normalized to reference cell counts and the results are shown in Table 2.2

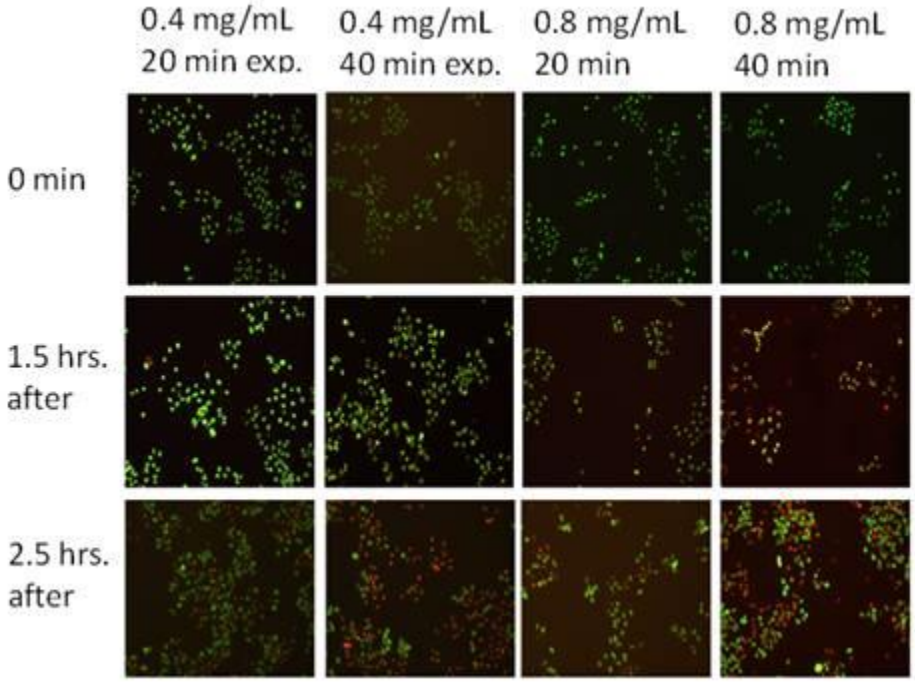

Figure 2.12: Examples of images taken of the cells using calcein AM and propidium iodide to give live cells green fluorescence and dead cells red fluorescence.

Time Exposure (min)	0.0 mg/mL % Alive	0.4 mg/mL % Alive	0.8 mg/mL % Alive	1.2 mg/mL % Alive
0	100	100	100	100
10	98	100	92	61
20	99	87	80	45
40	91	2	6	3

Table 2.2: Table of the cells still alive after being exposed to varying times of light and with varying concentrations of particles. All results were from 2.5 h after exposure.

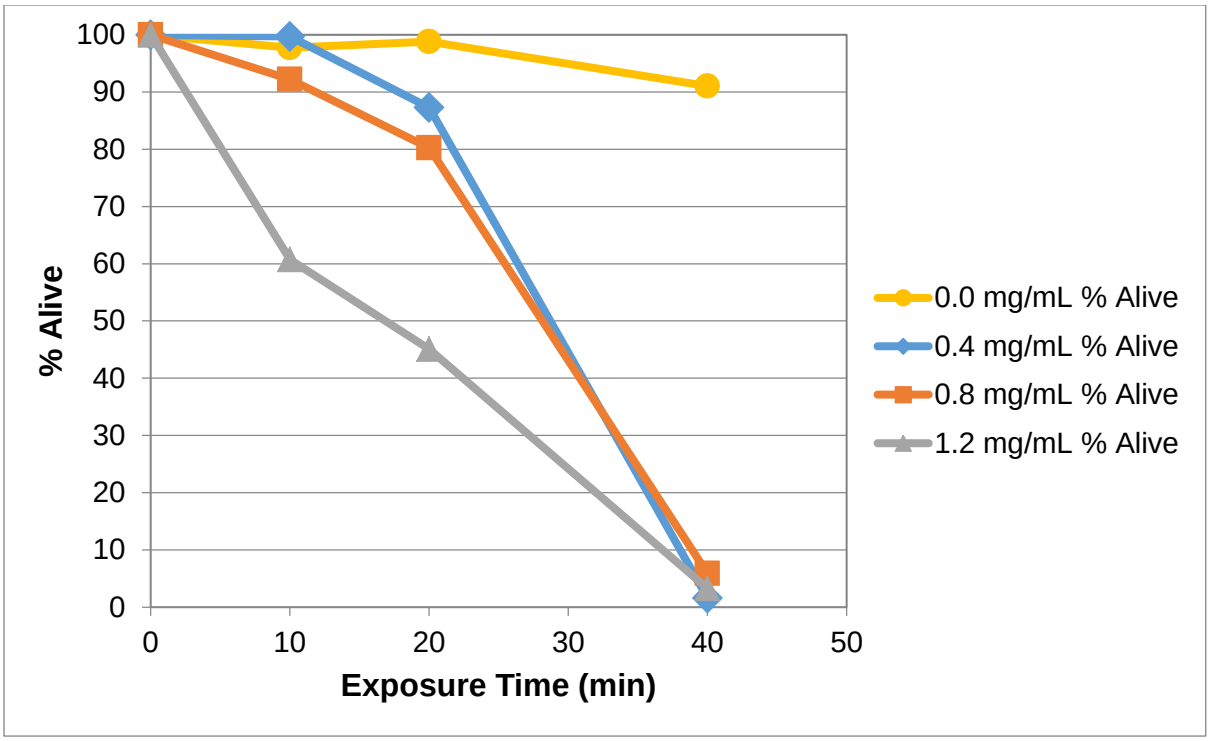

Figure 2.13: The effect of concentration of particles (in mg per mL) and exposure time on cell viability. Cells were exposed to 590 nm light with irradiance of 25.4 ± 1.6 mW/cm^2. Measurements were taken 2.5 h after exposure, using calcein AM and propidium iodide to measure the ratio of cell viability. Ten images were taken at each location on the petri dish. Each point represents about 800-2200 cells

The results plotted in Figure 2.13 indicate that there is a dependence on concentration and exposure time for cell viability. The dependence on concentration can easily be seen when looking at the 20 min exposure time. This is confirmed by some of the initial tests using CB-PAA in 9L cells (Figure 2.14). At the 40 min exposure time, most of the HeLa cells were dead. Therefore, either concentration would have provided nearly the same results. Also from the plot, it is possible to see that there is no major effect on the cell viability when no particles incubated with the cells.

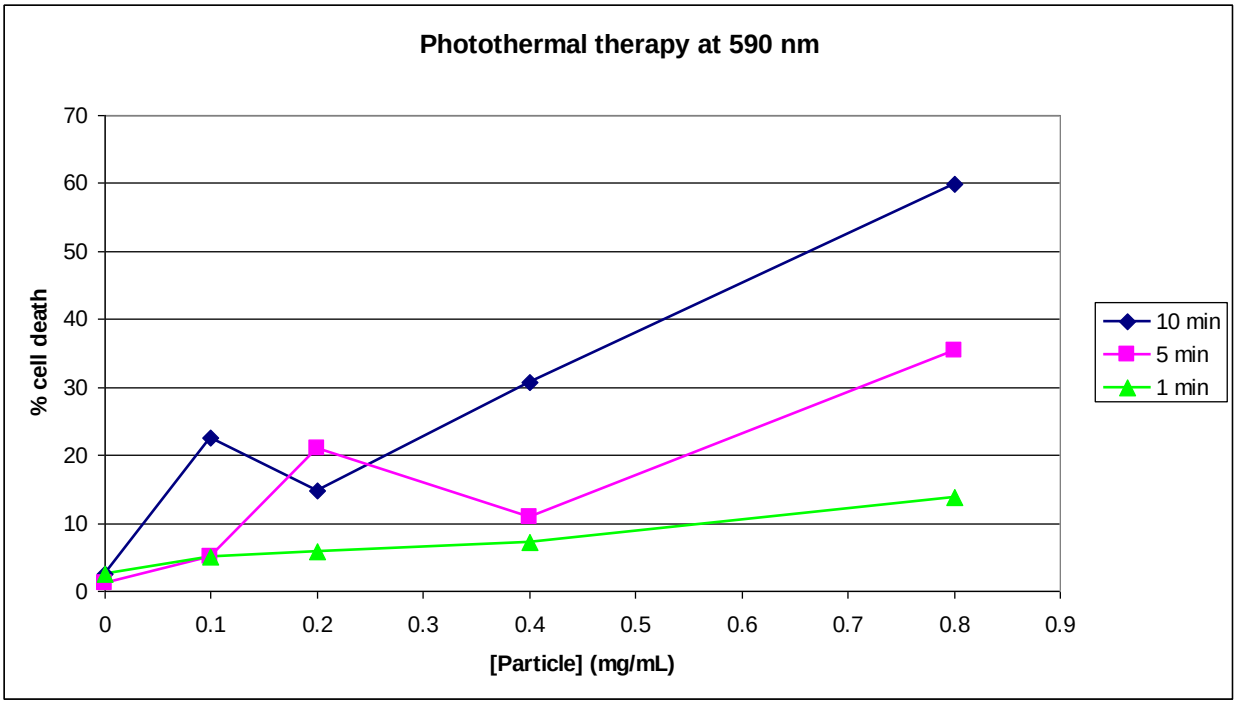

Figure 2.14: Initial results using CB-PAA nanoparticles on 9L cells. The particles were incubated in growth medium with cells at varying concentrations. Cells were then washed with DPBS. The cells were then exposed to the LED array. The particles were exposed for 1, 5, and 10 min. Using the live dead assay, cell viability was determined for each point. Results were produced by Matt Waugh with my collaboration.

2.4.4 Cell Viability as a Function of Incubation Time

Incubation time is an important variable that determines the functionality of the particle. To look at cell viability as a function of incubation time, cells were grown as in previous experiments, washed once, and then incubated with 0.8 mg/mL CB-PAA particles. Incubation times were measured from the time the particles were added until they were washed twice with DPBS. In this experiment, cells were placed in DMEM without phenol red to provide the cells with nutrients, and to ensure that the phenol red did not absorb or scatter any of the light. The calcein AM and propidium iodide were then added, and cells were placed in the incubator for 15 min. The cells were imaged as before, and exposed to 40 min of the LED array as in previous experiments. The

results of the cell counts can be seen in Figure 2.15, indicating an inverse relationship between cell viability and incubation time.

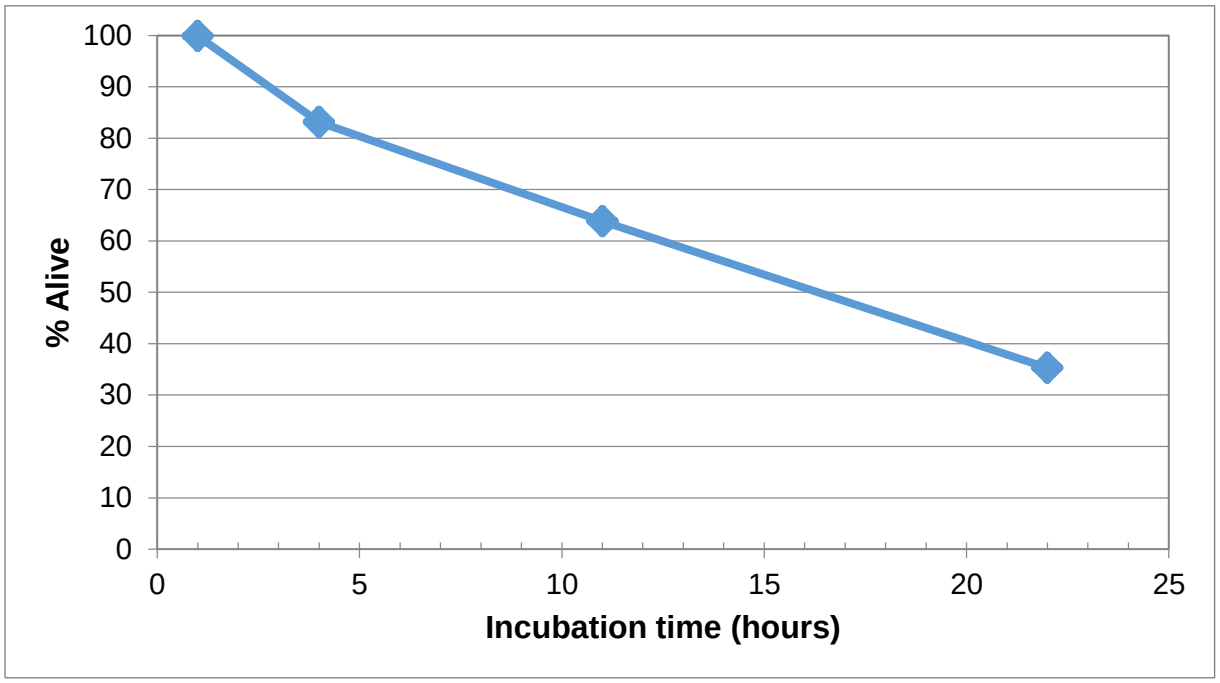

Figure 2.15: The effect that incubation time of the CB-PAA nanoparticles with the HeLa has on cell viability. Hela cells were incubated with 0.8 mg/mL CB-PAA particles and after washing the cells, they were exposed to 25.4 ± 1.6 mW/cm^2 for 40 min. Measurements were taken with counts from 10 different locations using a Live Dead assay of calcein AM and propidium iodide. Each point represents about 440 to 2800 cells.

2.4.5 Cell Viability as a Function of Intensity

This was done in the same manner as the incubation experiment, with 0.8 mg/mL CB-PAA growth media for cells while being exposed, but the incubation time was 24 h for each petri dish. The intensity of the petri dishes was varied by changing the voltage to the LED array. Intensities were measured at each voltage with a power meter to confirm intensity. The results of the varying intensities can be seen in Figure 2.16. There might be an inflection point after 13 mW/cm^2, but more experiments would need to be done to confirm that. Measurements for each point were only taken once, with an

average of 1640 cells for each data point. This made it difficult to determine if there is an inflection point. This result did continue to decrease as the intensity increased, as expected.

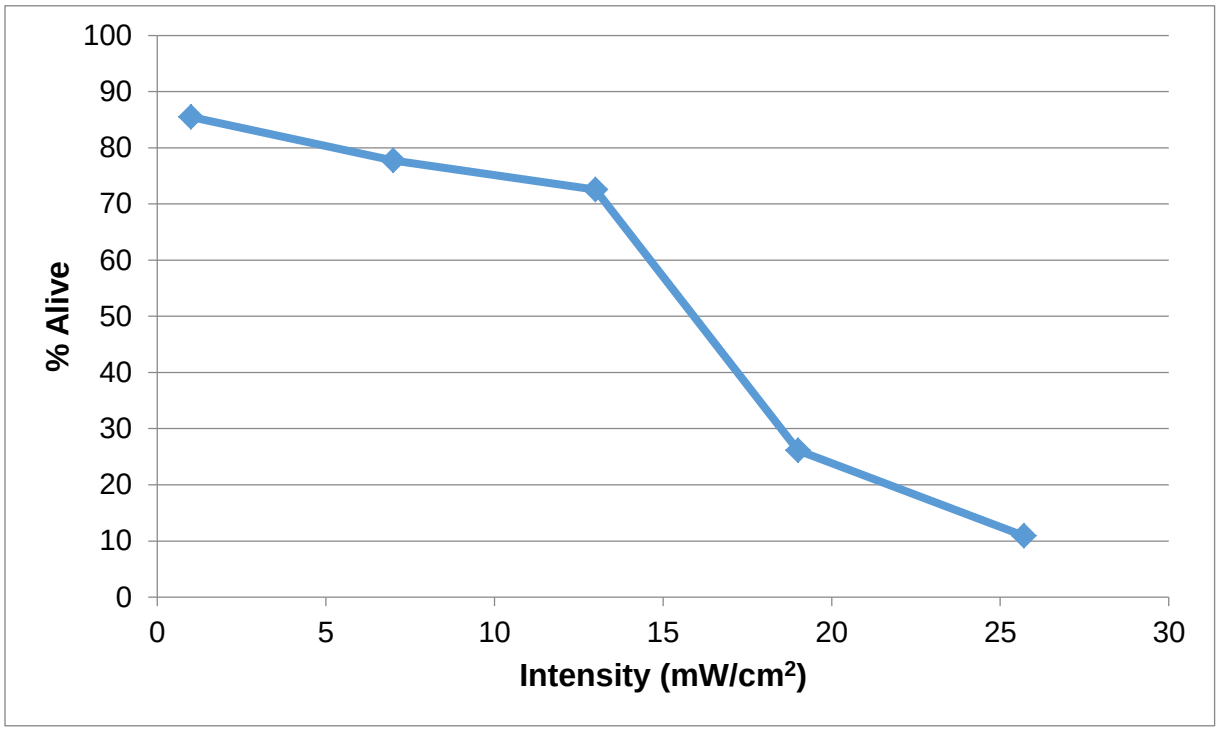

Figure 2.16: The effect of intensity of light on cell viability. Cells were incubated with 0.8 mg/mL CB-PAA particles for 24 h. Cells were exposed after washings for 40 min, and using a Live Dead assay, counts were taken from 10 different locations on the petri dishes 2.5 h after exposure. Each point represents about 1400-1800 cells.

2.4.6 Cell Viability as a Function of Time after Exposure

Again this experiment was similar to the previous two, except a 24 h incubation and maximum intensity were used. The dependence on time after exposure can be seen in Figure 2.17. Minimal cell death occurred immediately after the exposure time. With 0.8 mg/mL, 18% of the cells still remained alive after 2.5 h.

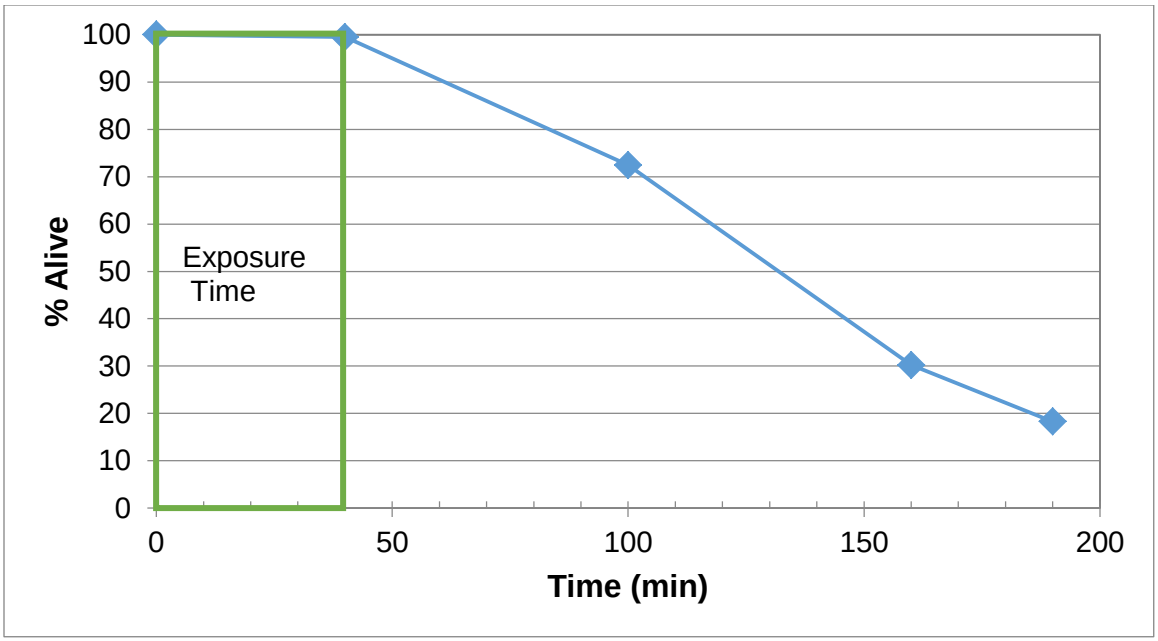

Figure 2.17: Time dependence of mortality of the HeLa cells using 0.8 mg/mL CB-PAA particles with 40 min exposure at 25.4 ± 1.6 mW/cm^2. Cell mortality was measured using a Live Dead assay. Each data point represents about 2600 to 3500 cells, and the data points were taken from 10 images captured at different locations on the petri dish.

2.4.7 Blank Particles and Dark Toxicity

To validate that the particle matrix was not affecting the cell viability, a petri dish of HeLa cells was incubated with a solution of 1.4 mg/mL blank PAA particles. After washing the cells, they were exposed to light for 40 min., and monitored 2.5 h later. This test showed no statistical cell death. This result, along with the result of the petri dish with no particles (shown in Figure 2.13), confirms that it is not the light source alone that is killing the cells. Another possibility tested was whether the particles themselves are toxic in the dark. To confirm that this was not the case, an MTT assay was done with varying concentrations. The results in this case can be seen in Figure 2.18. Evaluating the MTT assay and the fact that, after 24 hours of incubation, there were less than 1% dead cells measured by the live dead assay, it is possible to

conclude that the particles by themselves are not significantly toxic at these concentrations.

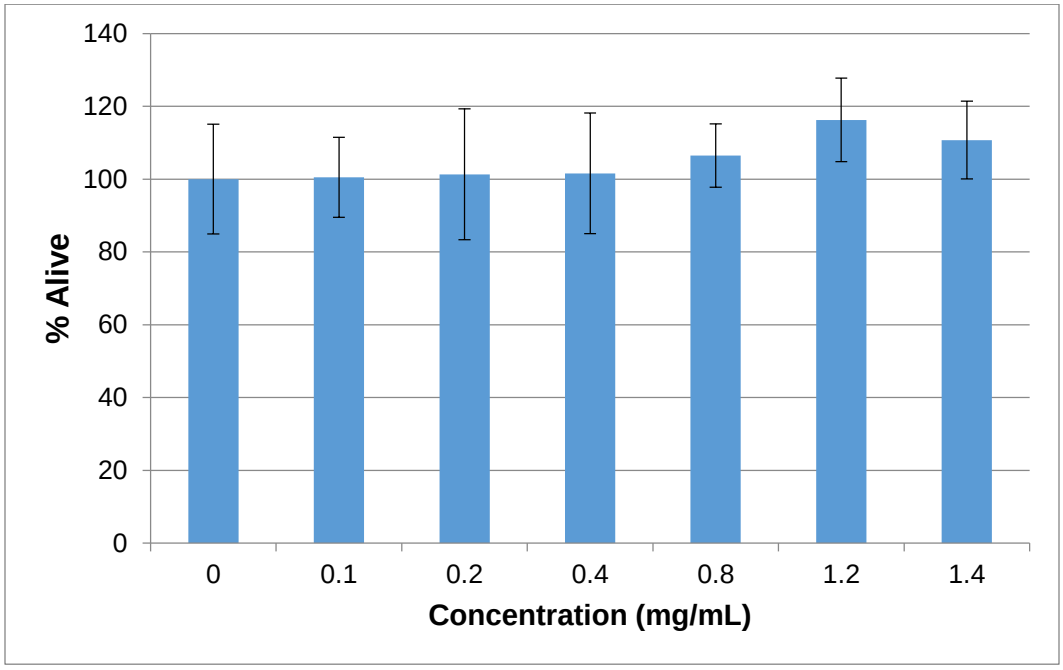

Figure 2.18: MTT assay results show the dark toxicity at varying concentrations of CB-PAA particles incubated with the HeLa cells for 4 h. Absorption depends on the MTT reagent that entered the living cells.

2.5 Discussion

There are a lot of different aspects to consider when describing the effectiveness of CB-PAA. Initially, the tools that were used to characterize the particle will be discussed. That will be followed by a discussion about HeLa cells, how cell viability was measured, toxicity of competing gold nanoparticles, absorption of particles compared to other systems, the light source, hyperthermic results compared to gold, how PTT compares to other thermal systems, where particles accumulate, biodegradation of particles, particle bioelimination, and other future work with tumor delineation.

2.5.1 Zeta Potential

The zeta potential of the CB-PAA particle was +6.9 mV. It is incorrect to believe that this is a direct measurement of charge, which has a major impact on particle uptake. The zeta potential is an electrokinectic property of the electrical double layer surrounding the object, or the particle in this case, but it is not an actual measurement of the surface charge. [203] It is actually the potential difference between the stationary layer surrounding the particle and the medium. So the particle charge does affect the zeta potential. The higher the zeta potential in a similar medium generally means the higher the surface charge. The machine measures the velocity of a particle in an electric field to determine the electrophoretic mobility (U_E). [203] Using this value in the Henry's equation (done by the computer), the zeta potential is calculated. [203] Since zeta potential is also dependent on the solution, there can be major changes in zeta potential when there is a change in pH or in salt concentrations. The change of 1 pH unit from 7 to 6 can result in a drop from -20 to -10 mV, as seen with carboxylated fullerene. [31] For this reason, the zeta potential was measured in Millipore water. There may be some error from the amount of dissolved carbon dioxide in the solution. Other sources of error are contaminants, like dust, bacteria, small molecules etc. Increasing the zeta potential by increasing the positive charge would be one method of increasing particle uptake, which will be discussed later.

2.5.2 Particle Size

There are multiple methods of measuring the size of particles, and in the case of CB-PAA, dynamic light scattering (DLS) was used. The particle size was determined to be 96 nm, with a large distribution of sizes. The reason DLS was used is because it is

one of the best methods for determining the size of polymers in solution. DLS measures the fluctuations in intensity from a pulsed laser, caused by the Brownian motion of the particles. Brownian motion is the motion of atoms, molecules, and particles caused by molecular collisions. Larger particles have fewer fluctuations because they have less Brownian motion. Both the shape of the particle and contaminants like dust can affect the results. [83] Another method to determine size is to measure them visually with a TEM or SEM, which works well with rigid and conductive particle materials. Since polymer particles are not conductive, they need to be coated with gold in order to measure the particle size. In the case of polymers that swell in water, TEM and SEM do not function well. The vacuum used during the coating process removes all the water from the particles, shrinking them in size. Therefore measurements do not give an accurate representation of their actual size in solution. There are a couple of properties that are affected by the size, such as toxicity and cellular uptake, which will be discussed later. To improve the properties, the particle size can easily be changed by increasing the quantity of free radicals or increasing the amount of surfactant.

2.5.3 Particle concentration

The concentration of particles was measured in mg per mL, and many of the gold experiments are measured in either μM of atomic gold concentration, or nM of particle concentration. The reason for the measurements in mg/mL results from the particles coming from a lyophilized stock and not a liquid solution with a known concentration of particles. Converting mass to particle concentrations requires the density of the particles, which varies with batches.

Particle concentrations ranged from 0.2 mg/mL to 1.2 mg/mL. Estimations were made on how much the particle swells in the solution by using SEM sizing of other PAA particles, with size determined by the DelsaNano particle sizer. Then the density of PAA was estimated. With these two estimations, and using the average particle size, the concentrations of the particles were estimated to be 39 nM (2.3×10^{13} particles/mL) for 1.2 mg/mL, and 13 nM (7.7×10^{12} particles/mL) for 0.4 mg/mL. That makes the concentration of 0.4 mg/mL (13 nM) about 100 times the concentration of gold colloids used for PTT of HSC and HOC cells. [14] Besides the Kopelman group, other groups have used similar concentrations, as in the drug delivery of pancitaxel on PANC-1 cells using mesoporous silica. [43] How CB-PAA particle concentrations affect the toxicity, uptake, and PTT effectiveness will be discussed later in this section.

2.5.4 HeLa cells

There are advantages and disadvantages to using HeLa cells to determine the effectiveness of PTT or other therapies. HeLa cells are very robust, as mentioned in the introduction. Second, HeLa cells have poor uniformity from years and years of cross contaminations. It is estimated that around 20% of all HeLa cell articles are using cell lines that have been contaminated, but the National testing service estimates the cross-contamination between cell lines to be as high as 36%. [201] The poor uniformity actually can be advantageous. Homogenous cell lines may be, more or maybe less, susceptible to certain treatments. This lowers the accuracy of the results when looking at single cell lines and trying to predict the results for other cell lines. Because of the heterogeneous nature of HeLa cell lines, they actually may be a better representation of the effectiveness of a treatment. There are various tests that can be performed to

eliminate the problem of uniformity. One of the main tests that could be used is DNA profiling. [201] [204] Standard DNA profiling can be used, but also using amplified polymorphic short tandem repeats (STR) loci with PCR primers. [204] This test can be used for human forensic applications, and can cost less than $200 to test each cell line. [204] [205]

As a side note, cross-contamination is not the only form of error, or variable. There is evidence of researchers lying and using different tumor cells, monkey cells, or mice cells. [201] Many times, HeLa cells are just simply mislabeled. These issues should not be a problem with the CB-PAA tests, but they can make one doubt the results when HeLa cells are used.

2.5.5 Measuring Cell Viability

There are various other methods to check cell viability, such as trypan blue, MTT, live dead kit (calcein AM and propidium iodide), flow cytometry and many others. Each method has different properties that will affect accuracy, precision, measurement rates, and the ability to do multiple measurements on the same sample. The rate of the test can be very important in determining cell viability. Many quick methods can determine if the cell is living, but cannot determine if the cell can reproduce. This is why some of the longer tests that measure the amount of viable cells after regrowth can be more accurate. In many cases, it is a tradeoff that has to be decided: fast and easier versus time consuming and more accurate. This is a general rule with many exceptions, depending on the given experiment.

One of the most common methods of checking cell viability is trypan blue. [14] [126] Trypan blue is a dye that penetrates through the cell membrane of dead cells.

Cells are then usually counted by a hemocytometer. This method, though common, does not function well with blue particles. Not only does the absorption of the blue particles interfere with the measurements of cell viability, the cells cannot be exposed to the illumination source after trypan blue is added. The trypan blue would be another source of absorption, therefore adding another variable to the cause of cell death. Some of the initial tests done by Matt Waugh were done with trypan blue to see the feasibility of methylene blue dye loaded particles for photothermal therapy. The results showed feasibility of the particles, but there were large deviations.

The MTT assay is the preferred method to determine cytotoxicity of particles. The assay measures the amount of reduction of the dye nitrotetrazolium blue, 3-(4,5-dimethylthiazol-2-yl)-2,5-diphenyltetrazolium bromide, by cellular enzymes in living cells to a purple formazan molecule. [83] [206] Figure 2.19 shows this reduction of the MTT reagent.

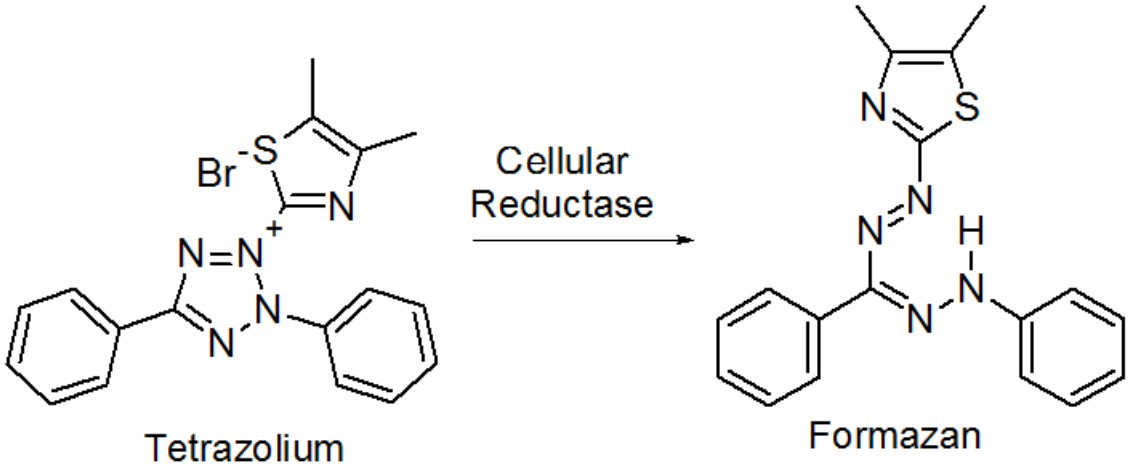

Figure 2.19: Reduction of the MTT reagent, tetrazolium, by cellular reductase, which is found in living cells. The final product is formazan, a violet dye that is soluble in DMSO. The percentage of viable cells is determined by comparing the absorption to that of a control. This reaction is not only affected by the enzymes present in living tissues that reduce nitrotetrazolium blue, it is also affected by cellular respiratory activity, and the phase of growth of the cell. [83]

The resulting formazan forms crystals that are not soluble in water and must be dissolved in DMSO or isopropanol/HCl. The absorption of the dissolved formazan crystals is measured in the range of 500-600 nm. [92] [206] Common errors with this test come from variations in absorbance between cell lines, errors from initial cell counts, and floating cells, which all together can cause deviations of ±15%. [206] Other errors may come from chemicals or enzymes that may reduce the dye. [206] This has been shown when there is mitochondrial oxidative stress caused by ROS. [46] [54] In fact, it is recommended that the MTT assay not be used when ROS can be created. [46] [54] There have also been some aberrant results with free amine groups on NP surface, as in case quantum dots. The problem with the results came from the lack of evidence to conclude if this is caused by surface charge of the particle, and not by the quantum dots themselves. [27] Another problem with MTT assay is that it cannot distinguish between cytostatic and cytocidal effects to the cell. [206] Overall reproducibility of MTT assays has been shown to be good, and is often ≤ 10% between replicated wells. [206]

In the case of CB-PAA, one of the main sources of error with the MTT assay to determine dark toxicity of the particles comes from the short incubation time with the particles. A 24 h to 48 h incubation would have been much more appropriate, or maybe even longer. Future experiments should be done to verify the long term effects of CB-PAA, whether there are any cytostatic or cytocidal effects to the cells.

Calcein AM and propidium iodide, live dead assay, was the method of choice to determine cell viability after PTT therapy. The reasons it was chosen are because it is simple, cells vitality can easily be determined under a microscope, and it is quick. The

calcein AM dye readily penetrates cellular membranes. After penetration, the acetoxymethyl ester is then hydrolyzed by intracellular esterases to form a fluorescent green dye at 514nm. [207] Nonviable cells lack the esterase necessary to convert the molecule to its fluorescent form, making it an ideal indicator for viable cells. The counterstain, propidium iodide (PI), a non-permanent molecule, binds to nucleic acids to produce a red fluorescent complex with emission peak at 617 nm. [208]

The main issues and errors arose from counting the cells and when the cells were undergoing blebbing. Often cell counts deviated from the time before exposure and immediately 2.5 h proceeding exposure. This came from cells floating to the surface of the solution, final image locations not matching the preexposure image locations, changes in cell density on the petri dish, and difficulty distinguishing dead from living. Many of the cells were in the process of dying when images were taken. There were ranges of red nuclei from barely visible to completely obvious.

There are several other methods to determine cellular viability. Crystal violet [137], Sulforhodamine B (SRB) [111], Cell Titer-Glo Luminescent cell viability assay [69], Cell Titer-Blue cell viability assay [69], WST-1 assay, XTT assay, MTS cytotoxicity test, LDH assay [46] [209], Comet assay [27], and propidium iodide with flow cytometry [27] are many of the different methods of determining cell viability. Many of these methods, WST-1 [83] [92], XTT [39] and MTS [16] [87], are very similar to the MTT assay, but utilize different chemicals. Each method has its advantages, as is the case with WST-1 assay, which utilizes a water soluble reagent, 4-[3-(4-iodophenyl)-2-(4-nitropheynyl)-2H-5-tetrazolio]-1,3-benzene disulfonate. This removes some error that is in the MTT assay of having to remove the solution from the wells to add a new solvent

to dissolve the final product, as is the case with formazan requiring the solvent DMSO. [83] [92] In the case of MTS, its change in color at 490 nm correlates with the cell's metabolic activity of mitochondrial dehydrogenases reducing MTS educts to formazan. [87] The others measure cell viability by quantification of ATP (Cell Titer-Glo Luminescent cell viability assay), metabolic activity of cells (Cell Titer-Blue cell viability assay), cell disruption (lactate dehydrogenase or LDH assay), and DNA damage through electrophoresis (Comet assay).

2.5.6 Toxicity of Competing Gold Nanoparticles

It is necessary to compare the toxicity of Coomassie Blue PAA nanoparticles to that of other particles. Currently, the standard particles are gold nanoparticles. Many assert that gold is not toxic, but there are actually conflicting results. [83] One of the major reasons for conflicting results, not only with gold, is caused by the lack of standards when determining the toxicity of particles. The experiments had variations in types of cells, particle types, particle functionality, particle shape, methodology of determining toxicity (MTT, Trypan blue), and concentration of particles. Most toxicity information about gold would state that it is nontoxic, but there are several cases where it shown that it may be extremely toxic to mildly toxic. Since there are different standards, it is difficult, if not impossible, to make solid conclusions on the toxicity of gold. In the next section there will be some examples of when gold or a method of implementing gold shows toxicity.

Often the toxicity of particles is determined by *in vitro* measurements, which lead to some false conclusions about the particle’s toxicity. In many cases, chemicals and particles that are deemed nontoxic *in vitro* cause inflammation. There are several

issues that have been observed when using particles *in vivo*, but let's first discuss the cytotoxicity of CTAB (Cetyl trimethylammonium bromide) nanoparticles *in vitro*.

As mentioned, toxicity is not always caused by the particle, but by impurities or remaining components from the production of the particles. One of the primary causes of toxicity in the literature is not caused by the gold nanoparticles but by CTAB, the surfactant used in the formation of gold particles. CTAB has been shown to be toxic with an IC_{50} < 1 μM, and because of this, it must be washed off or replaced from the surface of gold nanoparticles. [8] [9] [10] [83] [87] [210] [211] One of the reasons that CTAB on the surface of gold is so toxic is because of the rate that gold can desorb the CTAB and adsorbs different media proteins within just 5 min of being mixed. [209] This is also good because CTAB can be easily removed and replaced with coatings like BSA, PAA, or PAH. [9] Another reason CTAB on gold is so toxic is because it creates ROS on its release from the surface of gold. [87] The following are a few examples of the toxicity of CTAB based particles. For example, there is 65-75% loss of viability of HT-29 cells when introduced to a 0.4 nM nanorod particle concentration, but after replacing the CTAB with a PAA capping, there was almost no loss in viability. [9] There are still problems with cell dying with PAA gold particles when their concentration is above 1 nM. [9] Another example of the toxicity of CTAB showed that particles not washed were toxic at 0.05 μM to K562 cells, but citrate- and biotin- modified particles with a concentration of 250 μM were not cytotoxic. [211] It is important to note that they used the MTT assay, which is sensitive to ROS. With the removal of CTAB it is important to make sure the new coating is nontoxic. [83] Gold also needs to be

protected because unprotected gold particles are not stable and will aggregate in chloride solutions.

Gold nanoparticles, naked or with other coatings than CTAB, in most cases show no cytotoxicity *in vitro*, but there are instances of cytotoxicity. Using an MTT assay, K562 leukemia cells were incubated in gold nanoparticles for 5 days, B the concentration of gold being 25 μM. [211] The particles had sizes of 4, 12, and 18 nm, and each of them had no effect on cell viability. Another group determined, using MTT assay, that 10 to 50 nm GNPs, incubated in human dermal fibroblasts–fetal (HDF-f), showed no toxicity with concentrations up to 300 μM. They said gold nanoparticle concentration, but probably meant the gold atom concentration coming from the particle. [212] As the particle concentrations increased, the cell morphology changed, and was especially visible at 300 μM. There is another *in vitro* study that showed that gold nanoparticles are also nontoxic to HeLa cells. [91] Gold particles showing no sign of toxicity *in vitro* is very common. There are some cases that are different, though not as frequent as the nontoxic cases. For example, Tauredon gold particles and gold thiomalate had high IC_{50} values of greater than 10,000 μM for HeLa (Cervix Carcinoma), SK-Mel-28 (Human Melanoma), and L929 (mouse fibroblasts). However, with the j774A1 (mouse macrophages) cell line, Tauredon gold only had an IC_{50} value of 250 μM. [213] Another example is 13 nm citrate nanoparticles, which showed toxicity in human lung carcinoma cell line (A549), but not to human liver carcinoma (HepG2). [203] *In vitro*, 20 nm gold nanoparticles surface coated with fetal bovine serum caused oxidative damage to lung fibroblasts (MRC-5 human fetal lung fibroblasts). [214] The particles ranged in concentration from 0.1 nM to 1nM, and were incubated for 24 h, 48h,

and 72 h. Each time period showed about a 6-8% decrease in viability. As has been seen using MTT assay and other methods, the toxicity of gold depends heavily on cell type, size, and coating. [83] [213]

In vivo differs from *in vitro* studies because there are more cell types, biological systems, and interactions between them. Gold nanoparticles not only have shown signs of causing inflammation in the body, but they also cause an increase in leukocytes [18] [83], signs of acute liver inflammation, and apoptosis in the liver. [49] These were 13 nm PEGylated gold nanoparticles with concentrations of 0.17, 0.85 and 4.26 mg/kg in mice. Inflammation is not the only response. When concentrations of gold were 2000-3000 nanoparticles per cell, the cytoskeleton showed signs of damage. [87] In another study, rats showed various types of cellular damage done by PEGylated silica/gold nanoshells. [83] Most of the rats showed signs of necrosis of hepatocytes when injected with concentrations of 0.75, 0.150, 0.225, and 0.300 mg/kg. On the other hand, Mesogold, a common alternative medicine, has been ingested for years with no known side effects. [215] It is important to remember that even with concentrations of gold particles that are 100 nM, 20 ppm or 100 μM gold concentration, particles will have a much lower toxicity because they are ingested and not injected.

Size is one variable that can be altered on gold nanoparticles, and in fact, toxicity is also dependent on the size of the gold nanoparticles. Gold spheres, near the bottom of the nanometer scale, tend to be much more toxic than their larger counterparts. For example, in one study they showed that 1.4 nm gold clusters were toxic with an IC_{50} value ranging from 30 to 46 μM, while larger 15 nm nanoparticles showed no toxicity. [213] Another study showed that sizes ranging from 0.8 to 1.8 nm are toxic and have

IC_{50} values ranging from about 20 - 300 μM. [213] This is common, and it is often assumed that particles larger than 3 nm are chemically inert. [209] There is some variation in toxicity results when looking at naked gold nanoparticles. Naked gold nanoparticles, ranging in size from 8 to 37 nm, and at concentrations of 8mg/kg/week, cause severe sickness to mice, with the majority of them dying within 21 days. [91] [209] While 5, 50, and 100 nm naked gold nanoparticles administered to live mice at 8 mg/kg/week survived. [91] Modifications, such as pH5N1 and pFMDV peptides, can limit the toxic effects caused by size. [91] When 17 nm gold nanoparticles were modified, the lifespan of mice increased from 21 days to more than 50 days. Lysozyme and bovine serum albumin (BSA) modifications also increased the lifespan of mice, but it only increased it to 22.3 and 27.5 days respectively. [91]

Toxicity based on size is not unique to gold, and is seen in silver particles as well. [22] As mentioned in the introduction, the toxicity of PAA nanoparticles is minimal or zero even at extremely high concentrations, 500 mg/kg in a rat. To confirm the previous tests on the dark toxicity of CB-PAA, a MTT assay was done after 4 h of incubation, and it showed no toxicity all the way to 1.4 mg/mL (Figure 2.18). Another couple of reasons that CB-PAA are nontoxic to HeLa cells is because only 1% of cells from the LIVE/DEAD assay were dead, and the cells also continued to grow when incubated with cells for ≥ 24 h. Although not many dead cells were seen in the solution, some of the dead cells could have been washed away.

As can be seen above, gold particles also don't show much toxicity *in vitro*, but *in vivo* it is known to cause an inflammatory response, cell necrosis, or even death at concentrations well below that of CB-PAA or the concentrations previously tested in rats

(Please reference introduction for toxicity of PAA). As shown, gold nanoparticles, like PAA, also have toxicity issues arising from starting materials. The CB-PAA particles were thoroughly washed with ethyl alcohol and water. With the number of washings, and if the starting materials did not adhere to the particles, most of them would be washed way. In the case of Brij 30, if the surfactant was just in the solution, then with the 20 washings, it would be down to about 9.0×10^{-20} mg for the entire batch of particles, which would prevent any issues from starting materials. Another source of concern for CB-PAA particles are the latency effects of the Coomassie Blue derivative after biodegradation. At this time they are still unknown and could lead to future issues.

2.5.7 Absorption

Since Coomassie Blue has a strong absorbance at 600 nm (Figure 2.8), it is only a moderate candidate for PTT. The deep blue color that can be seen in Figure 2.5 makes the CB-PAA nanoparticles a great candidate for tumor delineation. Gold, on the other hand, does have an advantage over dye systems in tunability. By simply changing the size and shape of the particles, one can get different colors. Colloidal gold spheres can only be shifted a little, and their absorption peak is usually centered around 530 nm. On the other hand, gold nanorods and shells can be shifted to absorb in the red and be in the cells optical window. Nanorods can be tuned to one of their wide range of possible wavelengths by changing their aspect ratio, and gold shells can be tuned by changing their size and shell thickness. [42] With dyes, a different dye must be synthesized or found. Not only can that be difficult, but the new dyes will also have varying toxicities, photobleaching tolerances, and other issues. [19] One of the dyes

that have been used in PTT previously is Indocyanine Green, which has an absorption maximum at 778 nm.

The frequencies where the particles absorb are not the only important factor in choosing a photosensitizer, but also efficiency the dye or particle at absorbing light. Absorption coefficient depends on size of the particle, absorbing and scattering cross sections, shape of particle, surroundings, and material of the particle. [140] As previously mentioned in chapter 1, the molar extinction coefficient is the common method of comparing, but is not a completely accurate comparison. Molar absorption coefficients only are important when dye amounts are the same as particle concentrations. This is often not the case, and more often than not there will be significantly more dye molecules in the cell than particles that could fit in the cell. The high extinction coefficient of CB-PAA, 1.4 x 10^8 $M^{-1}cm^{-1}$, is due to 17% of the mass of the particle being Coomassie Blue. The extinction coefficient of 40 nm gold spheres is about 1.5 orders bigger than CB-PAA nanoparticles. [140]

Gold nanocages have the highest extinction coefficient, followed by gold nanorods, and then gold nanoshells when comparing particles with similar optical densities and that have a wavelength of 800 nm. [12] One issue with nanorods is that their absorption is dependent on the direction of the rod. [42] This effect will be more obvious when the excitation source is polarized.

2.5.8 Light Source

The light source used was a 256 LED array, which differs from most groups who use lasers. There are several different types of lasers used, including Ti:Sapphire, argon ion, and diode lasers. Irradiance (power/area) or fluency (energy/area), exposure

time, flux, wavelength, continuous wave or pulsed, pulse length, and pulse frequency are the main variables manipulated to increase the photothermal effect.

One of the most important variables to consider in choosing a light source is the overlap between the absorption peaks of the particles and the emission peak of the light source. In the case of CB-PAA, the emission peak of the LED array was at 590 nm, which matches up well with Coomassie Blue absorption peak at 600 nm (Figure 2.8). Other groups using gold will often use nanorods that absorb around 800 nm, and a Ti:Sapphire laser that emits around 800 nm.

The next thing to consider is the irradiance of the light source. The irradiance of the LED array was 25.4 ± 1.6 mW/cm^2, which is quite small compared to many of the gold nanoparticles therapies. HeLa cell death was even observed when the irradiance was down to 1 mW/cm^2 (2.4 J/cm^2), as can be seen in Figure 2.16. One of the simplest PTT experiments to compare to CB-PAA used a CW Argon ion laser (514 nm) to excite anti-EGFR spherical gold nanoparticles. [14] The particles were incubated with HSC (epithelial tumor), HOC (epithelial tumors), and HaCaT (human keratinocyte, non-tumorous cells that do not overexpress EGFR), with a concentration of ~0.2 nM for 40 min. The cells were then washed and irradiated for 4 min at various levels of irradiance. The HSC cells suffered some death at 25 W/cm^2, but none at 19 W/cm^2. They observed cell death of HOC cells at 19 W/cm^2, but none at 13 W/cm^2. HaCaT 57 cells did not die at any of the tested conditions. This experiment was later repeated with anti-EGFR gold nanorods that had an absorption maximum around 800 nm. The particles attached to both the HSC and HOC malignant epithelial cells, but not to HaCaT cells because they do not overexpress EGFR. [216] The particles were excited for 4 min with

CW Ti:Sapphire laser that had a wavelength of 800 nm. Cell death of HSC and HOC cells was observed at 10 W/cm^2 (2.4 kJ/cm^2), and complete cell death at 20 W/cm^2 (4.8 kJ/cm^2). HaCaT cells, also in presence of nanoparticles that had been washed away, didn't show cell death until around 15 W/cm^2 (3.6 kJ/cm^2). The fluencies were actually quite high. At the other lower end of fluencies, one can see effects, such as blebbing, at fluencies as low as 30 J/cm^2 (1 W/cm^2) for 30 s. [217] This was the case of KB cells when they endocytosed gold nanorods with an absorption at 815 nm, and excited at 795 nm. The exposures were 30 s, and the fluencies ranged from 15 to 120 J/cm^2. [217] The fluencies in the CB-PAA experiments showed almost complete death at 61 J/cm^2. This is much lower than the kilojoule level fluencies with some experiments, but just above the 30 J/cm^2 where other groups began seeing blebbing. [14] [217] In this case of photothermolysis (photoablation) the fluency is small but the irradiance is extremely high. Cells incubated with high concentrations of AuNR started showing signs of cell damage around 18 mJ/cm^2 (37 W/cm^2), but no cell death until the higher irradiances. This was done with a Ti:Sapphire laser tuned to 790 nm, the particle's absorption peak at 800 nm, pulses of 100 fs at 80 MHz, and exposure time of 504.60 μs. [10] Another group showed blebbing with internalized AuNR under fs-pulse power at 3 J/cm^2 (48.6 W/cm^2) when using photothermolysis of KB cells. [218]

The max intensity coming from the light source before it causes damage to the cell is dependent on the wavelength, irradiance and exposure time. For example, EMT-6 breast cancer cells could withstand fluencies of 93 mJ/cm^2 (185 W/cm^2), but died at fluencies of 113 mJ/cm^2 (222 W/cm^2). [10] Also, as mentioned, HaCaT cells did not die at 20 W/cm^2 when exposed for 4 min with no particles. Using these as references, and

knowing the maximum irradiance of the LED array was 25.4 ± 1.6 mW/cm^2, there should be no concern about damaging healthy tissue surrounding a tumor with the light source alone.

2.5.9 Hyperthermia of HeLa Cells

As mentioned previously in Chapter 1, apoptotic death, or programmed death, is the ideal method of cell death. The problem with this is that the temperature range is limited to about 42°C - 45°C, with some exceptions. With blood perfusion affecting the temperature of the cells, it may be difficult to stay within the range. Many groups, much of those working on gold nanoparticles, are actually doing photothermolysis instead of hyperthermia. This leads to necrosis which has its own issues. CB-PAA is believed to go through an apoptotic pathway, but that has not yet been confirmed. The cleavage of PARP is one method to determine apoptosis that could be tested. [219] Studying cell death as a function of time after photothermal exposure, seen in Figure 2.17, reveals that cell death is not immediate. This is most likely a result from apoptotic death taking time to conclude. In the case of gold nanoparticles, they usually caused necrosis, which is more immediate.

The 2.5 h timeline was used for the following reasons: most cells were dead after 2.5 h when concentration was 1.2 mg/mL (Figure 2.17), and to limit the time the cells were without nutrients in the experiments using DPBS. The cell death is dependent on illumination intensity, wavelength, exposure time, particle concentration, absorption coefficient of particles, particle location, cell type, and cell environment. Figure 2.13, Figure 2.15, and Figure 2.16 show how the cell environment (DPBS vs. cell media), incubation time, and illumination intensity affect cell death. When examining cell death

as a function of concentration, and comparing it to a function of incubation time, illumination, and time after exposure, it is possible to see the difference in cell viability from cells exposed to the light while in cell media and to those exposed to the light while in DPBS. The difference between the cells in DPBS (Figure 2.13) compared to average cells in media (Figure 2.15, Figure 2.16, and Figure 2.17) is approximately 10% increased viability. This is as expected, since the cells are not receiving nutrients during exposure and following exposure, which will make them weaker and more susceptible to die. The results from illumination, intensity, and incubation time are also as expected. They showed an increase of cell death with increases in intensity or incubation time.

Each of the experiments used a wide range of cells for each data point. Cell counts ranged from the low hundreds all the way to a few thousand depending on the experiment. Experiments did take a long time to complete, which is the reason that they were not repeated. Another source of inaccuracy is that cells have a higher cell survival rate when they are heated in mitotic phase and the S phases. [220] Some of my cells were in the growth phase and others were in the stationary phase, which will increase the inaccuracy of the measurements. In the future, work should be done to get better statistical results, error bars, instead of just relying solely on the high cell counts.

2.5.10 Required Heat for Cell Death

The heat required to kill cells is dependent on exposure time, cell type, blood flow, particle location, and other environmental factors. It was determined that it would be extremely difficult to calculate an accurate estimation of the heat in cells during the experiments using experimental results. So it was decided to compare the results to

other groups to estimate internal heat. HeLa cells are hardy cells that can grow well in harsh conditions. [134] [137] [221] They can survive at 41°C for over 57 h, but all the cells were dead after 96 h. [221] At 42°C, it takes 14 h to kill off all of the cells, and 3 h to kill all of the cells at 44°C. Another group who did a similar experiment had about just over 0.1% alive after 3 h at 44°C. When HeLa cells are heated to 46°C, some of the cells are still alive at 20 min, but none are living after 30 min of exposure. For 45°C it takes about 1 h 10 min to kill all of the cells. Knowing this, it can be concluded that the effect of the CB-PAA particles on HeLa cells is equivalent, in effectiveness, to heating HeLa cells to around 45-46°C. [134] [221]

One article calculates that cell colonies need to be greater than 1.1 mm in diameter for intercellular conditions to reach high enough temperatures for hyperthermia because of the rate of heat diffusing from the tumor. [222] They also figured that nano-scale heating effects are negligible. This work and other work other groups have shown cells can be still killed without a noticeable temperature change, or are much smaller than the 1.1 mm required. [14] [110]

Temperature is also dependent on the number of particles and their vicinity to one another. [223] [224] If there is a 4 x 4 array of 30 nm particles, separated by 150 nm, and exposed to 10 kW/cm^2 excitation, the particles will have a max temperature increase of about 18°C. For a single particle under the same conditions, it has a max temperature increase of 5°C. [224] Previously, it was assumed that the entire cell was heated. One other possibility is that the particles aggregate in one type of organelle in the cell, increasing the local concentration of particles to extent that they easily destroy that organelle upon exposure. This could lead to cell death, but not an immediate cell

death, as with photothermal ablation. With the very low irradiance of the LED array, this could be a possible pathway. If this is the case, the pathway and internal targeting of particles would be vital to increasing the effectiveness of PTT. There needs to be more work done on the pathways of cell death, location of the cells, and how PTT affects the various internal processes of the cell.

2.5.11 Thermotolerance

Thermotolerance, the ability to withstand raised cellular temperatures, can hinder the effectiveness of PTT. As mentioned previously in chapter 1, thermotolerance occurs after a pretreating of cells at a raised temperature. There is possibly some evidence that continuously heated cells also can gain a thermotolerance, but this could represent the point when only the more heat tolerant cells are remaining. Other therapies, such as antibiotics, have similar characteristics: the least tolerant cells go quickly, but sometimes the more tolerant cells are durable enough to last a much longer time, or even survive the therapy.

After a period of time, depending on the cell type, cells do begin to return to normal tolerance levels. With CHO fibroblasts it took just over 3 days to return to normal [225], and with most cells it takes about 1-3 days. [133] This is not the case with cells grown at 39°C for 2 and 4 days, instead of the 30 min to 1 h pretreatment, which showed resilience still after 3 months. [221] HeLa cells preheated at 42°C didn't show thermotolerance when reheated to 42°C [134], but HeLa cells heated for 1 h at 40°C were much more likely not to signal apoptosis at temperatures between 42-45°C. [120] Thermotolerance of HeLa cells lasts less than 13 days after being pretreated for 1 h at

44°C. [137] The level of thermotolerance begins to level off at or around 2 - 4 h and has shown to max out around 12 h between initial dose and the next dose. [137]

If thermotolerance becomes an issue *in vivo* for CB-PAA, there is a workaround, with the first being longer exposure times. [136] [226] Cell viability decreases exponentially with time at elevated temperatures. [137] Another is to wait until after the cells have returned to normal, not thermotolerant, which can be a couple of weeks. [137] If this does not work, it may be necessary to heat above the ideal temperatures that cause apoptosis so that the issues that arise from thermotolerance are overcome. [219]

2.5.12 Other Thermal Therapies

Indocyanine Green (ICG) has been used in the past for the photothermal therapy. There are several problems with using it as a free dye. First, the concentration and nature of the solvent lead to significant effects on it absorption properties. [227] [228] [229] Second, it is not very stable with increases in temperature or under excitation. [230] [231] Third, ICG binds readily to albumin and high-density lipoproteins (HDLs) in blood plasma, resulting in a red-shift in its optical absorption. [139] The dye itself is nonselective for cancer cells and is cleared rapidly from the body with a biexponential plasma clearance half-life of 2-4 min. [139] The last issue for using ICG solely for PTT is that it can also be used for photodynamic treatment. To overcome these issues, a group loaded ICG into a PAH (polyallylamine hydrochloride) cationic polymer matrix. [139] The particle had a high loading efficiency of 36%, but ranged in size from 60 nm to 2000 nm. There was still thermal degradation and the ICG was eliminated from interacting directly with the cellular environment. [232] Encapsulation

lowered the absorption of ICG by 35% at 780, and 25% at 700 nm. The particles were targeted with EGFR (epidermal growth factor receptor) antibody and used on hybridoma cell lines 1483, SiHa, and 435 at concentration of 0.4 mg /mL. EGFR is over expressed on breast, cervical, lung, and prostate cancer cells. The cells were excited with a continuous wave diode laser that emits at 808 nm and had an intensity of was 3-6 W/cm^2. After 200 s of exposure, the 6 W/cm^2 sample was about 100% dead, the 3 W/cm^2 was 30-65% dead, and uncoated was 10-50% dead. [139] CB-PAA particles took longer to kill, but they showed no cell death to uncoated particles.

The CB-PAA system described is advantageous because the Coomassie Blue dye is covalently linked to the matrix, unlike other dye-based systems such as Indocyanine Green. This is beneficial because the dye is part of the matrix and cannot leach out from the particle, which lowers absorption and can be toxic. Notably, CB does not fluoresce and does not create singlet oxygen under illumination. Thus, CB is not active as a PDT source under illumination. On the other hand, ICG's absorption is in the center of the optical window, instead of being on the edge like Coomassie Blue.

Some groups have been using magnetic particles, mostly $La_{0.73}Sr_{0.27}MnO_3$, magnetite (Fe3O4), and maghemite (Fe2O3 or γ-Fe2O3), in an oscilating magnetic field to produce heat through Néel relaxation. [110] [111] [125] The core size of the magnetic particles above is 5-15 nm with the most promising size ranging from 11- 13 nm. [125] These particles were delivered by cationic liposomes. [125] They were able to completely destroy a mammary carcinoma with tumor sizes up to 15 mm. [219] That is a very large tumor size to be affected by thermal therapies. There has been success with magnetite particles causing complete regression in clinical trials. [125] With time,

the magnetite particles aggregated in the liver and the spleen of MCL treated mice and within 30 days were cleared from the spleen by fixed macrophages and liver by Kupffer cells. [125] The problem with iron oxide is that the particles degrade rapidly in acidic conditions, such as is the case in the lysosomes, which raises the ROS levels in the cell. [46]

Using magnetism can be better than photothermal therapy for tumors deeper than 1 cm from the surface. The major problem with magnetic hyperthermia is that they are difficult to keep contained to a local volume without heating surrounding tissue. [124] Any free floating particle that is affected by the magnetic field will also be heated. This can cause major problems if there is a buildup of particles in a place like the liver or spleen.

Photothermal ablation uses high powered laser pulses, usually with particles, to destroy cells. It works by making small explosions, cavitations or bubble formations, by heating the particles above boiling points of the solution. [10] [210] [218] Not only has this technique been used with cancer cells, it has also been used to kill bacteria like Staphylococcus aureus. [233] In this instance, 10-40 nm gold spheres were pulsed 100 times with 8 ns pulses and with a fluency of 0.5 J/cm^2. The particles were heated to a temperature of 1250°C, with particle melting temperature being around 1063°C. The pressure caused by the extremely hot particles was 10^7 Pa and lasted for about 0.1-5 μs. This works fine with spheres because they will remain spheres after solidifying, but one must be careful with gold rods because they become spheres if they melt. [210]

A little less known thermal therapy is heating small gold nanoparticles with radiofrequencies. [147] The gold nanoparticles are heated with 200 W - 1000 W radio

waves with a frequency of 13.56 MHz. Gold nanoparticles that were administered at a concentration 67 μM/L showed about 98% cell death of Panc-1 and Hep3B when dosed for 2 min. This therapy has a lot of collateral damage. In the absence of gold nanoparticles, there was 21% and 26.4% cell death respectively, but with large standard deviations.

2.5.13 Accumulation, Biodegradability, and Bioelimination

What the particles do after therapy is almost as important as the therapy itself. As mentioned, many cancer therapies are extremely toxic and can cause severe side effects. Both gold particles and PAA based particles tend to accumulate in the spleen and liver, but this is dependent on size, shape, and surface functionality. [32] [60] [83] [209] [234] [235] Inside the cells, the particles were mostly found in the lysosomes to be degraded, but in the case with indigestible materials, such as gold, they will remain there. [82] [234] There is a chance that nonbiodegrable particles can be exocytosed from the cell, but they will generally remain within the cells for a considerable time before this occurs. [82]

When performing photothermal therapy, particles may need to be manipulated to increase concentrations in certain parts of the body or certain parts of the cells. Altering surface functionalization effects accumulation locations and pathways of endocytosis. One group showed that TAT peptide dextran capped iron oxide particles had a small increase in the quantity found in the lungs. [236] Changing the surface functionality might also change the pathway (e.g. BSA promotes caveolae-mediated endocytosis), which could lead to different organelles being targeted during treatment. [90]

The two main pathways of removal from the body are either by being filtered through the kidneys or by the reticuloendothelial system (RES, also known as mononuclear phagocyte system). The kidneys can filter particles smaller than 10 nm, and the larger particles are often taken in by Kupffer cells, or liver macrophages in direct contact with the blood. [32] [81] [60] After uptake they are then excreted out with the feces. Kupffer cells remove endogenous material, such as old or damaged erythrocytes, immune complexes, cancer cells, apoptotic cells and other cellular debris. [81] They can also endocytose various colloids, particles like latex beads, liposomes, cells like erythrocytes bacteria, denatured proteins, toxins like endotoxin, viruses, hormones like insulin antigens, and glycoproteins. [82] Size plays a major role in particle elimination, not only on the lower end of the spectrum, but also when particles are above 100 nm. As particles become bigger than 100 nm, the chance of being captured by RES dramatically increases. [84] Charge also plays a role in particle elimination. Both particles and products from biodegradation are less likely to be removed renally if they are neutral or anionic. [60]

Polyacrylamide nanoparticles have a plasma half-life of 24 h. [81] PAA is known to accumulate mostly in the liver and the spleen. [81] After about 120 h, PAA particles made with non-biodegradable cross-linker only have 2.2% of the PEGylated particles, and 3.3% of standard PAA particles bioeliminated. [81] When using biodegradable cross-linkers, ranges increased to 16.67% total recovery from feces and urine for 10% biodegradable cross-linker, and 7.68% total recovery for particles made with 20% biodegradable cross-linkers at 42 days. [81]

Gold nanoparticles are not biodegradable, therefore all particles around 10 nm or greater are required to go through the liver or spleen to be eliminated. After entering the RES, about 5% of 1.4 nm particles were bioeliminated in one day, and 0.5% of 18 nm particles were bioeliminated in one day. [235] In comparison, PAA particles made with 10% biodegradable cross-linkers had about 6% bioeliminated in one day. [81] Even though the 1.4 nm particles pass through the system faster than the larger particles, they have also shown to be toxic *in vivo.* Gold nanorods had even lower clearance, showing about a 1.5% clearance after 14 days when their size was 56 nm by 13 nm. [234] After 14 days, about 11.5% of PAA synthesized with 10% biodegradable cross-linkers were eliminated. [81] Another study of 40 nm gold nanoparticles showed that the amount of gold in the Kupffer cells only fell 9% after 6 months. [237] The inability of gold to biodegrade and be eliminated should be carefully considered when working with gold nanoparticles.

2.5.14 Cellular Uptake

The CB-PAA particles incubated for various times ranging from 1 h to 24 h showed a linear correlation between incubation time and cell death from PTT. Improving the rate and concentration of cellular uptake is one method of increasing the effectiveness of PTT. Cellular uptake is dependent on incubation time, particle size, surface functionality (e.g. charge of particle or surface proteins), concentration of the particle, and shape of the particle. Increasing the cellular uptake rates, or quantity taken in, is often accomplished by increasing the positive charge of the particle. [8] [23] Both negatively and positively charged particles have a higher rate of uptake than neutral particles. [50] One example of using charge to increase cellular uptake is PEI

(polyethylenimine), which has been used to increase cellular uptake of mesoporous silica nanoparticles loaded with drugs. [23] Another type of surface groups is peptides that have high amounts arginine and lysine (amino acids with positive charge) incorporated into their structure, such as TAT peptide. [45] [56] [236] TAT peptide (GRKKRRQRRRPQ) is widely known because it is also the peptide HIV uses to penetrate cells. [236] Changing the surface functionality doesn't always mean that there will be a higher concentration of particles, but sometimes just a faster rate of internalization. [33]

Antibodies are often used to target specific cells, which increases the number of particles around the cells. [66] There are many possible targeting moieties, such as F3 peptide. [33] It is important to remember that internalized particles are more effective than particles attached to the surface of the cells. [238] Knowing this, targeting should be designed so that more particles are also endocytosed by the cells. One problem that arises from changing the surface functionality is that the body often becomes hypersensitive to the targeted drug molecules or particles. [84] These methods could possibly be a way to increase the amount of particles that enter cells, therefore lowering the needed concentration of particles.

Most vary the incubation times based on the rate of uptake. If particles are slow, then incubation times can take a day or more, like CB-PAA, but in the case of target molecules, particle incubation times can be an hour or less. [14] [34] Targeting does not guarantee faster rates. Sometimes target particles take upwards of 48 h, as was the case anti-EGFR gold nanoparticles with HSC and HOC cancer cells. [15]

Currently CB-PAA particles have no surface modifications and required 24 h incubation, so there is room to improve the particle system. Often with other PAA based nanoparticles tested in our group, they only require 8 h to 20 h, and 1 to 4 h if functionalized with TAT peptide. [33] [34] Improved surface modifications could change the surface charge, noted by the relatively neutral zeta potential, to a higher positive charge that would be faster and better at being endocytosed. Particle uptake is not only surface dependent but it is also dependent on size and aspect ratio with the lower aspect ratio being better (in case of gold nanorods). [8] The current particles are spheres, so their shape is ideal, but the size distribution is much wider than desired. Ideally, particles should be under 100 nm, which means that the particles at the higher end of the distribution will have more troubles entering the cells. Changing the surface functionality will prevent aggregation of the particles, which could be one reason for the large size.

Cellular uptake is important and there are various different methods of measuring uptake. In the case of *in vitro* gold, they can use neutron activation analysis (INAA) and inductively coupled plasma-mass spectrometry (ICP-MS). [9] [83] ICP-MS would not work for our situation because we are not using metal nanoparticles. INAA would not work because it measures the amount of material, and since the particles are made of carbon nitrogen, there would be nothing to distinguish our particles from the tissue. One possibility is to use UV-VIS spectroscopy to determine the concentration of particles. There would be errors from the scattering of cells and cellular debris. Another possibility would be to use lower sensitivity atomic absorption spectroscopy (AAS). It is quite labor intensive and could be used *in-vivo* with a sacrificial animal.

This method would most likely require a target element being attached to the particle as a reference, which could change the properties of the particles. [83]

2.5.15 Tumor Delineation

Tumor delineation is when a contrast agent is used to increase visibility of the tumor to the naked eye or on an image, such as X-Ray or MRI. One of the first chemicals used was Gd^{3+} chelate, a first generation magnetic contrast agent for MRI. [124] There are an assortment of gadolinium contrast agents that have been approved by the FDA, including Magnavist®, Omniscan®, and Prohance®. [146] The new generation magnetic contrast agents for MRI use iron oxide as the core magnetic material. [124] [236] These are great for improving imaging contrast on a MRI, but when a surgeon is resecting a tumor it is almost impossible to remove the entire tumor without resecting extra healthy tissue when only referencing MRI images.

The reason tumor delineation is so important is because it is very difficult to achieve complete regression of a tumor by thermal therapy alone. [219] This is especially true for larger tumors and tumors past the penetration depth of the light source. So much of the tumor should be removed before photothermal therapy. Ideally, the tumor would be a different color so that a surgeon could easily distinguish between healthy tissue and the tumor. A few dyes that have been used are Coomassie Blue [239], Indocyanine Green [240] [241], and bromophenol blue [242]. The last two are known to have side effects at high concentrations. Below is an image of Coomassie Blue as a contrast agent (Figure 2.20).

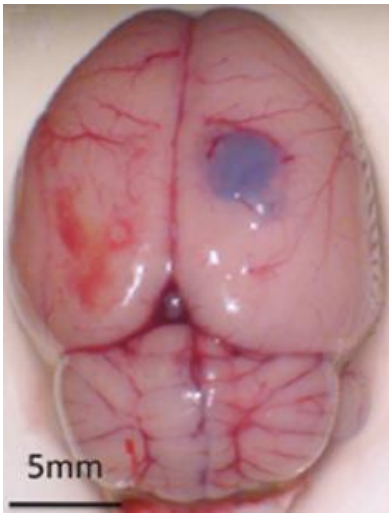

Figure 2.20: This is an example of tumor delineation on a rat brain using Coomassie Blue dye.*

*This image was taken from Orringer, D.; Chen, T.; Huang, D.; Armstead, W.; Hoff, B.; Koo, Y.; Keep, R.; Philbert, M.; Kopelman, R.; and Sagher, O.; The brain tumor window model: A combined cranial window and implanted glioma model for evaluating intraoperative contrast agents. Neurosurgery 2010 66(4) 736-743.

2.6 Conclusion

Gold nanoparticles have been used for years but very little work has been done with dye loaded particles in PTT. Alternative methods are extremely important in medicine in case one method does not pass FDA tests, has limited functionality (doesn't work on all tumor types), does not have fast enough bioelimination, costs are high to manufacture, or expensive for the customer because of a lack of competition. CB-PAA particles are strong absorbers that efficiently cause cell death under low light conditions, with 97% of cells dying when incubated with 1.2 mg/mL CB-PAA particles. One of the major reasons that this PAA delivery system is superior is because it is designed with biodegradable cross-linkers to speed up bioelimination. The initial examination of the dark toxicity is small, but more will be done to prove that this system is nontoxic. There is also the possibility of using CB-PAA not only for tumor delineation, but also to

increase effectiveness of radiation therapy. [133] [243] [244] These are all characteristics that make CB-PAA a strong alternative to gold in PTT devices.

Chapter 3 Photodynamic Killing of E. Coli O157:H7 using Covalently Linked Methylene Blue Nanoparticles

3.1 Abstract

Methylene blue nanoparticles have been previously used in photodynamic therapy to kill bacteria. [158] A couple of possible improvements to the particles were hypothesized in order to increase their efficacy. The first improvement was to increase the amount of methylene blue dye in the particle. This could lead to higher yields of singlet oxygen. Another possible improvement is to target the nanoparticles with antibodies, peptides, or aptamers. [14] [245] [246] Targeting the nanoparticles to a specific bacteria cell could increase the concentration of ROS species around that cell, which would increase cell death. To test these hypotheses, a polyacrylamide nanoparticle with MB-SE conjugated to the matrix was synthesized. Also, antibodies were attached to some of the same particles. The particles were then tested on E. coli. Cell death did not occur in either of the two cases. The highest concentration of particles was equivalent to the absorption of 400 μM of free methylene blue dye. Both tests were exposed to an irradiance of 20 ± 1 mW/cm^2 for up to 30 min. This chapter will discuss the reason for new antimicrobial therapies, dyes, photodynamic therapy, the light source, how the experiment was set up, the results, and some possible reasons for the results.

3.2 Introduction to Bacteria

Bacteria strains are becoming more antibiotic resistant. Examples of this are showing up all over the world, such as the Escherichia coli strain outbreak in Germany [247], and methicillin-resistant Staphylococcus aureus (MRSA) that is currently infecting many hospitals. [248] Bacterial strains often become more resistant if the antibiotic prescribed is below the minimal inhibitory concentration (MIC). The more tolerant cells will grow more and reproduce faster. This increases the MIC until the antibiotic is no considered effective at inhibiting the progression of the disease. For this reason, those in the medical profession need to determine the correct antibiotic and the required concentration to function properly.

Many researchers are currently working on determining the bacteria strain through various analytical measurements. This can be an effective method of determining the antibiotic, but it is no guarantee. The strain could still be resistant to the common antibiotics used on it. To counteract the chance of failure, a broad-spectrum antibiotic is often prescribed instead of the narrow-spectrum antibiotic. This often kills the harmful bacteria, but could lead to antibiotic resistance and limit the usefulness of some of the most functional antibiotics. Resistance can also occur when patients do not complete their course of antibiotics, leaving the bacteria that are more resilient to the prescribed antibiotic. There are two possible solutions: find a new method of destroying all types of bacteria, or determine the correct antibiotic for the specific infection. The latter will be discussed in more detail in the next chapter: nonlinear rotation. The various new therapies that are being probed include photodynamic therapy (PDT),

photothermal therapy (PTT), nanoparticle drug delivery, and novel antibiotics. [150] [249] [250] [251]

3.2.1 Dyes Used in Photodynamic Therapy of Bacteria

There are currently many different dyes used in photodynamic therapy of bacteria. Some of the more common photosensitizers used include toluidine blue O, methylene blue (MB), and chlorin e6. [149] [150] [151] Methylene blue was the chosen dye for multiple reasons. First, the dye molecule has a very low dark toxicity (not toxic when not excited by the light source). Another reason is because the dye has a maximum absorbance around 660 nm, which puts it in the optical window of tissue. With the dye being in the optical window, it has a deeper therapeutic range. If the photosensitizer absorbed more to the blue, the dye would only be effective at the immediate surface, or extremely shallow distances. The problem with methylene blue is that when it is in biological environments, it can be rendered inert by accepting electrons from NADH/NADPH. This changes it to its leuko form, leuokomethylene blue, a colorless molecule that has no photodynamic activity. [7] [38] [71] [73] [79] It has also been suggested that reduction of MB is done by thiazine dye reductase at the cell surface. For this reason, it so important that methylene blue is incorporated into a polymer matrix to be an effective therapeutic agent.

There are some limitations to dye loading, with the main limitation being leaching. Leaching is when the dye comes out of the particle. The most effective method to prevent dye leaching is by covalently linking the dye to the matrix. [34] Covalently linking the dye to the polymer matrix can also increase dye loading. Another limitation of dye loading is seen when the dye molecule concentration in the particle is high. The

dye molecules can quench each other when they are too close to each other, therefore making them inactive. [34] Previously, the methylene blue was not covalently linked to the polyacrylamide matrix. [158]

3.2.2 Light Source for Bacteria

The excitation source of most PDT experiments is a laser that has a close enough wavelength to the absorption of the photosensitizer. Several works used LED based systems instead because they are cheap and easily made to cover large surface areas. [252] [253] Fluencies for both lasers and LED excitation sources are often between 20 J/cm^2 to 60 J/cm^2. [150] [151] [158] [252] [253]

The variable of the light source used on cancer cells is very similar to that of bacteria. When targeting C6 with methylene blue nanoparticles, they used a 0.32 W/cm^2 laser with a wavelength of 647 nm. The cells were exposed for 45 minutes, which ends being a fluency of 864 J/cm^2. [7] A low dose is considered to be about 20 - 25 J/cm^2 for cancer [146]

3.2.3 Polyacrylamide

For more information of polyacrylamide, please refer back to chapter 2. In that chapter it describes in greater detail its toxicity, synthesis, biodegradability, and why it is used.

3.3 Experimental

3.3.1 Cell culturing

Escherichia coli O157:H7 (ATCC 35150) was solubilized using BD Tryptic Soy Media, and then plated onto petri dishes of BD Tryptic Soy Agar. Petri dishes were incubated in a Lab-Line Imperial III Incubator overnight, or until colonies were

approximately half of a millimeter in size. Solutions of E. coli were made by picking a colony, and regrowing the bacteria in Tryptic Soy Broth.

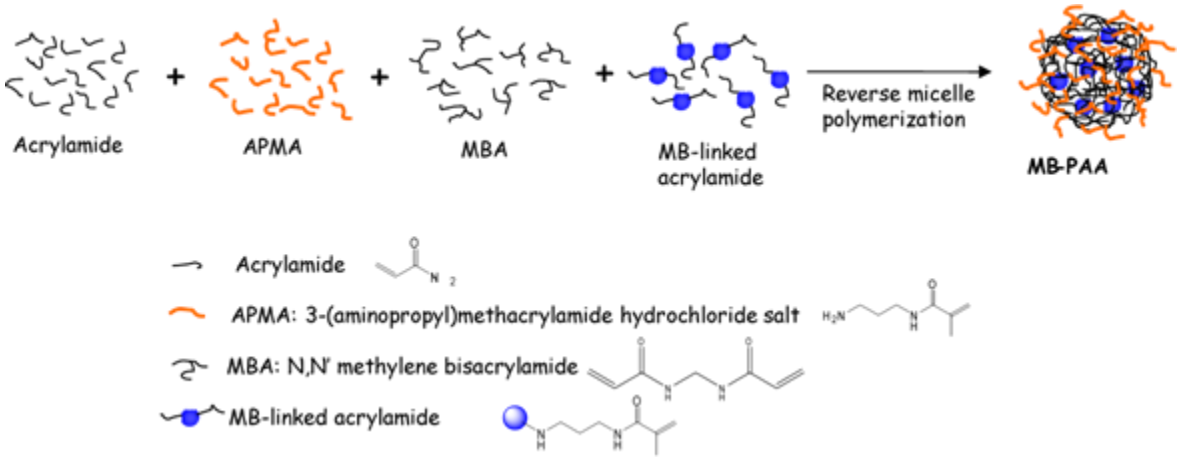

Figure 3.1: Synthesis scheme of the methylene blue polyacrylamide particles. The methylene blue linked to acrylamide was copolymerized with acrylamide APMA and MBA in a reverse micelle reaction.

3.3.2 Particle Synthesis

For these experiments, a MB-SE was covalently linked to a polyacrylamide matrix. [34] The synthesis was initiated by placing 1.6 g of AOT, 3.3 mL Brij 30, 45 mL of hexane (all from Sigma Aldrich), and a stir rod into a 100 mL round bottom flask. This solution was then deoxygenated by bubbling argon through the solution. In a separate scintillation vial, 610 mg of acrylamide from Sigma Aldrich, 45 mg of 3-(aminopropyl)-methacrylamide from Polysciences Inc., and N, N-methylenebis (acrylamide) from Sigma Aldrich were dissolved into 1.6 mL of Milli-Q water, from a Millipore A10 water purification system. After the monomer units were dissolved into the water, 2 mg of MB-SE was added and mixed until homogeneous. The monomer solution was stirred with a small magnetic spin rod, and then sonicated. After the solution was thoroughly mixed, it was added to the bubbling hexane solution. The solution was then bubbled for 20 min under inert conditions. To initiate the reaction, 40

μL of a 10% (w/v) ammonium persulfate in water solution, and 40 μL of N, N, N´, N´ tetramethylethylenediamine (TEMED) were added to the acrylamide solution. The solution was then stirred under inert conditions for 2 h. Figure 3.1 shows the general scheme of the synthesis. After the reaction was completed, the hexane was evaporated off using a Büch RII Rotavapor. The surfactant and unreacted monomers were then washed away from the particles by using an Amicon cell and Millipore Ultrafiltration Membrane 500,000 NMWL. The particles were washed 5 times with 200-proof ethyl alcohol from Decon Labs Inc., and 5 times with Milli-Q water. The clean particles were lyophilized to remove any water or minute quantities of remaining ethanol from the particles, and to keep the matrix intact.

3.3.3 LED Array

An excitation source was needed, and an LED array was designed and manufactured in the lab (See Figure 3.2). The LED array was made from 1242 wide angle LEDs from Kingbright Corp. The peak of the array was centered at 660 nm, which overlaps the absorption peak of the MB-PAA at 660 nm. An absorption spectrum of the nanoparticle can be seen in Figure 3.6. Mirrors were placed on each side of the array to increase uniformity of the light at the face, where samples were placed. There was about a 5% deviation in uniformity at the face of the mirrors. The max intensity, before power loss due to overheating, was 20 ± 1 mW /cm^2.

Figure 3.2: Experimental setup contains a 660 nm LED array of 1242 LEDs. The power output of the LED array was 20 ± 1 mW/cm2. The 1.5 mL cuvettes containing E. coli O157:H7, and either the methylene blue or MB-PAA nanoparticles, were placed at the face of the array.

3.3.4 MB PDT

To confirm functionality of the system shown in Figure 3.2, the initial examination was done using free methylene blue dye. E. coli O157:H7 was grown, centrifuged down, and decanted. A PBS peptone solution with a pH of 7.4 was added until the bacteria had an absorbance of 0.1 at 660 nm, which equates to approximately 1 x 10^{-8} cfu/mL. Then 1.5 milliliters of the bacteria solution was added to each of the 1.5 mL quartz cuvettes. Under a 468 nm blue LED, differing amounts of 15.1 mM MB dissolved in Milli-Q water were added to 1.5 mL cuvettes to get final concentrations of 0 µM, 0.1 µM, 1 µM, 10 µM, and 100 µM methylene blue. Cuvettes were then mixed and placed at the face of the mirrors. The cells were exposed to the LED array for 5 min. intervals, with small amounts of cells being removed to determine the number of colony forming

units per milliliter at each interval. Cells removed were serially diluted, then streaked in triplicate on Tryptic soy agar plates and incubated overnight. The proceeding day, colonies were counted.

3.3.5 MB-PAA PDT

The dried MB-PAA nanoparticles were dissolved in PBS solution with a pH of 7.4. A solution of bacteria with absorption greater than 1 at 660 nm, was centrifuged down and resuspended in a PBS peptone solution until the bacteria absorbance was 0.167. Then 1 mL of the solution was added to each cuvette, and 0.5 mL of varying concentrations of nanoparticles, determined by Figure 3.4, were added until the concentration of nanoparticles was equivalent to 0 μM, 0.1 μM, 1 μM, 5 μM, and 10 μM of free methylene blue. With the addition of 0.5 mL of dye solution, the final absorbance of the E. coli would have been around 0.1 at 660 nm. The MB-PAA solutions were exposed for 5 min intervals of 660 nm LED light at a power of 20 ± 1 mW/cm^2. There were small amounts of solution being removed for culturing at the end of each interval. This same experiment was repeated at the solubility limit of the nanoparticles, which is equivalent to approximately 400 μM of free MB.

3.3.6 Singlet Oxygen Production

Singlet oxygen of the MB-PAA particles was measured using the ADP method. [7] [254] 2 mg MB-PAA particles were dissolved in 2 mL of PBS buffer. The solution was then mixed with an ADPA solution 100 mM in a cuvette. The solution was constantly mixed and illuminated with 660 nm light through a 10 nm slit. The light source was Jobin Yvon Horiba 150 W ozone –free xenon-arc lamp. The fluorescence

of the ADPA excited at 378 nm was measured at different intervals during a 15 min period.

3.4 Results

Initially, methylene blue and the E. coli O157:H7 were used to test whether the LED system functioned properly and was an effective method of causing cell death in gram negative bacteria. After regrowth, the cells were centrifuged down and resuspended in PBS peptone solution to limit the interference that may come from the absorbance of the growth media at 660 nm. The PBS peptone was used to stabilize the cells. After the addition of methylene blue, the bacteria were placed under a microscope to image the effect of the MB. The E. coli was very dark blue from the uptake of MB free dye into the outer membrane, or possibly even deeper into the cell. This can be seen in Figure 3.5.

Figure 3.3 Staining of E. coli O157:H7 with methylene blue free dye. The methylene blue penetrates into the outer membrane of the bacteria staining them blue.

A different set of suspended E. coli cells were then prepared under 468 nm blue LEDs. The absorption of MB at 468 nm is low, which minimizes the amount of ROS produced before exposure to the 660 nm red LED array. These blue LEDs had a weak

intensity of about 50 μW/cm^2 where the samples were prepared. After the bacteria solution and MB were exposed to light at room temperature, small volumes were removed, serial diluted, and then plated. Generally, colony counts ranged from 300-400 colonies per plate, except for the MB concentrations that were effective at causing cell death. These had counts of 0 to 15 colonies per plate. The results shown in Figure 3.4 were taken from 3 plates made from each concentration. The average error was 9.0% and a median error of 6.4%. The difference between the average and median error comes from the colony counts of 10 μM and 100 μM. Concentrations of 1 μM MB and lower do not to have an effect greater than error in the measurements. At the higher concentrations of 10 μM and 100 μM, 99% of cell death occurred within the first 5 min of exposure at 20 ± 1 mW/cm^2.

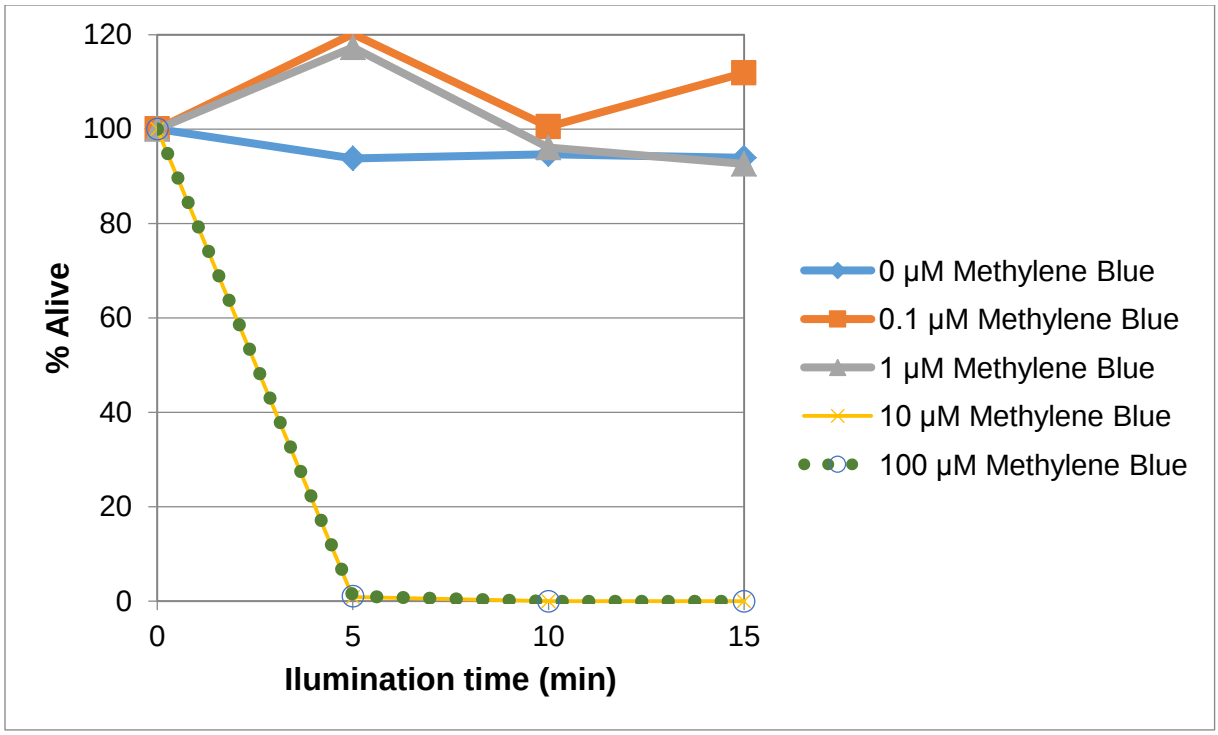

Figure 3.4: The effect methylene blue has at varying concentrations of MB and with varying illumination times. The colony counts of 3 different petri dishes were normalized to 0 to give each data point. The average error was 9.0% and a median error of 6.4%.

The ability of MB to kill the E. coli without an excitation source, known as dark toxicity, was also tested. E. coli O157:H7 showed no significant dark toxicity, which can be seen in Figure 3.5. These experiments were also prepared under the 468 nm blue LEDs to minimize the photodynamic effect caused by the absorption of light. There was an average error of 7.3%, with five petri dishes for each concentration.

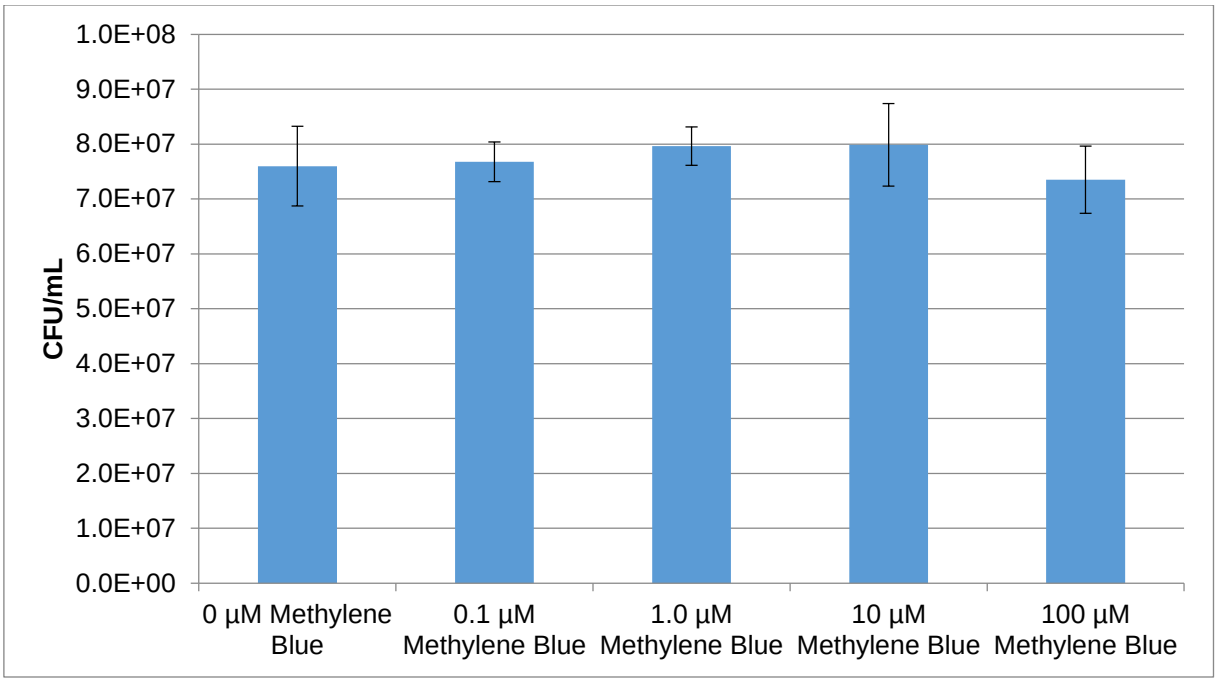

Figure 3.5: The average dark toxicity of the methylene blue at different concentrations. MB free dye was added to cuvettes with E. coli O157:H7 in PBS until concentrations of 0, 0.1, 1.0, 10 and 100 µM were reached. The absorption of the E. coli was 0.1 at 660 nm. All preparation was done under a blue LED. After allowing for 30 min incubation, the cells were then plated on five petri dishes for each concentration.

Before experimenting, the particles were characterized. When the methylene blue was bound in the particles there was a shift and a drop in absorption of the particles. This affect can be seen in Figure 3.6. Sometimes when dyes are in close proximity, they quench each other. The particles were then tested to confirm that they would produce singlet oxygen, and so an ADPA test was performed by using the 2 fluorescent peaks to measure singlet oxygen production. This can be seen in Figure 3.7, and the plots of the ratio between the peaks can be seen Figure 3.8. The singlet oxygen production per mg of particle is higher for MB-PAA than that of nonconjugated MB particles. The k-value of the nonconjugated MB nanoparticles was 1.1×10^{-4} s^{-1}, while that of MB-PAA at was 5×10^{-4} s^{-1}. [255] See Table 3.1 to see how MB-PAA compares to free methylene blue and methylene blue SE.

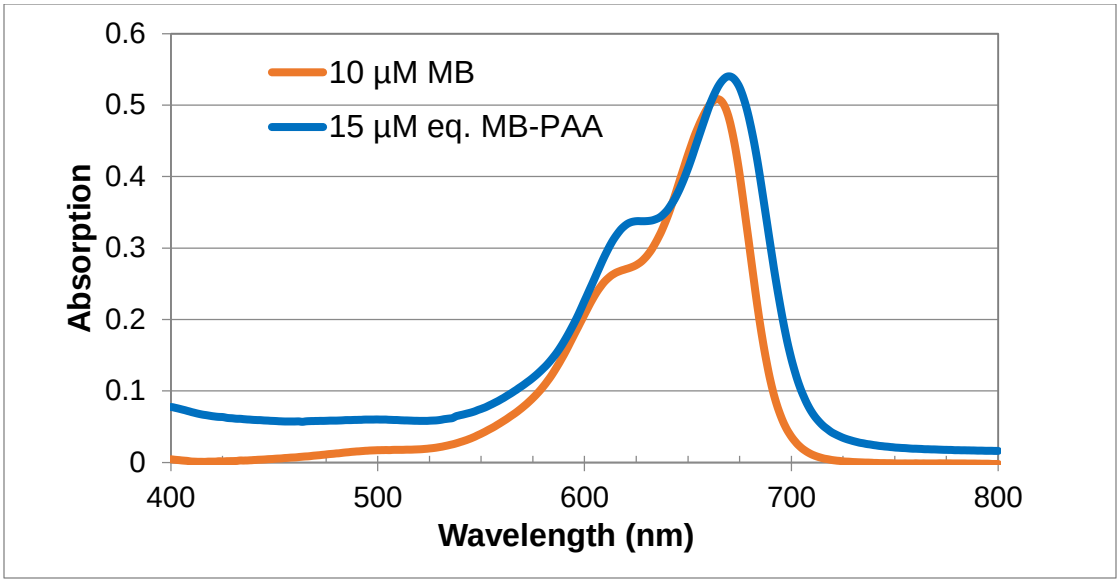

Figure 3.6: UV-Vis spectrum of 15 µM MB-PAA nanoparticles with similar absorbance to that of 10 µM of free methylene blue. The shift is caused by the dye molecules being in a polymer matrix.

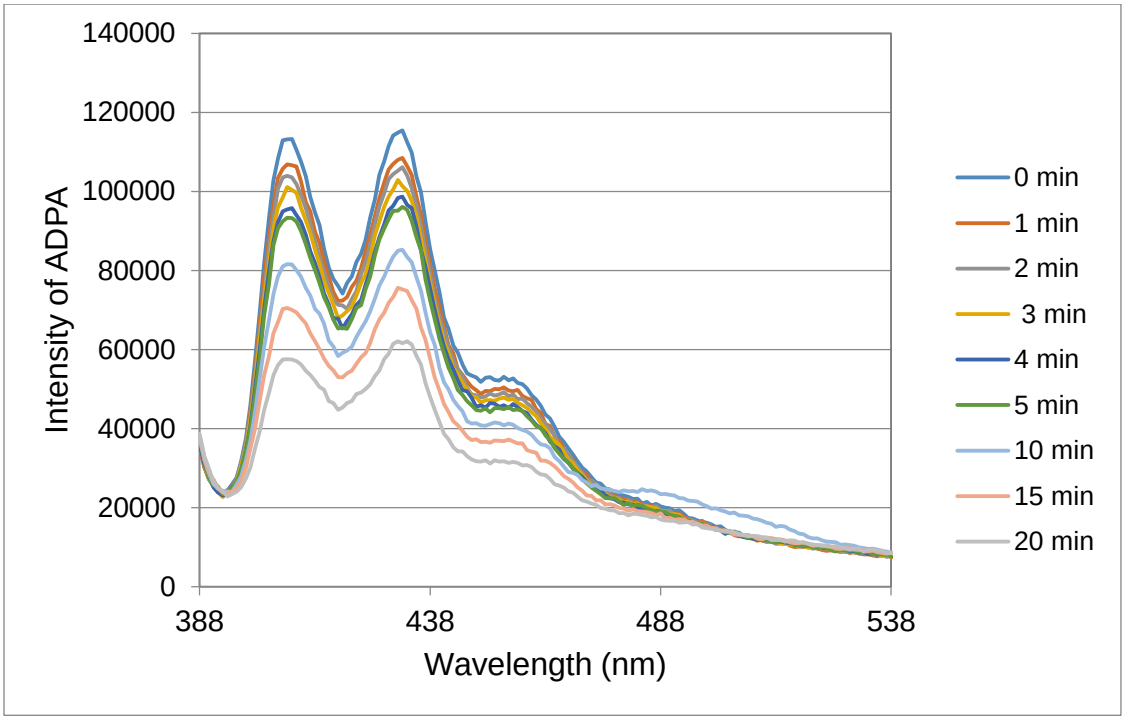

Figure 3.7: Fluorescent peaks of ADPA at different time intervals 0-20 min while being excited at 378 nm.

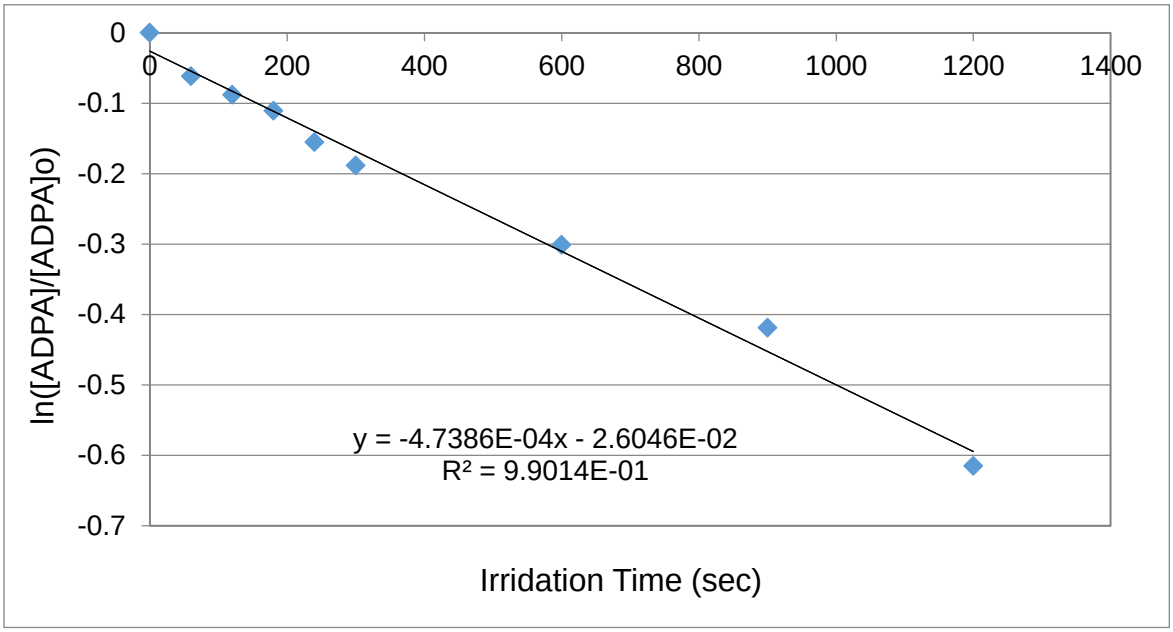

Figure 3.8: Singlet oxygen production of the 1 mg/mL MB-PAA nanoparticle using ADPA quenching to measure the amount of singlet oxygen being produced.

Dye	Solvent	Ex/Em	K value	k/k_{MB}
MB	PBS	667/688	$3.06 \times 10^{-3} s^{-1}$	100%
MB-SE	PBS	666/685	$2.54 \times 10^{-3} s^{-1}$	83%
MB-PAA	PBS	668/691	$0.5 \times 10^{-3} s^{-1}$	16%

Table 3.1: Different k values for MB dye, MB-SE dye, and MB-PAA particle. K values were determined from the singlet oxygen plots. All singlet oxygen plots were done using ADPA

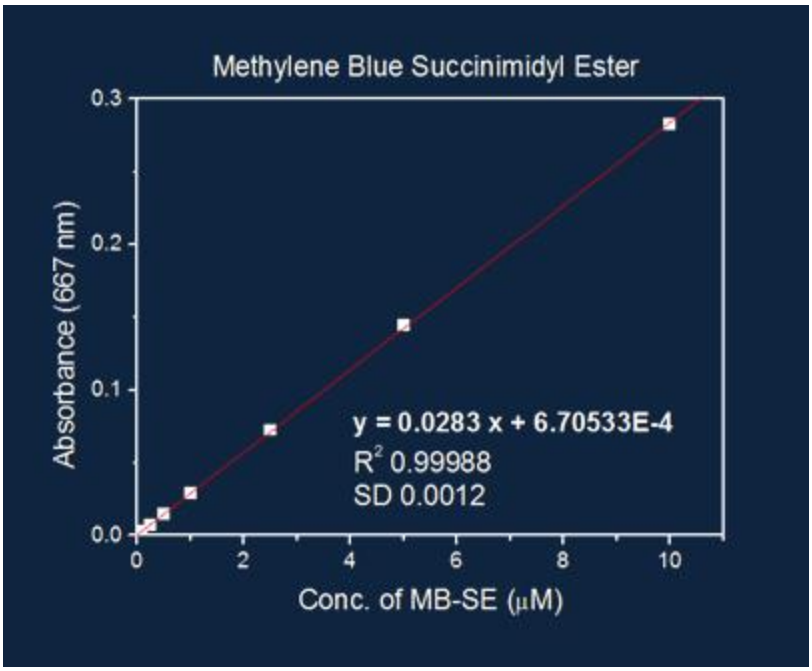

Figure 3.9: Calibration curve for methylene blue succinimidyl ester. Concentrations of dye in particles were determined from this plot.

In the MB-PAA particles test, the cuvettes were setup as they were for the methylene blue. A higher concentration of bacteria was used, but in smaller amounts because of the limited solubility of MB-PAA. Using the calibration curve (Figure 3.9) the different concentrations of particles were prepared. This experiment was repeated multiple times with varying concentrations. The results shown in Figure 3.10 and Figure 3.11 represent the experiments with the smallest errors. Each value is an average taken from three petri dishes. Unlike methylene blue, MB-PAA particles with equivalent absorbance to MB do not cause cell death, as can be seen in Figure 3.10. Even with the maximum amount of MB-PAA, which is equivalent to 400 μM of MB, there was still no cell death (Figure 3.11).

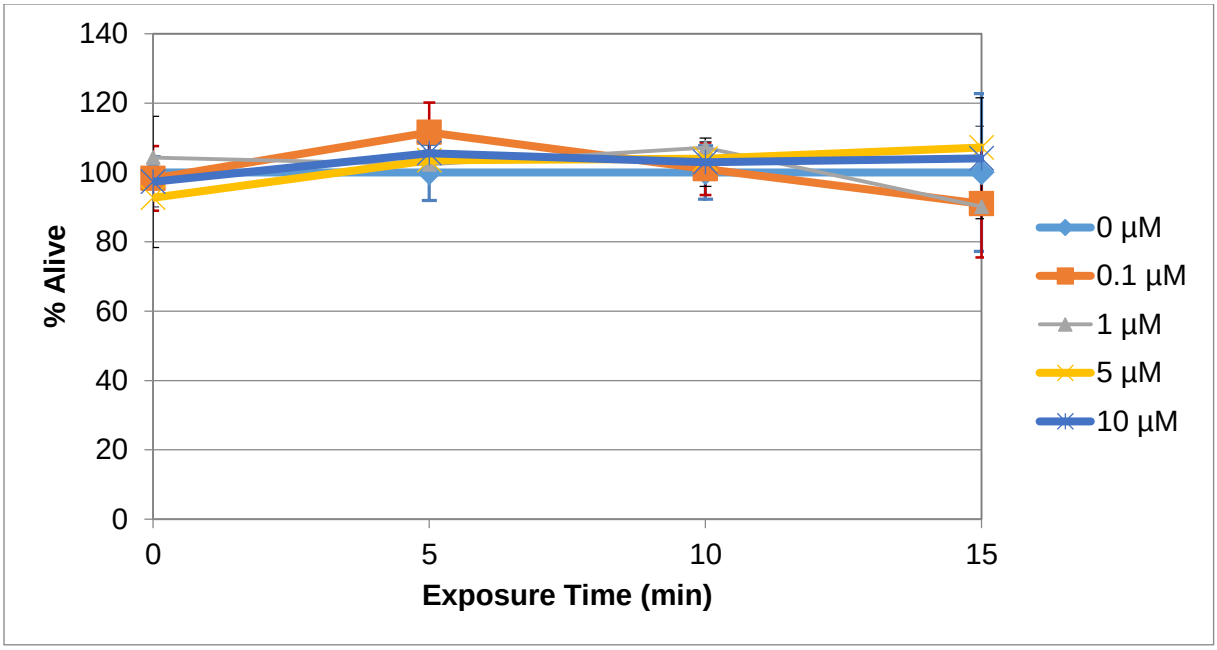

Figure 3.10: MB-PAA nanoparticles at concentrations with equivalent absorption 0 µM, 0.1 µM, 1 µM, 5 µM, and 10 µM of methylene blue free dye in a solution of E. coli O157:H7 with an Abs. of 0.1 at 660 nm. Each concentration was exposed using varying illumination time with colony forming units done in triplicate. The results were then normalized to time 0.

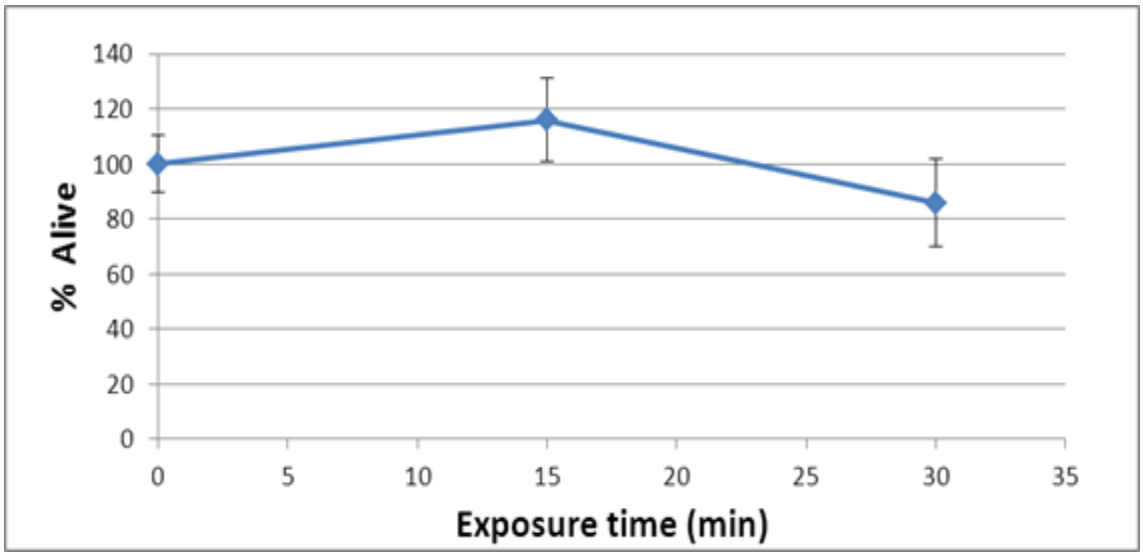

Figure 3.11: The effect of photodynamic therapy using MB-PAA nanoparticles with an absorption equivalent to 400 µM of methylene blue free dye. Each data point was from 3 petri dishes normalized to time 0.

MB-PAA particles with anti-E coli put with the bacteria under similar conditions to the methylene blue and the MB-PAA particles. There was no success with those either.

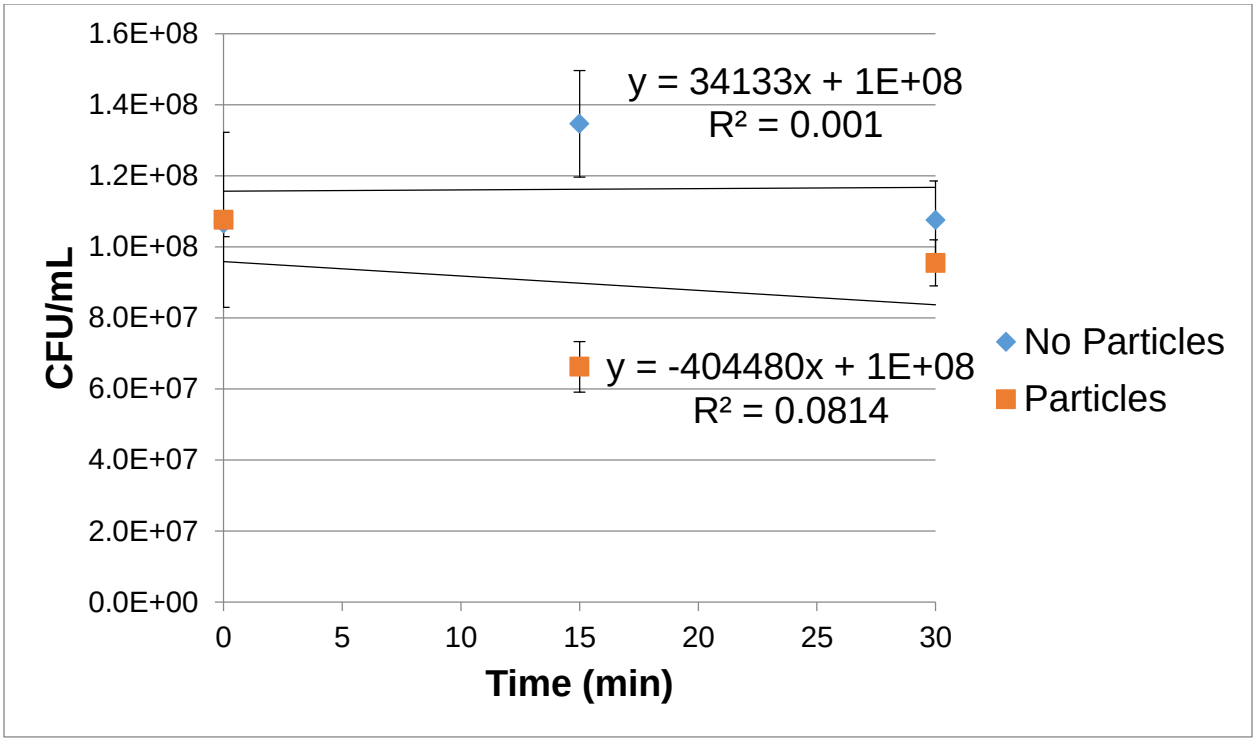

Figure 3.12 MB-PAA with anti-E coli attached to the surface were placed with E. coli O157:H7 with a concentration of particles equivalent absorption 10 μM of methylene blue free dye. The absorbance of the E. coli O157:H7 with an Abs. of 0.1 at 660 nm. The solution was exposed using varying illumination time with colony forming units done in triplicate.

3.5 Discussion

The results show promising PDT when just using the dye methylene blue, which has been observed in previous experiments. [256] Many groups are currently looking for cationic dyes that have better cell penetrations, i.e. zinc-phthalocyanine and tetra (4N, N, N-trimethyl-anilinium) porphine tetraiodide, which result in more cell death. [257] [258] [259] [260] Since ROS need to get inside a cell to kill the bacteria, it is better if the photosensitizer is deeper inside the cell. Without the dye penetration, cell death is minimal in certain strains. [259] Penetration is often better with gram positive bacteria because of a lack of an outer membrane, which is not the case in gram negative bacteria. [259]

Methylene blue loaded polyacrylamide nanoparticles have previously been shown to be effective at killing E. coli K-12, Staphylococcus aureus, Acinetobacter, and P. aeruginosa at concentrations of 5 mg/mL. [158] In comparison, MB-PAA could not kill E. coli O157:H7 at 89 mg/mL. There are a few possible reasons why this may have happened. First, the bacterial strains used for loaded MB particles could be easier to kill using PDT, which could be the reason for the deviation between particles. Looking at Xi's data alone, it is possible to see that all cell types are not equivalent.

Another likely scenario is that cell death in previous work was due to the methylene blue not being covalently linked to the particle. The speculation being that the MB molecules leached out of the particles and into the cells. While in the cells, the singlet oxygen produced by the methylene blue would be close enough to cause cell death. Figure 3.3 shows that methylene blue readily stains E. coli. The staining also works in gram positive bacteria and is believed to be caused by methylene blue's positive charge, low molecular weight, and hydrophilicity. [261] Taking the ability of methylene blue to enter cells into account, maybe the methylene blue in the previous work would have leached out since they were covalently not bound to the nanoparticle matrix. The particle worked as a delivery vehicle.

Since the MB-PAA was producing ROS, and methylene blue killed cells under similar conditions, the lack of cell death cannot be caused by the particles inability to produce singlet oxygen. The particles may not be producing enough singlet oxygen under the LED array to kill the bacteria without the particles actually being close enough, or inside the cells, as is the case for free MB molecules. The lower singlet

oxygen production could come from a lack of oxygen in the cuvettes, even though there was space at the top for air.

3.6 Conclusions

Methylene blue covalently linked nanoparticles were not effective for photodynamic killing of E. coli bacteria. In PDT on bacteria, it appears to be important to have the photosensitizer inside the cell in order to kill it. This common issue with PDT on bacteria has been seen with other dye molecules. The particles may not have worked because of the specific bacterial strains that were being used. It may have been better to use a gram positive bacteria strain. Another possibility to make the nanoparticles effective is by using cationic dyes on the surface to allow for more penetration of the ROS.

Chapter 4 Preparation and Experimentation using Nonlinear Rotation for Bacteria Detection

4.1 Abstract

As discussed in chapter 3, there is a need to find new methods of determining the best antibiotic when one has a bacterial infection. In order to determine the best antibiotic, one must know the bacteria strain or monitor its growth in an antibiotic. With my help, we determined that bacteria binding to a rotating particle will change the particle's rotation rate. In the case of a 2.0 μm magnetic sphere, the rotation rate lowered by a factor of 3.8 when E. coli BL21 was bound to its surface (Figure 2.1). Using this method will allow one to detect different bacteria strains.

4.2 Introduction

There are multiple examples of rotating magnetic particles in a magnetic field. Through simple microscopy techniques, one can monitor the rotation of different types of particles: single particles, rods, wires, chains of particles, Janus particles, etc. [262] [263] [264] [265] [266] Not only can the particles be monitored, but they can also be used as tools in other applications. They can be used to improve immunoassays, act as micromixers, study microorheology, magnetoresitive sensors, tunnel junction sensors, and increase signal to noise ratios in fluorescent spectroscopy. [267] [268] [263] [264] [266] [269]

Our laboratory had multiple people working on using nonlinear rotation of magnetic microparticles to detect and monitor the growth of bacteria. There were several issues that I worked on to assist in the research. The common issues we had were binding the particle to the bacteria, particles settling to the bottom of cell and sticking, particles and bacteria binding in groups, and uniformity of the magnetic field. W had a couple of theories on how to remove these problems, which was what I worked on with Brandon McNaughton and the others during the project. The rest of the chapter will discuss some of the issues and the results that we accomplished. This is the first time it has been used to measure the binding of a bacterium. [159] [160] [161]

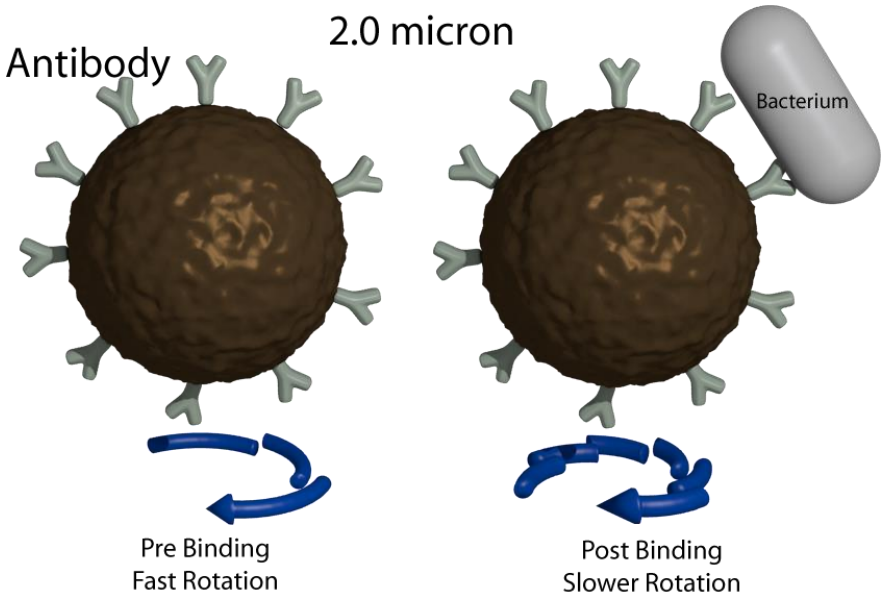

Figure 4.1: Diagram of the single cell detection, and changes in the rotational rate of a magnetic microsphere when it binds with a single bacterium. The antibody represents the multiple possible types of antibody configurations. In the case of this experiment, it was functionalized with a secondary antibody (goat anti-mouse IgG Ab2) and primary antibody (mouse anti-E.-Coli IgG Ab1).

4.3 Experiment

Initially, a precut slide was prepared with (1% W/V) 2.0 μm magnetic microspheres with anti-mouse IgG from Spherotech. This was done by spreading 20 μL

aliquots of particles onto the surface of the slide. After drying, the sample was coated with aluminum until the coating was about 50 nm. The particles were then placed in a magnetic field of 1.4kOe to change the magnetic moment of the particles to be perpendicular to the aluminum coating. The particles were then brushed off into a PBS buffer that had a pH of 7.2. Mouse anti-E coli antibodies from Cortex Biochem were then attached using the anti-mouse mouse interaction between the two antibodies. Many other types of interactions to connect the bacteria to the particles were tried too. Another type of particle that was used was streptavidin magnetic microspheres. The anti-E coli antibodies were biotinytalated, and therefore bound with the streptavidin.

In order see the bacteria as they rotated, a DsRed plasmid was introduced to the E. coli BL21(DE3). [270] The bacteria were grown until they had an optical density of 0.67 at 600 nm. The bacteria solution and the particles were mixed in a 1:1 ratio. A Rodney cell was then setup: two microscope cover slips of 100 μm were stuck together with double stick tape on the edges so that there was a space left in the middle for solution. The bacteria and particles were then magnetically separated so that there would not be too much bacteria in the solution. PBS (η = 0.001Pa's), or a PBS glycerol solution with a mass fraction of 0.5 (η = 0.006Pa's), was then added to the particles. After the addition of solution, the particle solution was then wicked into the Rodney cell and placed on the microscope for imaging and rotation.

The rotation of the particles was monitored by either fluorescence microscopy, bright-field microscopy, or reflection microscopy. The rotation was monitored by measuring the fluctuations in intensity of the particle with the Metamorph software from Molecular Devices. Brandon McNaughton did most of the work with Metamorph and

data acquisition. A more in depth description of this is described in various papers. [159] [160] The average rotational frequencies were determined using discrete Fourier transform. The higher harmonics were filtered out to make it easy to analyze the rotation dynamics of the particle.

4.4 Result and Discussion

My work in the nonlinear rotation was to find the different methods of binding the particles to the bacteria, to prevent particles from sticking to the surface of the slides, and to grow the bacteria. Various types of particles were used with bacteria. Initially, we attempted to use plain bacteria without antibodies. Sometimes we would find bacteria attached to the particles. It would take thousands of particles before Brandon or I would find a single particle with just a single bacterium attached. Much of our initial work together was using this method.

In order to increase the binding efficiency we looked into other methods. That is when we started working with antibodies. Most of the antibodies that we tested did not work, even though they were for E. coli. Each antibody is specific to a given antigen. Most of the antibodies we researched were not specific to a surface antigen on E. coli, nor were they specific to the strain of bacteria we were using at the time, BL21. I later set up a Biosafety Level 2 room for future work that was done with bacteria and nonlinear rotation. This allowed us to have the pathogenic bacteria that were used in chapter 3. I also assisted in many of the later experiments with bacteria growth by introducing new strains to be tested.

The particle with anti-E coli from Cortex was one of the few that we could get to bind. Even though it did bind, the binding was not great and it still required a lot of time to find particles with the correct amount of bacteria attached. In Figure 4.2

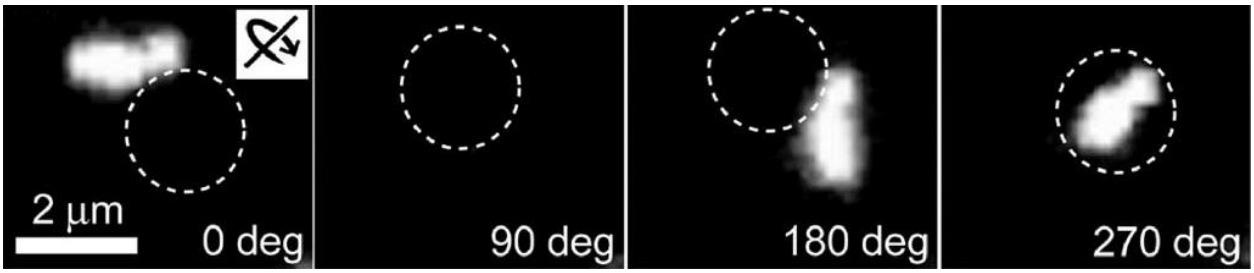

Figure 4.2: This is a series of successive fluorescence microscopy images of the magnetic microparticles rotating in the magnetic field [271]. The dotted lines represent the location of the 2.0 µm microsphere, and the bright spot is the fluorescing E. coli bacterium (BL21) attached to the surface of the particle. In this case, the particles are rotating where the axis of rotation lies in the plane of the sample.

Even after finding a good candidate to measure, there were still multiple issues to overcome in order to measure the average rotation frequency. For one, the particle would settle to the bottom of the vessel and rub against the bottom. This would increase the drag and change the rotational dynamics. Much of the time, the particles would stick to the surface. I worked on multiple different methods to eliminate this issue. I functionalized the slides with positively or negatively charged functional groups, and neither of those worked. Another method tested was to PEGylate the glass surface. Initially, PEG was spin coated or dried on to the surface the slide. This did not work because the PEG just dissolved back into solution. Not in this experiment, but in a later experiment, I covalently linked the PEG to the slide. [272] This didn't eliminate all sticking, it just took 5 times as long to stick. These slides were not used for bacteria rotation much, but they were used to monitor particle slipping on the surface of the slides. Instead of limiting sticking by changing the slides, it was decided to use a mixture

of glycerol and PBS. The mixture had a higher density, so the particles would not sink. This worked great for comparing particles with no bacteria and ones with bacteria attached, but this did not work for experiments where the bacteria needed to remain alive.

After finding the right particles, the average rotation of a particle as the driving frequency was measured. In Figure 4.3, it shows the average frequency for both a bare particle with nothing attached, and one with a bacterium. Both of these are in agreement with Equation 1.3. The critical frequency for the particle with the bacterium attached was determined to be 1.27 Hz, and the critical frequency of the bare particle was 2.2 Hz. Assuming that all of the forces are negligible, it was determined that the particle could be used to detect bacteria.

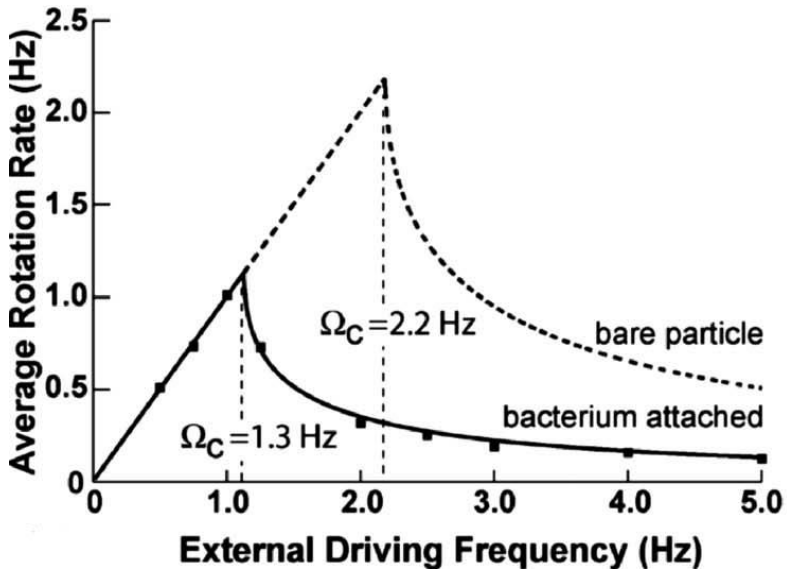

Figure 4.3: The plot shows the rotation rate of the 2.0 μm particle as driving frequencies increased with and without a single bacterium attached. The linear phase is seen on the left side, and the nonlinear phase of particle rotation is to the right of the Ω_C. Critical frequencies and the overall frequency both drop with the addition of the bacterium. [271]

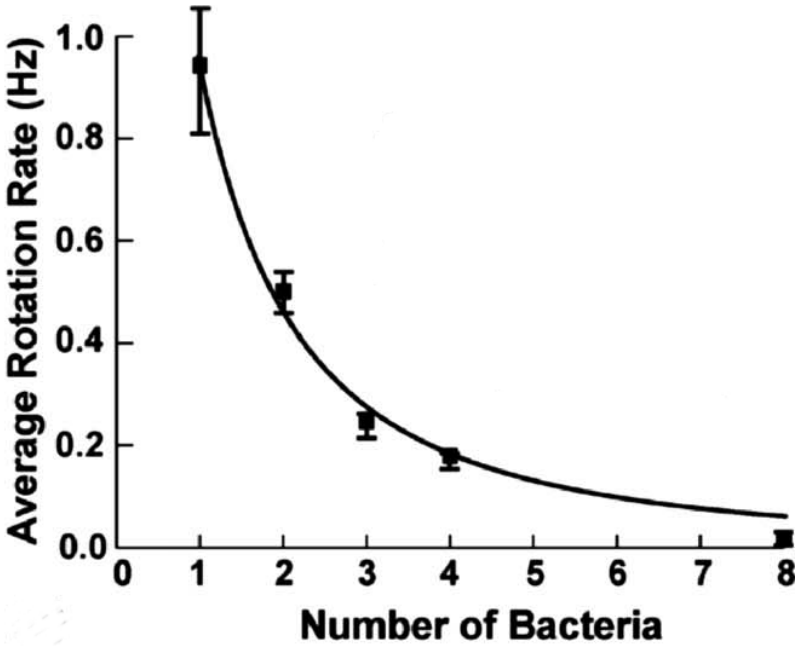

Figure 4.4: Plot shows the effect on the rotation rate of a dimer as 1, 2, 3, 4, and 8 bacteria bind. The magnetic particles were in a magnetic field rotating at 3.75 Hz. The trendline is a theoretical fit to represent estimations as other bacteria bind. [271]

Magnetic microparticles can also be used to detect multiple cells attaching. When cells attached to a dime, two particles connected to each other, we were also able to monitor the change in rotation. The dimer was able to detect the addition of 8 bacterium (Figure 4.4).

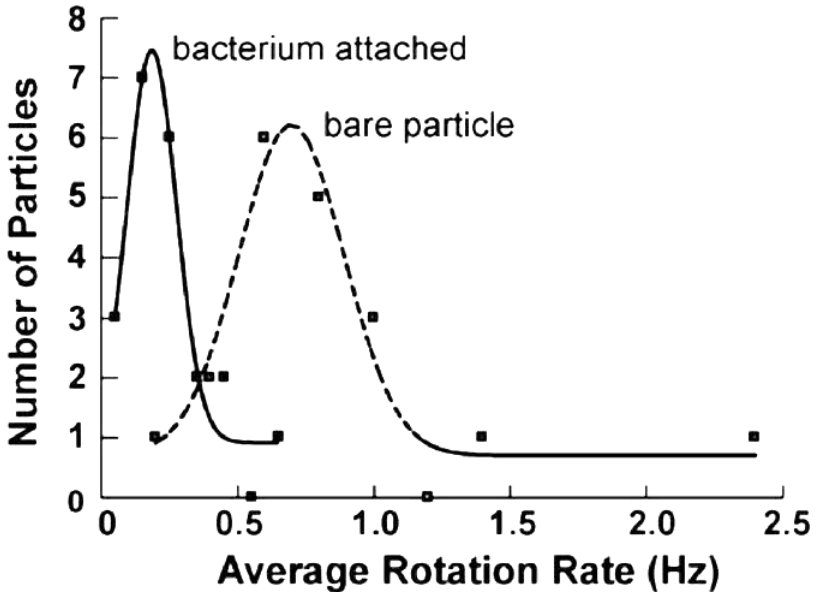

Figure 4.5: The change of the average rotation of 20 different particles when bacteria, not just a single bacterium, attach to the surface of the particles. [271]

To overcome the issue of too many bacteria binding to a particle, it was decided just to monitor the rotation rate of 20 different particles with bacteria attached. The bacteria on the surface of magnetic microspheres caused a significant change to the average rotation frequency. The driving frequency was 4.0 Hz, and the average frequency of the particles was 0.72 Hz without bacteria attached, and 0.19 Hz with bacteria attached, a decrease in rotation by a factor of 3.8 (Figure 4.5). These results are similar to a 1.0 μm sphere being attached to a 1.9 μm ferromagnetic particle. [160]

After these experiments, I worked on improving the uniformity of the magnetic field. The coils on the first magnetic fields were not the same size and the magnetic field had to be adjusted so that it was uniform. I later designed a new coil system that fit in the microscope that was more uniform (Figure 4.6). The coils were uniform in size, were able to rotate on any axis, had a built in incubator, allowed for 100x objective, and

fit on the microscope. Multiple members of the group used it as they were doing experiments.

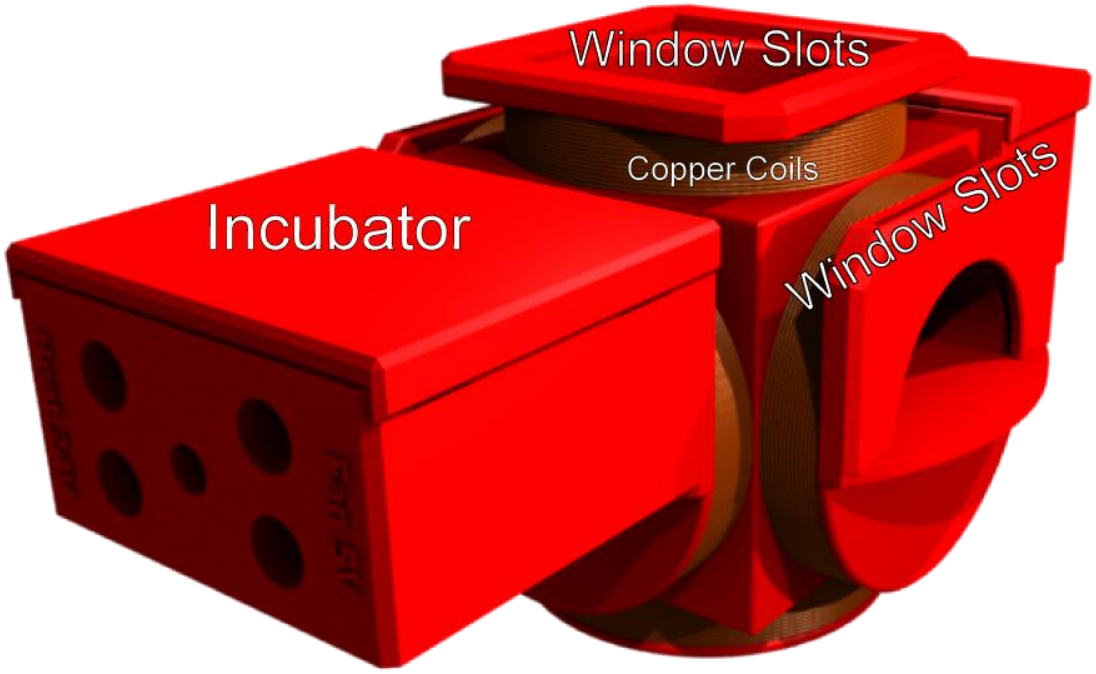

Figure 4.6: The magnetic coils I designed that were uniform in size, could rotate on any axis, had a built incubator, and could fit bigger microscope objectives.

A competing technology would be nanoelectromechanical systems (NEMS), which has been used to detect viruses and bacteria. [273] [274] [275] [276] With NEMS, a vibrating cantilever detects the presence of a microbiological agent attached to its surface by monitoring changes in its resonant frequency. The problem with NEMS is that it functions well in a vacuum, but it does not function well in the fluidic environment needed for bacteria. [277] [278]

When the bacteria are bound to the particle, the particle could be used to monitor the changes in the bacteria as it grows. [1] As the bacteria grows, its volume increases and so does its drag. This slows the particle rotation down in the nonlinear regime. Using this technique, one could monitor the effect of antibiotics on the growth dynamics

of bacteria attached to spheres. This method would directly determine the correct antibiotic and eliminate the need to name the strain attached. This has been one of the major research projects in the group. [1] [2] [279]

4.5 Conclusion

The rotation rate of 2.0 μm magnetic microspheres decreased by a factor 3.8 when a single bacterium was bound to their surface. The rotation decreased further on the binding of even more bacteria. These results show the ability of magnetic microparticles to detect bacteria bound to their surface in a liquid environment. It also shows that there is a potential of using this technique to monitor growth and division of microorganisms. Future work on increasing sensitivity and binding efficiencies will make this technique even stronger, and make it ready for industrial use.

Chapter 5 Conclusion and Future Work

5.1 Conclusions

Coomassie Blue polyacrylamide nanoparticles function well as photon absorbers for photothermal therapy. The particles are biodegradable and pass out from the body faster than the competing gold nanoparticles. The particles show no dark toxicity, but under exposure to low power LED array, the particles effectively kill the tumor cells. When cells are exposed to a fluency of 61 J/cm^2 after being incubated with concentrations of 1.2 mg/mL of Coomassie Blue nanoparticles, 97% of the HeLa cells were killed.

A study was done using methylene blue covalently linked to polyacrylamide nanoparticles for photodynamic therapy on E. coli O157:H7. The nanoparticles were ineffective at killing the bacteria, even when concentrations of the methylene blue in the nanoparticles were equivalent to 400 μM of methylene blue free dye. A similar study was done using noncovalently linked methylene blue nanoparticles on various strains of bacteria. Noncovalently linked methylene blue nanoparticles were able to reduce cell viability in various strains. [158] It is believed that the reason the covalently linked nanoparticles did not show cell death is because the singlet oxygen could not penetrate deep enough to kill the cells. In the noncovalently bound methylene blue nanoparticles, the dye could possibly leach out of the particle into the bacteria. This would allow the singlet oxygen produced to penetrate deeper into the bacteria, causing cell death.

Nonlinear rotation magnetic microparticles show promise for bacteria detection. The microparticles showed the ability to detect individual binding events of E. coli. This was done by optically watching the change in the rotation of the particles. As each binding event occurred, the rotation rate of the particles slowed down, on average, by a factor 3.8.

5.2 Future directions

Several steps can be taken to improve the current Coomassie Blue polyacrylamide particle system. The uptake of the particles by the HeLa cells took about 24 h, which is longer than that of other polyacrylamide particles. Incubation times could be lowered by increasing the positive charge on the nanoparticles. Some different potential surface modifications for increasing the positive charge include a short peptide residue containing arginines, or the TAT peptide that facilitates HIV uptake into cells. Both methods are known to assist internalization with other nanoparticles. [45] [56] [236] Since the particles are easily functionalized with targeting peptides, antibodies, or aptamers, targeting the Coomassie Blue nanoparticles to specific tumor cells should be tested. A more exhaustive study of the correlation between light irradiance and cell viability should be undertaken. This could be accomplished by comparing the LED array to a higher-powered laser system, which could also give more information on the manner of cell death. Another interesting direction to take is to study the concentration of particles inside the cells, and then determine the heat each concentration produces. Along the same line, the pathway of internalization and where the particles accumulate should also be examined. These experiments could give some more insight into the temperature surrounding each particle and how the cells die. Also,

since the particles are adept at killing tumor cells *in vitro,* the nanoparticles should be tested *in vivo.*

There are a couple of experiments that could be done in the future to solidify the result that covalently linked methylene blue nanoparticles are not going to be useful for PDT on bacteria, and also to help move forward with what has worked so far. First, the two different types of particles, covalently and noncovalently bound methylene blue polyacrylamide particles, should be tested on the same bacteria strains. Another experiment would involve taking noncovalently bound methylene blue polyacrylamide particles and attaching targeting moieties to their surface. It would be interesting to see if this would increase the effectiveness of the particles.

Nonlinear rotation already has a bright future, as members of our group have started a spin-off company with it. [1] [2] [279] However, there are still advancements to be made in the field. One idea would be to attach a universal targeting moiety to the rotating particles that will attach to any bacteria. With this particle, it may be possible to determine the bacteria strain by monitoring how each type of bacteria affects the rotation of the particle as the bacteria grow. Monitoring growth has been done, [1] [2] [279] but comparing growth in different strains of bacteria has not been studied.

Bibliography

[1] McNaughton, B. H.; Kinnunen, P.; Smith, R. G.; Pei, S. N.; Torres-Isea, R.; Kopelman, R.; and Clarke, R.; *Compact sensor for measuring nonlinear rotational dynamics of driven magnetic microspheres with biomedical applications.* Journal of Magnetism and Magnetic Materials **2009** 321(10) 1648-1652.

[2] Kinnunen, P.; Sinn, I.; McNaughton, B. H.; Newton, D. W.; Burns, M. A.; and Kopelman, R.; *Monitoring the growth and drug susceptibility of individual bacteria using asynchronous magnetic bead rotation sensors.* Biosensors and Bioelectronics **2011** 26(5) 2751-2755.

[3] Haukanes, B.; and Kvam, C.; *Application of Magnetic Beads in Bioassays.* Nat Biotech **1993** 11(1) 60-63.

[4] Olsvik, O.; Popovic, T.; Skjerve, E.; Cudjoe, K. S.; Hornes, E.; Ugelstad, J.; and Uhlén, M.; *Magnetic separation techniques in diagnostic microbiology.* Clinical Microbiology Reviews **1994** 7(1) 43-54.

[5] Gu, H.; Ho, P.; WT Tsang, K.; Yu, C.; and Xu, B.; *Using biofunctional magnetic nanoparticles to capture Gram-negative bacteria at an ultra-low concentration.* Chemical Communications **2003** (15) 1966-1967.

[6] Kimelberg, H.; Mayhew, E.; and Papahadjopoulos, D.; *Distribution of liposome-entrapped cations in tumor-bearing mice.* Life Sciences **1975** 17(5) 715-723.

[7] Tang, W.; Xu, H.; Park, E. J.; Philbert, M. A.; and Kopelman, R.; *Encapsulation of methylene blue in polyacrylamide nanoparticle platforms protects its photodynamic effectiveness.* Biochemical and Biophysical Research Communications **2008** 369(2) 579-583.

[8] Qiu, Y.; Liu, Y.; Wang, L.; Xu, L.; Bai, R.; Ji, Y.; Wu, X.; Zhao, Y.; Li, Y.; and Chen, C.; *Surface chemistry and aspect ratio mediated cellular uptake of Au nanorods.* Biomaterials **2010** 31(30) 7606-7619.

[9] Alkilany, A. M.; Nagaria, P. K.; Hexel, C. R.; Shaw, T. J.; Murphy, C. J.; and Wyatt, M. D.; *Cellular Uptake and Cytotoxicity of Gold Nanorods: Molecular Origin of Cytotoxicity and Surface Effects.* Small **2009** 5(6) 701-708.

[10] Chen, C.; Kuo, L.; Chang, C.; Hwu, Y.; Huang, C.; Lee, S.; Chen, K.; Lin, S.; Huang, J.; and Chen, Y.; *In situ real-time investigation of cancer cell photothermolysis mediated by excited gold nanorod surface plasmons.* Biomaterials **2010** 31(14) 4104-4112.

[11] Dickerson, E. B.; Dreaden, E. C.; Huang, X.; El-Sayed, I. H.; Chu, H.; Pushpanketh, S.; McDonald, J. F.; and El-Sayed, M. A.; *Gold nanorod assisted near-infrared*

plasmonic photothermal therapy (PPTT) of squamous cell carcinoma in mice. Cancer Letters **2008** 269(1) 57-66.

[12] Khlebtsov, B.; Khanadeev, V.; Maksimova, I.; Terentyuk, G.; and Khlebtsov, N.; *Silver nanocubes and gold nanocages: Fabrication and optical and photothermal properties.* Nanotechnologies in Russia **2010** 5(7) 454-468.

[13] Millstone, J. E.; Hurst, S. J.; Métraux, G. S.; Cutler, J. I.; and Mirkin, C. A.; *Colloidal Gold and Silver Triangular Nanoprisms.* Small **2009** 5(6) 646-664.

[14] El-Sayed, I. H.; Huang, X.; and El-Sayed, M. A.; *Selective laser photo-thermal therapy of epithelial carcinoma using anti-EGFR antibody conjugated gold nanoparticles.* Cancer Letters **2006** 239(1) 129-135.

[15] El-Sayed, I. H.; Huang, X.; and El-Sayed, M. A.; *Surface Plasmon Resonance Scattering and Absorption of anti-EGFR Antibody Conjugated Gold Nanoparticles in Cancer Diagnostics: Applications in Oral Cancer.* Nano Letters **2005** 5(5) 829-834.

[16] Gratton, S. E.; Ropp, P. A.; Pohlhaus, P. D.; Luft, J. C.; Madden, V. J.; Napier, M. E.; and DeSimone, J. M.; *The effect of particle design on cellular internalization pathways.* Proceedings of the National Academy of Sciences **2008** 105(33) 11613-11618.

[17] Cheong, S.; Watt, J. D.; and Tilley, R. D.; *Shape control of platinum and palladium nanoparticles for catalysis.* Nanoscale **2010** 2(10) 2045-2053.

[18] Pacheco, G.; *Studies on the Action of Metallic Colloids on Immunisation.* Mem. Inst. Oswaldo Cruz **1925** 18(1) 119-149.

[19] Jain, P. K.; El-Sayed, I. H.; and El-Sayed, M. A.; *Au nanoparticles target cancer.* Nano Today **2007** 2(1) 18-29.

[20] Chen, C.; Lin, Y.; Wang, C.; Tzeng, H.; Wu, C.; Chen, Y.; Chen, C.; Chen, L.; and Wu, Y.; *DNA−Gold Nanorod Conjugates for Remote Control of Localized Gene Expression by near Infrared Irradiation.* Journal of the American Chemical Society **2006** 128(11) 3709-3715.

[21] Cheng, H.; Huan, S.; and Yu, R.; *Nanoparticle-based substrates for surface-enhanced Raman scattering detection of bacterial spores.* Analyst **2012** 137(16) 3601-3608.

[22] Wani, I. A.; Khatoon, S.; Ganguly, A.; Ahmed, J.; and Ahmad, T.; *Structural characterization and antimicrobial properties of silver nanoparticles prepared by inverse microemulsion method.* Colloids and Surfaces B: Biointerfaces **2013** 101(0) 243-250.

[23] Xia, T.; Kovochich, M.; Liong, M.; Meng, H.; Kabehie, S.; George, S.; Zink, J. I.; and Nel, A. E.; *Polyethyleneimine Coating Enhances the Cellular Uptake of Mesoporous Silica Nanoparticles and Allows Safe Delivery of siRNA and DNA Constructs.* ACS Nano **2009** 3(10) 3273-3286.

[24] Kopelman, R.; Lee Koo, Y.; Philbert, M.; Moffat, B. A.; Ramachandra Reddy, G.; McConville, P.; Hall, D. E.; Chenevert, T. L.; Bhojani, M. S.; Buck, S. M.;

Rehemtulla, A.; and Ross, B. D.; *Multifunctional nanoparticle platforms for in vivo MRI enhancement and photodynamic therapy of a rat brain cancer.* Journal of Magnetism and Magnetic Materials **2005** 293(1) 404-410.

[25] Smijs, T.; and Pavel, S.; *Titanium dioxide and zinc oxide nanoparticles in sunscreens: Focus on their safety and effectiveness.* Nanotechnology, Science and Applications **2011** 4(1) 95-112.

[26] Jiang, X.; Röcker, C.; Hafner, M.; Brandholt, S.; Dörlich, R. M.; and Nienhaus, G. U.; *Endo- and Exocytosis of Zwitterionic Quantum Dot Nanoparticles by Live HeLa Cells.* ACS Nano **2010** 4(11) 6787-6797.

[27] Hoshino, A.; Fujioka, K.; Oku, T.; Suga, M.; Sasaki, Y. F.; Ohta, T.; Yasuhara, M.; Suzuki, K.; and Yamamoto, K.; *Physicochemical Properties and Cellular Toxicity of Nanocrystal Quantum Dots Depend on Their Surface Modification.* Nano Letters **2004** 4(11) 2163-2169.

[28] Delehanty, J. B.; Medintz, I. L.; Pons, T.; Brunel, F. M.; Dawson, P. E.; and Mattoussi, H.; *Self-Assembled Quantum Dot−Peptide Bioconjugates for Selective Intracellular Delivery.* Bioconjugate Chemistry **2006** 17(4) 920-927.

[29] Miller, C. R.; Bondurant, B.; McLean, S. D.; McGovern, K. A.; and O'Brien, D. F.; *Liposome−Cell Interactions in Vitro: Effect of Liposome Surface Charge on the Binding and Endocytosis of Conventional and Sterically Stabilized Liposomes†.* Biochemistry **1998** 37(37) 12875-12883.

[30] Kam, N. W.; O'Connell, M.; Wisdom, J. A.; and Dai, H.; *Carbon nanotubes as multifunctional biological transporters and near-infrared agents for selective cancer cell destruction.* Proceedings of the National Academy of Sciences of the United States of America **2005** 102(33) 11600-11605.

[31] Li, W.; Chen, C.; Ye, C.; Wei, T.; Zhao, Y.; Lao, F.; Chen, Z.; Meng, H.; Gao, Y.; Yuan, H.; Xing, G.; Zhao, F.; Chai, Z.; Zhang, X.; Yang, F.; Han, D.; Tang, X.; and Zhang, Y.; *The translocation of fullerenic nanoparticles into lysosome via the pathway of clathrin-mediated.* Nanotechnology **2008** 19(14) 145102.

[32] Wang, X.; Wang, Y.; Chen, Z. G.; and Shin, D. M.; *Advances of Cancer Therapy by Nanotechnology.* Cancer Res Treat **2009** 41(1) 1-11.

[33] Koo, Y. L.; Ulbrich, E. E.; Kim, G.; Hah, H.; Strollo, C.; Fan, W.; Gurjar, R.; Koo, S.; and Kopelman, R.; *Near Infrared Luminescent Oxygen Nanosensors with Nanoparticle Matrix Tailored Sensitivity.* Analytical Chemistry **2010** 82(20) 8446-8455.

[34] Hah, H. J.; Kim, G.; Lee, Y. K.; Orringer, D. A.; Sagher, O.; Philbert, M. A.; and Kopelman, R.; *Methylene Blue-Conjugated Hydrogel Nanoparticles and Tumor-Cell Targeted Photodynamic Therapy.* Macromolecular Bioscience **2011** 11(1) 90-99.

[35] Gref, R.; Minamitake, Y.; Peracchia, M. T.; Trubetskoy, V.; Torchilin, V.; and Langer, R.; *Biodegradable Long-Circulating Polymeric Nanospheres.* Science **1994** 263(5153) 1600-1603.

[36] Stolnik, S.; Dunn, S. E.; Garnett, M. C.; Davies, M. C.; Coombes, A. G.; Taylor, D. C.; Irving, M. P.; Purkiss, S. C.; Tadros, T. F.; Davis, S. S.; and Illum, L.; *Surface Modification of Poly(lactide-co-glycolide) Nanospheres by Biodegradable Poly(lactide)-Poly(ethylene glycol) Copolymers.* Pharmaceutical Research **1994** 11(12) 1800-1808.

[37] Benjaminsen, R. V.; Mattebjerg, M. A.; Henriksen, J. R.; Moghimi, S. M.; and Andresen, T. L.; *The Possible "Proton Sponge" Effect of Polyethylenimine (PEI) Does Not Include Change in Lysosomal pH.* Mol Ther **2013** 21(1) 149-157.

[38] Xu, H.; Aylott, J. W.; Kopelman, R.; Miller, T. J.; and Philbert, M. A.; *A Real-Time Ratiometric Method for the Determination of Molecular Oxygen Inside Living Cells Using Sol−Gel-Based Spherical Optical Nanosensors with Applications to Rat C6 Glioma.* Analytical Chemistry **2001** 73(17) 4124-4133.

[39] Myc, A.; Kukowska-Latallo, J.; Cao, P.; Swanson, B.; Battista, J.; Dunham, T.; and Baker, J.; *Targeting the efficacy of a dendrimer-based nanotherapeutic in heterogeneous xenograft tumors in vivo.* Anti-Cancer Drugs **2010** 21(2) 186-192.

[40] Niidome, T.; Yamagata, M.; Okamoto, Y.; Akiyama, Y.; Takahashi, H.; Kawano, T.; Katayama, Y.; and Niidome, Y.; *PEG-modified gold nanorods with a stealth character for in vivo applications.* Journal of Controlled Release **2006** 114(3) 343-347.

[41] Wang, X.; Yang, L.; Chen, Z. (.; and Shin, D. M.; *Application of Nanotechnology in Cancer Therapy and Imaging.* CA: A Cancer Journal for Clinicians **2008** 58(2) 97-110.

[42] Khlebtsov, B.; Zharov, V.; Melnikov, A.; Tuchin, V.; and Khlebtsov, N.; *Optical amplification of photothermal therapy with gold nanoparticles and nanoclusters.* Nanotechnology **2006** 17(20) 5167-5180.

[43] Lu, J.; Liong, M.; Sherman, S.; Xia, T.; Kovochich, M.; Nel, A.; Zink, J.; and Tamanoi, F.; *Mesoporous Silica Nanoparticles for Cancer Therapy: Energy-Dependent Cellular Uptake and Delivery of Paclitaxel to Cancer Cells.* NanoBioTechnology **2007** 3(2) 89-95.

[44] Clark, H. A.; Merritt, G.; and Kopelman, R.; *Novel optical biosensors using a gold colloid monolayer substrate.* Scanning and Force Microscopies for Biomedical Applications II **2000** 3922(1) 138-146.

[45] Lagerholm, B. C.; Wang, M.; Ernst, L. A.; Ly, D. H.; Liu, H.; Bruchez, M. P.; and Waggoner, A. S.; *Multicolor Coding of Cells with Cationic Peptide Coated Quantum Dots.* Nano Letters **2004** 4(10) 2019-2022.

[46] Soenen, S. J.; and De Cuyper, M.; *Assessing iron oxide nanoparticle toxicity in vitro: current status and future prospects.* Nanomedicine **2010** 5(8) 1261-1275.

[47] Gupta, A. K.; and Gupta, M.; *Synthesis and surface engineering of iron oxide nanoparticles for biomedical applications.* Biomaterials **2005** 26(18) 3995-4021.

[48] SHAMIM, N.; PENG, Z.; HONG, L.; HIDAJAT, K.; and UDDIN, M. S.; *SYNTHESIS AND CHARACTERIZATION OF DOUBLE SURFACTANT COATED MAGNETIC PARTICLES.* International Journal of Nanoscience **2005** 04(02) 187-195.

[49] Cho, W.; Cho, M.; Jeong, J.; Choi, M.; Cho, H.; Han, B. S.; Kim, S. H.; Kim, H. O.; Lim, Y. T.; Chung, B. H.; and Jeong, J.; *Acute toxicity and pharmacokinetics of 13 nm-sized PEG-coated gold nanoparticles.* Toxicology and Applied Pharmacology **2009** 236(1) 16-24.

[50] Harush-Frenkel, O.; Rozentur, E.; Benita, S.; and Altschuler, Y.; *Surface Charge of Nanoparticles Determines Their Endocytic and Transcytotic Pathway in Polarized MDCK Cells.* Biomacromolecules **2008** 9(2) 435-443.

[51] Derossi, D.; Joliot, A. H.; Chassaing, G.; and Prochiantz, A.; *The third helix of the Antennapedia homeodomain translocates through biological membranes.* Journal of Biological Chemistry **1994** 269(14) 10444-10450.

[52] Pooga, M.; Hällbrink, M.; Zorko, M.; and Langel, U.; *Cell penetration by transportan.* The FASEB Journal **1998** 12(1) 67-77.

[53] Zhao, F.; Zhao, Y.; Liu, Y.; Chang, X.; Chen, C.; and Zhao, Y.; *Cellular Uptake, Intracellular Trafficking, and Cytotoxicity of Nanomaterials.* Small **2011** 7(10) 1322-1337.

[54] Soenen, S. J.; Brisson, A. R.; and De Cuyper, M.; *Addressing the problem of cationic lipid-mediated toxicity: The magnetoliposome model.* Biomaterials **2009** 30(22) 3691-3701.

[55] Haider, M.; Hatefi, A.; and Ghandehari, H.; *Recombinant polymers for cancer gene therapy: A minireview.* Journal of Controlled Release **2005** 109(1–3) 108-119.

[56] Kumar, S.; Harrison, N.; Richards-Kortum, R.; and Sokolov, K.; *Plasmonic Nanosensors for Imaging Intracellular Biomarkers in Live Cells.* Nano Letters **2007** 7(5) 1338-1343.

[57] Myc, A.; Majoros, I. J.; Thomas, T. P.; and Baker, J. R.; *Dendrimer-Based Targeted Delivery of an Apoptotic Sensor in Cancer Cells.* Biomacromolecules **2006** 8(1) 13-18.

[58] Reddy, G. R.; Bhojani, M. S.; McConville, P.; Moody, J.; Moffat, B. A.; Hall, D. E.; Kim, G.; Koo, Y. L.; Woolliscroft, M. J.; Sugai, J. V.; Johnson, T. D.; Philbert, M. A.; Kopelman, R.; Rehemtulla, A.; and Ross, B. D.; *Vascular Targeted Nanoparticles for Imaging and Treatment of Brain Tumors.* Clinical Cancer Research **2006** 12(22) 6677-6686.

[59] Koo, Y. L.; Reddy, G. R.; Bhojani, M.; Schneider, R.; Philbert, M. A.; Rehemtulla, A.; Ross, B. D.; and Kopelman, R.; *Brain cancer diagnosis and therapy with nanoplatforms.* Advanced Drug Delivery Reviews **2006** 58(14) 1556-1577.

[60] Acharya, S.; and Sahoo, S. K.; *PLGA nanoparticles containing various anticancer agents and tumour delivery by EPR effect.* Advanced Drug Delivery Reviews **2011** 63(3) 170-183.

[61] Iyer, A. K.; Khaled, G.; Fang, J.; and Maeda, H.; *Exploiting the enhanced permeability and retention effect for tumor targeting.* Drug Discovery Today **2006** 11(17–18) 812-818.

[62] Konno, T.; *Targeting chemotherapy for hepatoma: Arterial administration of anticancer drugs dissolved in lipiodol.* European Journal of Cancer **1992** 28(2–3) 403-409.

[63] Maeda, H.; *The enhanced permeability and retention (EPR) effect in tumor vasculature: the key role of tumor-selective macromolecular drug targeting.* Advances in Enzyme Regulation **2001** 41(1) 189-207.

[64] Gao, X.; Cui, Y.; Levenson, R. M.; Chung, L. W.; and Nie, S.; *In vivo cancer targeting and imaging with semiconductor quantum dots.* Nat Biotech **2004** 22(8) 969-976.

[65] Cai, W.; Shin, D.; Chen, K.; Gheysens, O.; Cao, Q.; Wang, S. X.; Gambhir, S. S.; and Chen, X.; *Peptide-Labeled Near-Infrared Quantum Dots for Imaging Tumor Vasculature in Living Subjects.* Nano Letters **2006** 6(4) 669-676.

[66] Sokolov, K.; Follen, M.; Aaron, J.; Pavlova, I.; Malpica, A.; Lotan, R.; and Richards-Kortum, R.; *Real-Time Vital Optical Imaging of Precancer Using Anti-Epidermal Growth Factor Receptor Antibodies Conjugated to Gold Nanoparticles.* Cancer Research **2003** 63(9) 1999-2004.

[67] Kang, B.; Mackey, M. A.; and El-Sayed, M. A.; *Nuclear Targeting of Gold Nanoparticles in Cancer Cells Induces DNA Damage, Causing Cytokinesis Arrest and Apoptosis.* Journal of the American Chemical Society **2010** 132(5) 1517-1519.

[68] Jiang, W.; Kim, B. Y.; Rutka, J. T.; and Chan, W. C.; *Nanoparticle-mediated cellular response is size-dependent.* Nat Nano **2008** 3(3) 145-150.

[69] Asharani, P.; Xinyi, N.; Hande, M. P.; and Valiyaveettil, S.; *DNA damage and p53-mediated growth arrest in human cells treated with platinum nanoparticles.* Nanomedicine **2009** 5(1) 51-64.

[70] Koo, Y. L.; Agayan, R.; Philbert, M. A.; Rehemtulla, A.; Ross, B. D.; and Kopelman, R.; *New Approaches in Biomedical Spectroscopy Chapter 14: Photonic Explorers Based on Multifunctional Nanoplatforms: In Vitro and In Vivo Biomedical Applications.* (2007) New York, American Chemical Society.

[71] Park, E. J.; Brasuel, M.; Behrend, C.; Philbert, M. A.; and Kopelman, R.; *Ratiometric Optical PEBBLE Nanosensors for Real-Time Magnesium Ion Concentrations Inside Viable Cells.* Analytical Chemistry **2003** 75(15) 3784-3791.

[72] Clark, H. A.; Hoyer, M.; Philbert, M. A.; and Kopelman, R.; *Optical Nanosensors for Chemical Analysis inside Single Living Cells. 1. Fabrication, Characterization, and Methods for Intracellular Delivery of PEBBLE Sensors.* Analytical Chemistry **1999** 71(21) 4831-4836.

[73] Sumner, J. P.; Aylott, J. W.; Monson, E.; and Kopelman, R.; *A fluorescent PEBBLE nanosensor for intracellular free zinc.* Analyst **2002** 127(1) 11-16.

[74] Sumner, J. P.; Westerberg, N. M.; Stoddard, A. K.; Fierke, C. A.; and Kopelman, R.; *Cu+- and Cu2+-sensitive PEBBLE fluorescent nanosensors using DsRed as the recognition element.* Sensors and Actuators B: Chemical **2006** 113(2) 760-767.

[75] Sumner, J. P.; and Kopelman, R.; *Alexa Fluor 488 as an iron sensing molecule and its application in PEBBLE nanosensors.* Analyst **2005** 130(4) 528-533.

[76] Koo, Y. L.; Cao, Y.; Kopelman, R.; Koo, S. M.; Brasuel, M.; and Philbert, M. A.; *Real-Time Measurements of Dissolved Oxygen Inside Live Cells by Organically Modified Silicate Fluorescent Nanosensors.* Analytical Chemistry **2004** 76(9) 2498-2505.

[77] Cao, Y.; Lee Koo, Y.; and Kopelman, R.; *Poly(decyl methacrylate)-based fluorescent PEBBLE swarm nanosensors for measuring dissolved oxygen in biosamples.* Analyst **2004** 129(8) 745-750.

[78] Gregoriadis, G.; and Ryman, B. E.; *Fate of Protein-Containing Liposomes Injected into Rats.* European Journal of Biochemistry **1972** 24(3) 485-491.

[79] Gabrielli, D.; Belisle, E.; Severino, D.; Kowaltowski, A. J.; and Baptista, M. S.; *Binding, aggregation and photochemical properties of methylene blue in mitochondrial suspensions.* Photochemistry and Photobiology **2004** 79(3) 227-232.

[80] Svenson, S.; Wolfgang, M.; Hwang, J.; Ryan, J.; and Eliasof, S.; *Preclinical to clinical development of the novel camptothecin nanopharmaceutical CRLX101.* Journal of Controlled Release **2011** 153(1) 49-55.

[81] Schneider, R. J.; *Characterization of polyacrylamide nanoparticles for biomedical applications: Toxicology, pharmacology, and therapy.* Ph.D. Dissertation, University of Michigan, United States -- Michigan **2005** () .

[82] Wake, K.; Decker, K.; Kirn, A.; Knook, D.; McCuskey, R.; Bouwens, L.; Wisse, E.; and G.H. Bourne, K. J.; *Cell Biology and Kinetics of Kupffer Cells in the Liver.* International Review of cytology **1989** 118() 173-229.

[83] Khlebtsov, N.; and Dykman, L.; *Biodistribution and toxicity of engineered gold nanoparticles: a review of in vitro and in vivo studies.* Chemical Society Reviews **2011** 40(3) 1647-1671.

[84] Davis, M. E.; Chen, Z. (.; and Shin, D. M.; *Nanoparticle therapeutics: an emerging treatment modality for cancer.* Nat Rev Drug Discov **2008** 7(9) 771-782.

[85] Ulbrich, K.; and Šubr, V.; *Polymeric anticancer drugs with pH-controlled activation.* Advanced Drug Delivery Reviews **2004** 56(7) 1023-1050.

[86] Kratz, F.; Beyer, U.; and Schütte, M.; *Drug-polymer conjugates containing acid-cleavable bonds.* Critical Reviews in Therapeutic Drug Carrier Systems **1999** 16(3) 245-288.

[87] Tarantola, M.; Pietuch, A.; Schneider, D.; Rother, J.; Sunnick, E.; Rosman, C.; Pierrat, S.; Sönnichsen, C.; Wegener, J.; and Janshoff, A.; *Toxicity of gold-nanoparticles: Synergistic effects of shape and surface functionalization on micromotility of epithelial cells.* Nanotoxicology **2010** 5(2) 254-268.

[88] Dobrovolskaia, M. A.; and McNeil, S. E.; *Immunological properties of engineered nanomaterials.* Nat Nano **2007** 2(8) 469-478.

[89] Oh, J.; Choi, S.; Lee, G.; Kim, J.; and Choy, J.; *Inorganic Metal Hydroxide Nanoparticles for Targeted Cellular Uptake Through Clathrin-Mediated Endocytosis.* Chemistry – An Asian Journal **2009** 4(1) 67-73.

[90] Wang, Z.; Tiruppathi, C.; Minshall, R. D.; and Malik, A. B.; *Size and Dynamics of Caveolae Studied Using Nanoparticles in Living Endothelial Cells.* ACS Nano **2009** 3(12) 4110-4116.

[91] Chen, Y.; Hung, Y.; Liau, I.; and Huang, G.; *Assessment of the In Vivo Toxicity of Gold Nanoparticles.* Nanoscale Research Letters **2009** 4(8) 858-864.

[92] Pulskamp, K.; Diabaté, S.; and Krug, H. F.; *Carbon nanotubes show no sign of acute toxicity but induce intracellular reactive oxygen species in dependence on contaminants.* Toxicology Letters **2007** 168(1) 58-74.

[93] Koo Lee, Y.; Smith, R.; and Kopelman, R.; *Nanoparticle PEBBLE Sensors in Live Cells and In Vivo.* Annual Review of Analytical Chemistry **2009** 2(1) 57-76.

[94] Brasuel, M.; Kopelman, R.; Miller, T. J.; Tjalkens, R.; and Philbert, M. A.; *Fluorescent Nanosensors for Intracellular Chemical Analysis: Decyl Methacrylate Liquid Polymer Matrix and Ion-Exchange-Based Potassium PEBBLE Sensors with Real-Time Application to Viable Rat C6 Glioma Cells.* Analytical Chemistry **2001** 73(10) 2221-2228.

[95] Clark, H. A.; Hoyer, M.; Parus, S.; Philbert, M. A.; and Kopelman, R.; *Optochemical Nanosensors and Subcellular Applications in Living Cells.* Microchimica Acta **1999** 131(1) 121-128.

[96] Chan, W. C.; and Nie, S.; *Quantum Dot Bioconjugates for Ultrasensitive Nonisotopic Detection.* Science **1998** 281(5385) 2016-2018.

[97] Åkerman, M. E.; Chan, W. C.; Laakkonen, P.; Bhatia, S. N.; and Ruoslahti, E.; *Nanocrystal targeting in vivo.* Proceedings of the National Academy of Sciences **2002** 99(20) 12617-12621.

[98] Tang, W.; *Development and in vitro investigation of methylene blue-containing nanoparticle platforms for photodynamic therapy. Ph.D. dissertation.* (2007) University of Michigan, Ann Arbor Sciences , .

[99] Huang, J. G.; Leshuk, T.; and Gu, F. X.; *Emerging nanomaterials for targeting subcellular organelles.* Nano Today **2011** 6(5) 478-492.

[100] Nishikawa, T.; Iwakiri, N.; Kaneko, Y.; Taguchi, A.; Fukushima, K.; Mori, H.; Morone, N.; and Kadokawa, J.; *Nitric Oxide Release in Human Aortic Endothelial Cells Mediated by Delivery of Amphiphilic Polysiloxane Nanoparticles to Caveolae.* Biomacromolecules **2009** 10(8) 2074-2085.

[101] Bartczak, D.; Sanchez-Elsner, T.; Louafi, F.; Millar, T. M.; and Kanaras, A. G.; *Receptor-Mediated Interactions between Colloidal Gold Nanoparticles and Human Umbilical Vein Endothelial Cells.* Small **2011** 7(3) 388-394.

[102] Bulte, J. W.; de Cuyper, M.; Despres, D.; and Frank, J. A.; *Short- vs. long-circulating magnetoliposomes as bone marrow-seeking MR contrast agents.* Journal of Magnetic Resonance Imaging **1999** 9(2) 329-335.

[103] Clark, H. A.; Barker, S. L.; Brasuel, M.; Miller, M. T.; Monson, E.; Parus, S.; Shi, Z.; Song, A.; Thorsrud, B.; Kopelman, R.; Ade, A.; Meixner, W.; Athey, B.; Hoyer, M.; Hill, D.; Lightle, R.; and Philbert, M. A.; *Subcellular optochemical nanobiosensors: probes encapsulated by biologically localised embedding (PEBBLEs).* Sensors and Actuators B: Chemical **1998** 51(1–3) 12-16.

[104] Sasaki, K.; Shi, Z.; Kopelman, R.; and Masuhara, H.; *Three-Dimensional pH Microprobing with an Optically-Manipulated Fluorescent Particle.* Chemistry Letters **1996** 25(2) 141-142.

[105] Harrell, J. A.; and Kopelman, R.; *Biocompatible Probes Measure Intracellular Activity.* Biophotonics International **2000** 7() 22-24.

[106] Rhyner, M. N.; Smith, A. M.; Gao, X.; Mao, H.; Yang, L.; and Nie, S.; *Quantum dots and multifunctional nanoparticles: new contrast agents for tumor imaging.* Nanomedicine **2006** 1(2) 209-217.

[107] Doyen, E. L.; *Traité de thérapeutique chirurgicale et de technique opératoire. Tome troisième: chirurgie du cou, du thorax et du membre supérieur.* (1910) Paris, .

[108] Griffin, R. J.; Dings, R. P.; Jamshidi-Parsian, A.; and Song, C. W.; *Mild temperature hyperthermia and radiation therapy: Role of tumour vascular thermotolerance and relevant physiological factors.* International Journal of Hyperthermia **2010** 26(3) 256-263.

[109] Oleson, J. R.; and Dewhirst, M. W.; *Hyperthermia: An overview of current progress and problems.* Current Problems in Cancer **1983** 8(6) 1-62.

[110] Creixell, M.; Bohórquez, A. C.; Torres-Lugo, M.; and Rinaldi, C.; *EGFR-Targeted Magnetic Nanoparticle Heaters Kill Cancer Cells without a Perceptible Temperature Rise.* ACS Nano **2011** 5(9) 7124-7129.

[111] Prasad, N. K.; Rathinasamy, K.; Panda, D.; and Bahadur, D.; *TC-tuned biocompatible suspension of La0.73Sr0.27MnO3 for magnetic hyperthermia.* Journal of Biomedical Materials Research Part B: Applied Biomaterials **2008** 85B(2) 409-416.

[112] Crile Jr., G.; *Heat as an adjunct to the treatment of cancer; experimental studies.* Cleveland Clinic quarterly **1961** 28() 75-89.

[113] American Cancer Society Inc.; *Hyperthermia.* American Cancer Society Inc. **8/30/2011** Accessed(28/8/2011) http://www.cancer.org/treatment/treatmentsandsideeffects/treatmenttypes/hyperthermia.

[114] Song, C.; *Physiological factors in hyperthermia.* National Cancer Institute monograph **1982** 61() 169-176.

[115] Song, C. W.; Kang, M. S.; Rhee, J. G.; and Levitt, S. H.; *The effect of hyperthermia on vascular function, pH, and cell survival.* Radiology **1980** 137(3) 795-803.

[116] Harisiadis, L.; Sung, D. I.; and Hall, E. J.; *Thermal Tolerance and Repair of Thermal Damage by Cultured Cells.* Radiology **1977** 123(2) 505-509.

[117] Dickson, J. A.; and Muckle, D. S.; *Total-Body Hyperthermia versus Primary Tumor Hyperthermia in the Treatment of the Rabbit VX-2 Carcinoma.* Cancer Research **1972** 32(9) 1916-1923.

[118] Song, C. W.; Park, H.; and Griffin, R. J.; *Improvement of Tumor Oxygenation by Mild Hyperthermia.* Radiation Research **2001** 155(4) 515-528.

[119] Vujaskovic, Z.; and Song, C. W.; *Physiological mechanisms underlying heat-induced radiosensitization.* International Journal of Hyperthermia **2004** 20(2) 163-174.

[120] Bettaieb, A.; and Averill-Bates, D. A.; *Thermotolerance induced at a fever temperature of 40 °C protects cells against hyperthermia-induced apoptosis mediated by death receptor signalling.* Biochemistry and Cell Biology **2008** 86(6) 521-538.

[121] Daniel, P.; *Dissecting the pathways to death.* Leukemia **2000** 14(12) 2035-2044.

[122] Cherukuri, P.; Glazer, E. S.; and Curley, S. A.; *Targeted hyperthermia using metal nanoparticles.* Advanced Drug Delivery Reviews **2010** 62(3) 339-345.

[123] Vauthier, C.; Tsapis, N.; and Couvreur, P.; *Nanoparticles: heating tumors to death?.* Nanomedicine **2010** 6(1) 99-109.

[124] Duguet, E.; Vasseur, S.; Mornet, S.; and Devoisselle, J.; *Magnetic nanoparticles and their applications in medicine.* Nanomedicine **2006** 1(2) 157-168.

[125] Kobayashi, T.; *Cancer hyperthermia using magnetic nanoparticles.* Biotechnology Journal **2011** 6(11) 1342-1347.

[126] Muckle, D. S.; and Dickson, J. A.; *The Selective Inhibitory Effect of Hyperthermia on the Metabolism and Growth of Malignant Cells.* British Journal of Cancer **1971** 25(4) 771-778.

[127] Mondovi', B.; Strom, R.; Rotilio, G.; Agro', A. F.; Cavaliere, R.; and Fanelli, A. R.; *The biochemical mechanism of selective heat sensitivity of cancer cells: I. Studies on cellular respiration.* European Journal of Cancer **1969** 5(2) 129-136.

[128] Vaupel, P.; Ostheimer, K.; and Müller-Klieser, W.; *Circulatory and metabolic responses of malignant tumors during localized hyperthermia.* Journal of Cancer Research and Clinical Oncology **1980** 98(1) 15-29.

[129] Gullino, P.; Nyong Yi, P.; and Grantham, F.; *Relationship between temperature and blood supply or consumption of oxygen and glucose by rat mammary carcinomas.* Journal of the National Cancer Institute **1978** 60(4) 835-847.

[130] Kirkpatrick, J. P.; Brizel, D. M.; and Dewhirst, M. W.; *A Mathematical Model of Tumor Oxygen and Glucose Mass Transport and Metabolism with Complex Reaction Kinetics.* Radiation Research **2003** 159(3) 336-344.

[131] Okajima, K.; Griffin, R. J.; Iwata, K.; Shakil, A.; and Song, C. W.; *Tumor Oxygenation after Mild-Temperature Hyperthermia in Combination with Carbogen Breathing: Dependence on Heat Dose and Tumor Type.* Radiation Research **1998** 149(3) 294-299.

[132] Ogawa, A.; Griffin, R. J.; and Song, C. W.; *Effect of a Combination of Mild-Temperature Hyperthermia and Nicotinamide on the Radiation Response of Experimental Tumors.* Radiation Research **2000** 153(3) 327-331.

[133] Connor, W. G.; Gerner, E. W.; Miller, R. C.; and Boone, M. L.; *Prospects for Hyperthermia in Human Cancer Therapy: Part II: Implications of Biological and Physical Data for Applications of Hyperthermia to Man.* Radiology **1977** 123(2) 497-503.

[134] Palzer, R. J.; and Heidelberger, C.; *Studies on the Quantitative Biology of Hyperthermic Killing of HeLa Cells.* Cancer Research **1973** 33(2) 415-421.

[135] Wike-Hooley, J. L.; van der Zee, J.; van Rhoon, G. C.; van den Berg, A. P.; and Reinhold, H. S.; *Human tumour pH changes following hyperthermia and radiation therapy.* European Journal of Cancer and Clinical Oncology **1984** 20(5) 619-623.

[136] Crile, G.; *The Effects of Heat and Radiation on Cancers Implanted on the Feet of Mice.* Cancer Research **1963** 23(3) 372-380.

[137] Gerner, E. W.; Boone, R.; Connor, W. G.; Hicks, J. A.; and Boone, M. L.; *A Transient Thermotolerant Survival Response Produced by Single Thermal Doses in HeLa Cells.* Cancer Research **1976** 36(3) 1035-1040.

[138] Henle, K. J.; and Dethlefsen, L. A.; *Heat Fractionation and Thermotolerance: A Review.* Cancer Research **1978** 38(7) 1843-1851.

[139] Yu, J.; Javier, D.; Yaseen, M. A.; Nitin, N.; Richards-Kortum, R.; Anvari, B.; and Wong, M. S.; *Self-Assembly Synthesis, Tumor Cell Targeting, and Photothermal Capabilities of Antibody-Coated Indocyanine Green Nanocapsules.* Journal of the American Chemical Society **2010** 132(6) 1929-1938.

[140] Jain, P. K.; Lee, K. S.; El-Sayed, I. H.; and El-Sayed, M. A.; *Calculated Absorption and Scattering Properties of Gold Nanoparticles of Different Size, Shape, and Composition: Applications in Biological Imaging and Biomedicine.* The Journal of Physical Chemistry B **2006** 110(14) 7238-7248.

[141] Urbanska, K.; Romanowska-Dixon, B.; Matuszak, Z.; Oszajca, J.; Nowak-Sliwinska, P.; and Stochel, G.; *Indocyanine green as a prospective sensitizer for photodynamic therapy of melanomas.* Acta Biochimica Polonica **2002** 49(2) 387-391.

[142] Cheong, W.; Prahl, S.; and Welch, A.; *A review of the optical properties of biological tissues.* Quantum Electronics, IEEE Journal of **1990** 26(12) 2166-2185.

[143] Delpy, D. T.; and Cope, M.; *Quantification in tissue near–infrared spectroscopy.* Philosophical Transactions of the Royal Society of London. Series B: Biological Sciences **1997** 352(1354) 649-659.

[144] Ntziachristos, V.; Bremer, C.; and Weissleder, R.; *Fluorescence imaging with near-infrared light: new technological advances that enable in vivo molecular imaging.* European Radiology **2003** 13(1) 195-208.

[145] Tromberg, B. J.; Shah, N.; Lanning, R.; Cerussi, A.; Espinoza, J.; Pham, T.; Svaasand, L.; and Butler, J.; *Non-Invasive In Vivo Characterization of Breast Tumors Using Photon Migration Spectroscopy.* Neoplasia **2000** 2(1-2) 26-40.

[146] Ethirajan, M.; Chen, Y.; Joshi, P.; and Pandey, R. K.; *The role of porphyrin chemistry in tumor imaging and photodynamic therapy.* Chemical Society Reviews **2011** 40(1) 340-362.

[147] Gannon, C.; Patra, C.; Bhattacharya, R.; Mukherjee, P.; and Curley, S.; *Intracellular gold nanoparticles enhance non-invasive radiofrequency thermal destruction of human gastrointestinal cancer cells.* Journal of Nanobiotechnology **2008** 6(1) 2.

[148] Vermeersch, G.; Ronfard-Haret, J. C.; Bazin, M.; Carillet, V.; Morliere, P.; and Santus, R.; *TYPE I and TYPE II PHOTOSENSITIZATION BY THE ANTIBACTERIAL DRUG NALIDIXIC ACID. A LASER FLASH PHOTOLYSIS STUDY*.* Photochemistry and Photobiology **1991** 54(5) 661-666.

[149] Williams, J.; Pearson, G.; Colles, M.; and Wilson, M.; *The Photo-Activated Antibacterial Action of Toluidine Blue O in a Collagen Matrix and in Carious Dentine.* Caries Research **2004** 38(6) 530-536.

[150] Fimple, J. L.; Fontana, C. R.; Foschi, F.; Ruggiero, K.; Song, X.; Pagonis, T. C.; Tanner, A. C.; Kent, R.; Doukas, A. G.; Stashenko, P. P.; and Soukos, N. S.; *Photodynamic Treatment of Endodontic Polymicrobial Infection In Vitro.* Journal of Endodontics **2008** 34(6) 728-734.

[151] Park, J.; Moon, Y.; Bang, I.; Kim, Y.; Kim, S.; Ahn, S.; and Yoon, J.; *Antimicrobial effect of photodynamic therapy using a highly pure chlorin e6.* Lasers in Medical Science **2010** 25(5) 705-710.

[152] Lovell, J. F.; Liu, T. W.; Chen, J.; and Zheng, G.; *Activatable Photosensitizers for Imaging and Therapy.* Chemical Reviews **2010** 110(5) 2839-2857.

[153] Yaseen, M. A.; Diagaradjane, P.; Pikkula, B. M.; Yu, J.; Wong, M. S.; and Anvari, B.; *Photothermal and photochemical effects of laser light absorption by indocyanine green (ICG).* **2005** () 27-35.

[154] DeRosa, M. C.; and Crutchley, R. J.; *Photosensitized singlet oxygen and its applications.* Coordination Chemistry Reviews **2002** 233–234(0) 351-371.

[155] Wilkinson, F.; Helman, W. P.; and Ross, A. B.; *Rate Constants for the Decay and Reactions of the Lowest Electronically Excited Singlet State of Molecular Oxygen in Solution. An Expanded and Revised Compilation.* Journal of Physical and Chemical Reference Data **1995** 24(2) 663-677.

[156] Moan, J.; and Boye, E.; *Photodynamic effect on DNA and cell survival of human cells sensitized by hematoporphyrin.* Photobiochemistry and Photobiophysics **1981** 2(4-5) 301-307.

[157] Reindl, S.; Penzkofer, A.; Gong, S.; Landthaler, M.; Szeimies, R.; Abels, C.; and Bäumler, W.; *Quantum yield of triplet formation for indocyanine green.* Journal of Photochemistry and Photobiology A: Chemistry **1997** 105(1) 65-68.

[158] Wu, J.; Xu, H.; Tang, W.; Kopelman, R.; Philbert, M. A.; and Xi, C.; *Eradication of Bacteria in Suspension and Biofilms Using Methylene Blue-Loaded Dynamic Nanoplatforms.* Antimicrobial Agents and Chemotherapy **July** 53(7) 3042-3048.

[159] McNaughton, B. H.; Kehbein, K. A.; Anker, J. N.; and Kopelman, R.; *Sudden Breakdown in Linear Response of a Rotationally Driven Magnetic Microparticle and Application to Physical and Chemical Microsensing†.* The Journal of Physical Chemistry B **2006** 110(38) 18958-18964.

[160] McNaughton, B. H.; Agayan, R. R.; Wang, J. X.; and Kopelman, R.; *Physiochemical microparticle sensors based on nonlinear magnetic oscillations.* Sensors and Actuators B: Chemical **2007** 121(1) 330-340.

[161] Cēbers, A.; and Ozols, M.; *Dynamics of an active magnetic particle in a rotating magnetic field.* Physical Review E **2006** 73(2) 021505-.

[162] Shelton, W. A.; Bonin, K. D.; and Walker, T. G.; *Nonlinear motion of optically torqued nanorods.* Physical Review E **2005** 71(3) 036204-.

[163] Helgesen, G.; Pieranski, P.; and Skjeltorp, A. T.; *Nonlinear phenomena in systems of magnetic holes.* Physical Review Letters **1990** 64(12) 1425-1428.

[164] Anker, J. N.; Behrend, C.; and Kopelman, R.; *Aspherical magnetically modulated optical nanoprobes (MagMOONs).* Journal of Applied Physics **2003** 93(10) 6698-6700.

[165] Jemal, A.; Bray, F.; Center, M. M.; Ferlay, J.; Ward, E.; and Forman, D.; *Global cancer statistics.* CA: A Cancer Journal for Clinicians **2011** 61(2) 69-90.

[166] National Cancer Institute; *What is Cancer?.* National Cancer Institute **9/2/2013** Accessed(9/2/2013) http://www.cancer.gov/cancertopics/cancerlibrary/what-is-cancer.

[167] Fucic, A.; Gamulin, M.; Ferencic, Z.; Rokotov, D. S.; Katic, J.; Bartonova, A.; Lovasic, I. B.; and Merlo, D. F.; *Lung Cancer and Environmental Chemical Exposure: A Review of Our Current State of Knowledge With Reference to the Role of Hormones and Hormone Receptors as an Increased Risk Factor for Developing Lung Cancer in Man.* Toxicologic Pathology **2010** 38(6) 849-855.

[168] Hu, Y.; Zheng, M.; Zhang, R.; Liang, Y.; and Han, H.; *Notch signaling pathway and cancer metastasis.* Advances in Experimental Medicine and Biology **2012** 727() 186-198.

[169] Per, O.; *Biological low-dose radiation effects.* Mutation Research/Reviews in Genetic Toxicology **1991** 258(2) 191-205.

[170] Sage, E.; Girard, P.; and Francesconi, S.; *Unravelling UVA-induced mutagenesis.* Photochemical & Photobiological Sciences **2012** 11(1) 74-80.

[171] Moan, J.; Baturaite, Z.; Porojnicu, A. C.; Dahlback, A.; and Juzeniene, A.; *UVA, UVB and incidence of cutaneous malignant melanoma in Norway and Sweden.* Photochemical & Photobiological Sciences **2012** 11(1) 191-198.

[172] Wang, Y.; and Chemical Rubber Company, .; *CRC handbook of radioactive nuclides.* (1969) Cleveland, Chemical Rubber Co..

[173] United States. Public Health Service. Office on Smoking and Health and United States. Public Health Service. Office of the Surgeon General; *The Health Consequences of Smoking.* (1982) Rockville, Maryland, United States. Public Health Service. Office on Smoking and Health.

[174] Perfetti, T. A.; and Rodgman, A.; *The Complexity of Tobacco and Tobacco Smoke.* Beiträge zur Tabakforschung International/Contributions to Tobacco Research **2011** 24(5) 215-232.

[175] Fowles, J.; and Dybing, E.; *Application of toxicological risk assessment principles to the chemical constituents of cigarette smoke.* Tobacco Control **2003** 12(4) 424-430.

[176] Sung, M.; Yeon, J.; Park, S.; Park, J. H.; and Choi, M.; *Obesity-induced metabolic stresses in breast and colon cancer.* Annals of the New York Academy of Sciences **2011** 1229(1) 61-68.

[177] Xing, M.; *Oxidative stress: a new risk factor for thyroid cancer.* Endocrine-Related Cancer **2011** () .

[178] Andrea, H.; *The role of DNA repair in benzene-induced carcinogenesis.* Chemico-Biological Interactions **2010** 184(1-2) 269-272.

[179] Sarma, S. N.; Kim, Y.; Song, M.; and Ryu, J.; *Induction of apoptosis in human leukemia cells through the production of reactive oxygen species and activation of HMOX1 and Noxa by benzene, toluene, and o-xylene.* Toxicology **2011** 280(3) 109-117.

[180] Wu, X.; Xue, M.; Li, X.; Wang, Y.; Wang, J.; Han, Q.; and Yi, Z.; *Phenolic metabolites of benzene inhibited the erythroid differentiation of K562 cells.* Toxicology Letters **2011** 203(3) 190-199.

[181] Broaddus, V. C.; Everitt, J. I.; Black, B.; and Kane, A. B.; *Non-Neoplastic and Neoplastic Pleural Endpoints Following Fiber Exposure.* Journal of Toxicology and Environmental Health, Part B **2011** 14(1-4) 153-178.

[182] Marty S., K.; *Mesothelioma from Chrysotile Asbestos: Update.* Annals of Epidemiology **2011** 21(9) 688-697.

[183] Yarborough, C.; *The risk of mesothelioma from exposure to chrysotile asbestos.* Current Opinion in Pulmonary Medicine **2007** 13(4) 334-338.

[184] Bartlett, D. L.; and Chu, E.; *Can Metastatic Colorectal Cancer Be Cured?.* Oncology (Williston Park) **2012** 26(3) 266-275.

[185] Scheele, J.; Stang, R.; Altendorf-Hofmann, A.; and Paul, M.; *Resection of colorectal liver metastases.* World Journal of Surgery **1995** 19(1) 59-71.

[186] Abrams, M. J.; and Murrer, B. A.; *Metal Compounds in Therapy and Diagnosis.* Science **1993** 261(5122) 725-730.

[187] Jonker, D.; Spithoff, K.; and Maroun, J.; *Adjuvant Systemic Chemotherapy for Stage II and III Colon Cancer after Complete Resection: An Updated Practice Guideline.* Clinical Oncology **2011** 23(5) 314-322.

[188] Gullino, P. M.; Grantham, F. H.; Smith, S. H.; and Haggerty, A. C.; *Modifications of the Acid-Base Status of the Internal Milieu of Tumors.* Journal of the National Cancer Institute **1965** 34(6) 857-869.

[189] Caulfield, M. J.; Qiao, G. G.; and Solomon, D. H.; *Some Aspects of the Properties and Degradation of Polyacrylamides.* Chemical Reviews **2002** 102(9) 3067-3084.

[190] Van Dyke, J. D.; and Kasperski, K. L.; *Thermogravimetric study of polyacrylamide with evolved gas analysis.* Journal of Polymer Science Part A: Polymer Chemistry **1993** 31(7) 1807-1823.

[191] DeWoskin, R. S.; Hogan, K.; Wohlers, D. W.; McClure, P. R.; Rhoades, J.; Salinas, K.; and Teeguarden, J. G.; *Toxicological Review of Acrylamide.* (2010) Washington D.C., U.S. Environmental Protection Agency.

[192] King, D.; and Noss, R.; *Toxicity of polyacrylamide and acrylamide monomer.* Reviews on Environmental Health **1989** 8(1-4) 3-16.

[193] Ono, S.; Ogawa, R.; and Hyakusoku, H.; *Complications after polyacrylamide hydrogel injection for soft-tissue augmentation.* Plastic and Reconstructive Surgery **2010** 126(4) 1349-1357.

[194] Christensen, L.; Breiting, V.; Aasted, A.; Jørgensen, A.; and Kebuladze, I.; *Long-term effects of polyacrylamide hydrogel on human breast tissue.* Plastic and Reconstructive Surgery **2003** 111(6) 1883-1890.

[195] Cheng, N.; Wang, Y.; Wang, J.; Zhang, X.; and Zhong, H.; *Complications of Breast Augmentation with Injected Hydrophilic Polyacrylamide Gel.* Aesthetic Plastic Surgery **2002** 26(5) 375-382.

[196] Smith, E.; and Oehme, F.; *Acrylamide and polyacrylamide: A review of production, use, environmental fate and neurotoxicity.* Reviews on Environmental Health **1991** 9(4) 215-228.

[197] CHRISTENSEN, L. H.; NIELSEN, J. B.; MOURITSEN, L.; SØRENSEN, M.; and LOSE, G.; *Tissue Integration of Polyacrylamide Hydrogel: An Experimental Study of Periurethral, Perivesical, and Mammary Gland Tissue in the Pig.* Dermatologic Surgery **2008** 34() S68-S77.

[198] Cheng, N.; Xu, S.; Deng, H.; Ding, X.; Zhang, X.; Wu, D.; Zhong, H.; and Sun, Z.; *Migration of implants: A problem with injectable polyacrylamide gel in aesthetic plastic surgery.* Aesthetic Plastic Surgery **2006** 30(2) 215-225.

[199] Cássia Novaes, W.; and Berg, A.; *Experiences with a New Nonbiodegradable Hydrogel (Aquamid): A Pilot Study.* **2003** 27(5) 376-380.

[200] Remy, M.; Thaler, S.; Schumann, R. G.; May, C. A.; Fiedorowicz, M.; Schuettauf, F.; Grüterich, M.; Priglinger, S. G.; Nentwich, M. M.; Kampik, A.; and Haritoglou, C.; *An in vivo evaluation of Brilliant Blue G in animals and humans.* British Journal of Ophthalmology **2008** 92(8) 1142-1147.

[201] Masters, J. R.; *HeLa cells 50 years on: the good, the bad and the ugly.* Nature Reviews Cancer **2002** 2(4) 315-319.

[202] Jones Jr., H.; McKusick, V.; Harper, P.; and Wuu, K.; *George Otto Gey. (1899-1970). The HeLa cell and a reappraisal of its origin.* Obstetrics and Gynecology **1971** 38(6) 945-949.

[203] Patra, H. K.; Banerjee, S.; Chaudhuri, U.; Lahiri, P.; and Dasgupta, A. K.; *Cell selective response to gold nanoparticles.* Nanomedicine: Nanotechnology, Biology and Medicine **2007** 3(2) 111-119.

[204] Masters, J. R.; Thomson, J. A.; Daly-Burns, B.; Reid, Y. A.; Dirks, W. G.; Packer, P.; Toji, L. H.; Ohno, T.; Tanabe, H.; Arlett, C. F.; Kelland, L. R.; Harrison, M.; Virmani, A.; Ward, T. H.; Ayres, K. L.; and Debenham, P. G.; *Short tandem repeat profiling provides an international reference standard for human cell lines.* Proceedings of the National Academy of Sciences **2001** 98(14) 8012-8017.

[205] Oldroyd, N. J.; Urquhart, A. J.; Kimpton, C. P.; Millican, E. S.; Watson, S. K.; Downes, T.; and Gill, P. D.; *A highly discriminating octoplex short tandem repeat polymerase chain reaction system suitable for human individual identification.* ELECTROPHORESIS **1995** 16(1) 334-337.

[206] Carmichael, J.; DeGraff, W. G.; Gazdar, A. F.; Minna, J. D.; and Mitchell, J. B.; *Evaluation of a Tetrazolium-based Semiautomated Colorimetric Assay: Assessment of Chemosensitivity Testing.* Cancer Research **1987** 47(4) 936-942.

[207] Life Technologies Corporation; *Calcein, AM.* Life Technologies Corporation ***II*** Accessed(6/16/) http://products.invitrogen.com/ivgn/product/C3099?ICID=search-product.

[208] Life Technologies Corporation; *Propidium Iodide - 1.0 mg/mL Solution in Water.* Life Technologies Corporation ***II*** Accessed(6/16/) https://products.invitrogen.com/ivgn/product/P3566?ICID=search-product.

[209] Alkilany, A.; and Murphy, C.; *Toxicity and cellular uptake of gold nanoparticles: what we have learned so far?.* Journal of Nanoparticle Research **2010** 12(7) 2313-2333.

[210] Tong, L.; Wei, Q.; Wei, A.; and Cheng, J.; *Gold Nanorods as Contrast Agents for Biological Imaging: Optical Properties, Surface Conjugation and Photothermal Effects†.* Photochemistry and Photobiology **2009** 85(1) 21-32.

[211] Connor, E.; Mwamuka, J.; Gole, A.; Murphy, C.; and Wyatt, M.; *Gold Nanoparticles Are Taken Up by Human Cells but Do Not Cause Acute Cytotoxicity.* Small **2005** 1(3) 325-327.

[212] Qu, Y.; and Lü, X.; *Aqueous synthesis of gold nanoparticles and their cytotoxicity in human dermal fibroblasts-fetal.* Biomedical Materials **2009** 4(2) .

[213] Pan, Y.; Neuss, S.; Leifert, A.; Fischler, M.; Wen, F.; Simon, U.; Schmid, G.; Brandau, W.; and Jahnen-Dechent, W.; *Size-Dependent Cytotoxicity of Gold Nanoparticles.* Small **2007** 3(11) 1941-1949.

[214] Li, J.; Zou, L.; Hartono, D.; Ong, C.; Bay, B.; and Lanry Yung, L.; *Gold Nanoparticles Induce Oxidative Damage in Lung Fibroblasts In Vitro.* Advanced Materials **2008** 20(1) 138-142.

[215] Purest Colloids; *MesoGold - Nanoparticle Colloidal Gold.* Purest Colloids, Inc. ***//*2013** Accessed(6/16/2013) http://www.purestcolloids.com/mesogold.htm?utm_source=searchalliance&utm_medium=ppc&utm_campaign=Meso-Gold&partner=11&utm_term=colloidal%20gold.

[216] Huang, X.; El-Sayed, I. H.; Qian, W.; and El-Sayed, M. A.; *Cancer Cell Imaging and Photothermal Therapy in the Near-Infrared Region by Using Gold Nanorods.* Journal of the American Chemical Society **2006** 128(6) 2115-2120.

[217] Huff, T. B.; Tong, L.; Zhao, Y.; Hansen, M. N.; Cheng, J.; and Wei, A.; *Hyperthermic effects of gold nanorods on tumor cells.* Nanomedicine **2007** 2(1) 125-132.

[218] Tong, L.; Zhao, Y.; Huff, T.; Hansen, M.; Wei, A.; and Cheng, J.; *Gold Nanorods Mediate Tumor Cell Death by Compromising Membrane Integrity.* Advanced Materials **2007** 19(20) 3136-3141.

[219] Ito, K.; Tanaka, O.; Honda, I.; Abe, H.; Yamaguchi, I.; and Kobayashi, A.; *Complete Regression of Mouse Mammary Carcinoma with a Size Greater than 15 mm by Frequent Repeated Hyperthermia Using Magnetite Nanoparticles.* Journal of Bioscience and Bioengineering **2003** 96(4) 364-369.

[220] Westra, A.; and Dewey, W. C.; *Variation in Sensitivity to Heat Shock during the Cell-cycle of Chinese Hamster Cells in Vitro.* International Journal of Radiation Biology **1971** 19(5) 467-477.

[221] Selawry, O. S.; Goldstein, M. N.; and McCormick, T.; *Hyperthermia in Tissue-cultured Cells of Malignant Origin.* Cancer Research **1957** 17(8) 785-791.

[222] Rabin, Y.; *Is intracellular hyperthermia superior to extracellular hyperthermia in the thermal sense?.* International Journal of Hyperthermia **2002** 18(3) 194-202.

[223] Govorov, A. O.; and Richardson, H. H.; *Generating heat with metal nanoparticles.* Nano Today **2007** 2(1) 30-38.

[224] Govorov, A.; Zhang, W.; Skeini, T.; Richardson, H.; Lee, J.; and Kotov, N.; *Gold nanoparticle ensembles as heaters and actuators: melting and collective plasmon resonances.* Nanoscale Research Letters **2006** 1(1) 84-90.

[225] Henle, K. J.; and Leeper, D. B.; *Interaction of Hyperthermia and Radiation in CHO Cells: Recovery Kinetics.* Radiation Research **1976** 66(3) 505-518.

[226] Thrall, D. E.; Gillette, E. L.; and Bauman, C. L.; *Effect of heat on the C3H mouse mammary adenocarcinoma evaluated in terms of tumor growth.* European Journal of Cancer (1965) **1973** 9(11–12) 871-875.

[227] Landsman, M. L.; Kwant, G.; Mook, G. A.; and Zijlstra, W. G.; *Light-absorbing properties, stability, and spectral stabilization of indocyanine green.* Journal of Applied Physiology **1976** 40(4) 575-583.

[228] Philip, R.; Penzkofer, A.; Bäumler, W.; Szeimies, R.; and Abels, C.; *Absorption and fluorescence spectroscopic investigation of indocyanine green.* Journal of Photochemistry and Photobiology A: Chemistry **1996** 96(1–3) 137-148.

[229] Mordon, S.; Devoisselle, J. M.; Soulie-Begu, S.; and Desmettre, T.; *Indocyanine Green: Physicochemical Factors Affecting Its Fluorescencein Vivo.* Microvascular Research **1998** 55(2) 146-152.

[230] Holzer, W.; Mauerer, M.; Penzkofer, A.; Szeimies, R.; Abels, C.; Landthaler, M.; and Bäumler, W.; *Photostability and thermal stability of indocyanine green.* Journal of Photochemistry and Photobiology B: Biology **1998** 47(2–3) 155-164.

[231] Saxena, V.; Sadoqi, M.; and Shao, J.; *Degradation kinetics of indocyanine green in aqueous solution.* Journal of Pharmaceutical Sciences **2003** 92(10) 2090-2097.

[232] Yu, J.; Yaseen, M. A.; Anvari, B.; and Wong, M. S.; *Synthesis of Near-Infrared-Absorbing Nanoparticle-Assembled Capsules.* Chemistry of Materials **2007** 19(6) 1277-1284.

[233] Zharov, V. P.; Mercer, K. E.; Galitovskaya, E. N.; and Smeltzer, M. S.; *Photothermal Nanotherapeutics and Nanodiagnostics for Selective Killing of Bacteria Targeted with Gold Nanoparticles.* Biophysical Journal **2006** 90(2) 619-627.

[234] Wang, L.; Li, Y.; Zhou, L.; Liu, Y.; Meng, L.; Zhang, K.; Wu, X.; Zhang, L.; Li, B.; and Chen, C.; *Characterization of gold nanorods in vivo by integrated analytical techniques: their uptake, retention, and chemical forms.* **2010** 396(3) 1105-1114.

[235] Semmler-Behnke, M.; Kreyling, W. G.; Lipka, J.; Fertsch, S.; Wenk, A.; Takenaka, S.; Schmid, G.; and Brandau, W.; *Biodistribution of 1.4- and 18-nm Gold Particles in Rats.* Small **2008** 4(12) 2108-2111.

[236] Lewin, M.; Carlesso, N.; Tung, C.; Tang, X.; Cory, D.; Scadden, D. T.; and Weissleder, R.; *Tat peptide-derivatized magnetic nanoparticles allow in vivo tracking.* Nat Biotech **2000** 18(4) 410-414.

[237] Sadauskas, E.; Danscher, G.; Stoltenberg, M.; Vogel, U.; Larsen, A.; and Wallin, H.; *Protracted elimination of gold nanoparticles from mouse liver.* Nanomedicine: Nanotechnology, Biology and Medicine **2009** 5(2) 162-169.

[238] Bartczak, D.; Muskens, O. L.; Millar, T. M.; Sanchez-Elsner, T.; and Kanaras, A. G.; *Laser-Induced Damage and Recovery of Plasmonically Targeted Human Endothelial Cells.* Nano Letters **2011** 11(3) 1358-1363.

[239] Orringer, D.; Chen, T.; Huang, D.; Armstead, W.; Hoff, B.; Koo, Y.; Keep, R.; Philbert, M.; Kopelman, R.; and Sagher, O.; *The brain tumor window model: A*

combined cranial window and implanted glioma model for evaluating iIntraoperative contrast agents. Neurosurgery **2010** 66(4) 736-743.

[240] Britz, G.; Ghatan, S.; Spence, A.; and Berger, M.; *Intracarotid RMP-7 enhanced indocyanine green staining of tumors in a rat glioma model.* Journal of Neuro-Oncology **2002** 56(3) 227-232.

[241] Hansen, D. A.; Spence, A. M.; Carski, T.; and Berger, M. S.; *Indocyanine green (ICG) staining and demarcation of tumor margins in a rat glioma model.* Surgical Neurology **1993** 40(6) 451-456.

[242] Ozawa, T.; Britz, G.; Kinder, D.; Spence, A.; VandenBerg, S.; Lamboorn, K.; Deen, D.; and Berger, M.; *Bromophenol blue staining of tumors in a rat glioma model.* Neurosurgery **2005** 57(5) 1041-1046.

[243] Little, J. B.; *Repair of Sub-lethal and Potentially Lethal Radiation Damage in Plateau Phase Cultures of Human Cells.* Nature **1969** 224(5221) 804-806.

[244] Horsman, M.; and Overgaard, J.; *Hyperthermia: a Potent Enhancer of Radiotherapy.* Clinical Oncology **2007** 19(6) 418-426.

[245] Winer, I.; Wang, S.; Lee, Y. K.; Fan, W.; Gong, Y.; Burgos-Ojeda, D.; Spahlinger, G.; Kopelman, R.; and Buckanovich, R. J.; *Correction: F3-Targeted Cisplatin-Hydrogel Nanoparticles as an Effective Therapeutic that Targets Both Murine and Human Ovarian Tumor Endothelial Cells In vivo.* Cancer Research **2011** 71(1) 289-289.

[246] Farokhzad, O. C.; Jon, S.; Khademhosseini, A.; Tran, T. T.; LaVan, D. A.; and Langer, R.; *Nanoparticle-Aptamer Bioconjugates.* Cancer Research **2004** 64(21) 7668-7672.

[247] *Resistant to Antibiotics: E. Coli Outbreak in Germany Claims First Victim.* Spiegel Online International **5/24/2011** Accessed(8/12/2011) http://www.spiegel.de/international/germany/resistant-to-antibiotics-e-coli-outbreak-in-germany-claims-first-victim-a-764656.html.

[248] Begier, E. M.; Frenette, K.; Barrett, N. L.; Mshar, P.; Petit, S.; Boxrud, D. J.; Watkins-Colwell, K.; Wheeler, S.; Cebelinski, E. A.; Glennen, A.; Nguyen, D.; and Hadler, J. L.; *A High-Morbidity Outbreak of Methicillin-Resistant Staphylococcus aureus among Players on a College Football Team, Facilitated by Cosmetic Body Shaving and Turf Burns.* Clinical Infectious Diseases **2004** 39(10) 1446-1453.

[249] Norman, R. S.; Stone, J. W.; Gole, A.; Murphy, C. J.; and Sabo-Attwood, T. L.; *Targeted Photothermal Lysis of the Pathogenic Bacteria, Pseudomonas aeruginosa, with Gold Nanorods.* Nano Letters **2007** 8(1) 302-306.

[250] Fawaz, F.; Bonini, F.; Maugein, J.; and Lagueny, A.; *Ciprofloxacin-loaded polyisobutylcyanoacrylate nanoparticles: pharmacokinetics and in vitro antimicrobial activity.* International Journal of Pharmaceutics **1998** 168(2) 255-259.

[251] *FDA Approves Teflaro for Bacterial Infections.* U.S. Department of Health & Human Services **10/29/2010** Accessed(8/12/2010)

http://www.fda.gov/NewsEvents/Newsroom/PressAnnouncements/2010/ucm231594.htm.

[252] Tsai, J.; Chiang, C.; Chen, H.; Huang, S. B.; Wang, C. W.; Lee, M. I.; Hsu, Y.; Chen, C.; and Tsai, T.; *Photodynamic Therapy of oral dysplasia with topical 5-aminolevulinic acid and light-emitting diode array.* Lasers in Surgery and Medicine **2004** 34(1) 18-24.

[253] Giusti, J.; Santos-Pinto, L.; Pizzolitto, A.; Kurachi, C.; and Bagnato, V.; *Effectiveness of Photogem® activated by LED on the decontamination of artificial carious bovine dentin.* Laser Physics **2006** 16(5) 859-864.

[254] Moreno, M. J.; Monson, E.; Reddy, R. G.; Rehemtulla, A.; Ross, B. D.; Philbert, M.; Schneider, R. J.; and Kopelman, R.; *Production of singlet oxygen by Ru(dpp(SO3)2)3 incorporated in polyacrylamide PEBBLES.* Sensors and Actuators B: Chemical **2003** 90(1–3) 82-89.

[255] Tang, W.; Xu, H.; Kopelman, R.; and Philbert, M. A.; *Photodynamic Characterization and In Vitro Application of Methylene Blue-containing Nanoparticle Platforms*¶. Photochemistry and Photobiology **2005** 81(2) 242-249.

[256] Zolfaghari, P.; Packer, S.; Singer, M.; Nair, S.; Bennett, J.; Street, C.; and Wilson, M.; *In vivo killing of Staphylococcus aureus using a light-activated antimicrobial agent.* BMC Microbiology **2009** 9(1) 27.

[257] Merchat, M.; Bertolini, G.; Giacomini, P.; Villaneuva, A.; and Jori, G.; *Meso-substituted cationic porphyrins as efficient photosensitizers of gram-positive and gram-negative bacteria.* Journal of Photochemistry and Photobiology B: Biology **1996** 32(3) 153-157.

[258] Minnock, A.; Vernon, D. I.; Schofield, J.; Griffiths, J.; Howard Parish, J.; and Brown, S. B.; *Photoinactivation of bacteria. Use of a cationic water-soluble zinc phthalocyanine to photoinactivate both Gram-negative and Gram-positive bacteria.* Journal of Photochemistry and Photobiology B: Biology **1996** 32(3) 159-164.

[259] Jori, G.; and Brown, S. B.; *Photosensitized inactivation of microorganisms.* Photochemical & Photobiological Sciences **2004** 3(5) 403-405.

[260] Nitzan, Y.; Salmon-Divon, M.; Shporen, E.; and Malik, Z.; *ALA induced photodynamic effects on Gram positive and negative bacteria.* Photochemical & Photobiological Sciences **2004** 3(5) 430-435.

[261] Usacheva, M. N.; Teichert, M. C.; and Biel, M. A.; *Comparison of the methylene blue and toluidine blue photobactericidal efficacy against gram-positive and gram-negative microorganisms.* Lasers in Surgery and Medicine **2001** 29(2) 165-173.

[262] Anker, J. N.; and Kopelman, R.; *Magnetically modulated optical nanoprobes.* Applied Physics Letters **2003** 82(7) 1102-1104.

[263] Biswal, S. L.; and Gast, A. P.; *Micromixing with Linked Chains of Paramagnetic Particles.* Analytical Chemistry **2004** 76(21) 6448-6455.

[264] Lapointe, C.; Cappallo, N.; Reich, D. H.; and Leheny, R. L.; *Static and dynamic properties of magnetic nanowires in nematic fluids (invited).* Journal of Applied Physics **2005** 97(10) 10Q304-6.

[265] Korneva, G.; Ye, H.; Gogotsi, Y.; Halverson, D.; Friedman, G.; Bradley, J.; and Kornev, K. G.; *Carbon Nanotubes Loaded with Magnetic Particles.* Nano Letters **2005** 5(5) 879-884.

[266] Behrend, C. J.; Anker, J. N.; McNaughton, B. H.; and Kopelman, R.; *Microrheology with modulated optical nanoprobes (MOONs).* Journal of Magnetism and Magnetic Materials **2005** 293(1) 663-670.

[267] Rife, J.; Miller, M.; Sheehan, P.; Tamanaha, C.; Tondra, M.; and Whitman, L.; *Design and performance of GMR sensors for the detection of magnetic microbeads in biosensors.* Sensors and Actuators A: Physical **2003** 107(3) 209-218.

[268] Shen, W.; Liu, X.; Mazumdar, D.; and Xiao, G.; *In situ detection of single micron-sized magnetic beads using magnetic tunnel junction sensors.* Applied Physics Letters **2005** 86(25) 253901-3.

[269] Petkus, M. M.; McLauchlin, M.; Vuppu, A. K.; Rios, L.; Garcia, A. A.; and Hayes, M. A.; *Detection of FITC-cortisol via Modulated Supraparticle Lighthouses.* Analytical Chemistry **2006** 78(5) 1405-1411.

[270] Shaner, N. C.; Campbell, R. E.; Steinbach, P. A.; Giepmans, B. N.; Palmer, A. E.; and Tsien, R. Y.; *Improved monomeric red, orange and yellow fluorescent proteins derived from Discosoma sp. red fluorescent protein.* Nat Biotech **2004** 22(12) 1567-1572.

[271] McNaughton, B. H.; Agayan, R. R.; Clarke, R.; Smith, R. G.; and Kopelman, R.; *Single bacterial cell detection with nonlinear rotational frequency shifts of driven magnetic microspheres.* Applied Physics Letters **2007** 91(22) 224105-3.

[272] Agayan, R. R.; Smith, R. G.; and Kopelman, R.; *Slipping friction of an optically and magnetically manipulated microsphere rolling at a glass-water interface.* Journal of Applied Physics **2008** 104(5) 054915-11.

[273] Ilic, B.; Czaplewski, D.; Craighead, H. G.; Neuzil, P.; Campagnolo, C.; and Batt, C.; *Mechanical resonant immunospecific biological detector.* Applied Physics Letters **2000** 77(3) 450-452.

[274] Ilic, B.; Czaplewski, D.; Zalalutdinov, M.; Craighead, H. G.; Neuzil, P.; Campagnolo, C.; and Batt, C.; *Single cell detection with micromechanical oscillators.* J. Vac. Sci. Technol. B **2001** 19(6) 2825-2828.

[275] Ilic, B.; Yang, Y.; and Craighead, H. G.; *Virus detection using nanoelectromechanical devices.* Applied Physics Letters **2004** 85(13) 2604-2606.

[276] Burg, T. P.; Godin, M.; Knudsen, S. M.; Shen, W.; Carlson, G.; Foster, J. S.; Babcock, K.; and Manalis, S. R.; *Weighing of biomolecules, single cells and single nanoparticles in fluid.* Nature **2007** 446(7139) 1066-1069.

[277] Ekinci, K. L.; and Roukes, M. L.; *Nanoelectromechanical systems.* Review of Scientific Instruments **2005** 76(6) 061101-12.

[278] Vignola, J. F.; Judge, J. A.; Jarzynski, J.; Zalalutdinov, M.; Houston, B. H.; and Baldwin, J. W.; *Effect of viscous loss on mechanical resonators designed for mass detection.* Applied Physics Letters **2006** 88(4) 041921-3.

[279] Sinn, I.; Kinnunen, P.; Albertson, T.; McNaughton, B. H.; Newton, D. W.; Burns, M. A.; and Kopelman, R.; *Asynchronous magnetic bead rotation (AMBR) biosensor in microfluidic droplets for rapid bacterial growth and susceptibility measurements.* Lab on a Chip **2011** 11(15) 2604-2611.

[280] Woods, L.; Powell, P.; Paxon, T.; and Ewing, A.; *Analysis of Mammalian Cell Cytoplasm with Electrophoresis in Nanometer Inner Diameter Capillaries.* Electroanalysis **2005** 17(13) 1192-1197.

[281] Stohrer, M.; Boucher, Y.; Stangassinger, M.; and Jain, R. K.; *Oncotic Pressure in Solid Tumors Is Elevated.* Cancer Research **2000** 60(15) 4251-4255.

[282] Shi, Y.; Ryu, D. D.; and Park, S. H.; *Performance of mammalian cell culture bioreactor with a new impeller design.* Biotechnology and Bioengineering **1992** 40(2) 260-270.

[283] Shi, Y.; Ryu, D. D.; and Ballica, R.; *Rheological properties of mammalian cell culture suspensions: Hybridoma and HeLa cell lines.* Biotechnology and Bioengineering **1993** 41(7) 745-754.

[284] Sahay, G.; Alakhova, D. Y.; and Kabanov, A. V.; *Endocytosis of nanomedicines.* Journal of Controlled Release **2010** 145(3) 182-195.

[285] Mineo, C.; and Anderson, R.; *Potocytosis.* **2001** 116(2) 109-118.

[286] Lai, S. K.; Hida, K.; Man, S. T.; Chen, C.; Machamer, C.; Schroer, T. A.; and Hanes, J.; *Privileged delivery of polymer nanoparticles to the perinuclear region of live cells via a non-clathrin, non-degradative pathway.* Biomaterials **2007** 28(18) 2876-2884.

[287] Giberson, R. T.; and Demaree, R. S.; *The influence of immunogold particle size on labeling density.* Microscopy Research and Technique **1994** 27(4) 355-357.

[288] GERNER, E. W.; and SCHNEIDER, M. J.; *Induced thermal resistance in HeLa cells.* Nature **1975** 256(5517) 500-502.

[289] Conner, S. D.; and Schmid, S. L.; *Regulated portals of entry into the cell.* Nature **2003** 422(6927) 37-44.

[290] Boonstra, J.; van Bergen en Henegouwen, P. M.; van Belzen, N.; Rijken, P. J.; and Verkleij, A. J.; *Immunogold labelling in combination with cryoultramicrotomy, freeze-etching, and label-fracture.* Journal of Microscopy **1991** 161(1) 135-147.